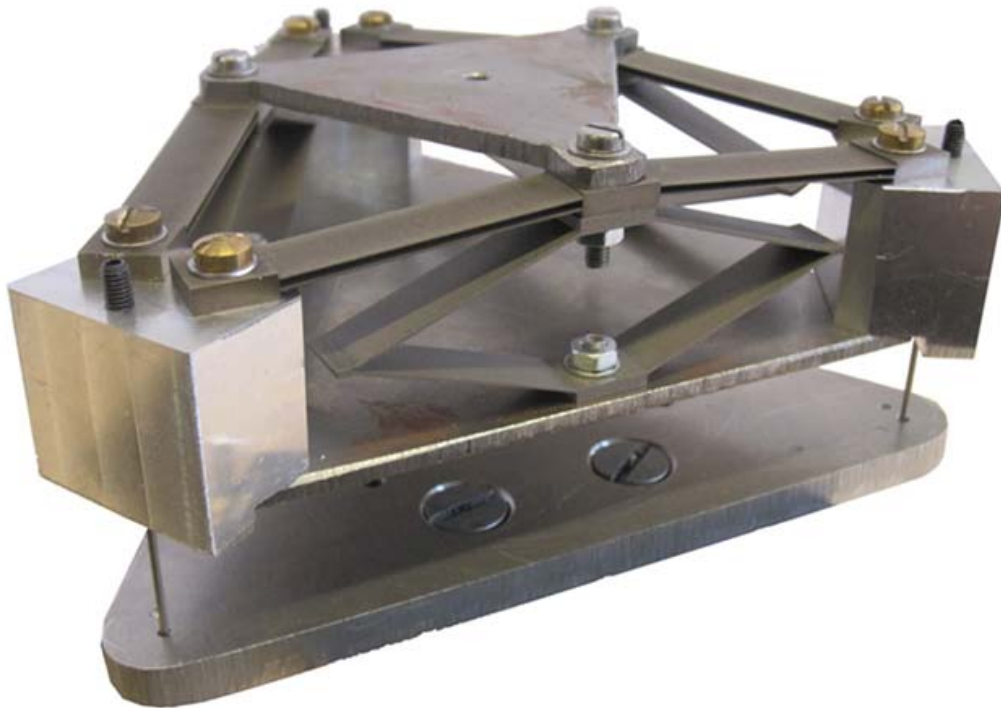Master of Science Thesis

DESIGN OF A ZERO STIFFNESS SIX DEGREES OF FREEDOM COMPLIANT PRECISION STAGE

September 16, 2011   A.G. Dunning

TU**Delft** Delft
University of
Technology

Challenge the future

Title: Design of a zero stiffness six degrees of freedom compliant precision stage

Author: A.G. Dunning

Date: September 16, 2011

Student nr: 1172514

Institute: Delft University of Technology
Faculty of Mechanical Engineering
Department of Biomechanical Engineering

Board of examiners:

     Prof. Dr. F.C.T. van der Helm, Biomechanical Engineering, 3mE, TUDelft
     Dr. Ir. J.L. Herder, Biomechanical Engineering, 3mE, TUDelft
     Ir. J.J.M. Peijster, Mapper Lithography
     Ir. J.W. Spronck, Mechatronic Systems Design, 3mE, TUDelft
     Mr. N. Tolou, Biomechanical Engineering, 3mE, TUDelft

Preface

This thesis contains the research I have performed on the design of a zero stiffness 6 DoF compliant precision stage. I did this project in collaboration with the company Mapper Lithography, Delft, The Netherlands.

First, I did a literature research towards the design of a statically balanced six degrees of freedom compliant precision stage. I made an overview of the existing of the available six degrees of freedom compliant stages and looked to the possibilities to combine such a mechanism with static balancing. The paper is published in Mechanical Sciences.

During the design phase of this project I encountered that there was no numerical method available to model the design I proposed, the use of bi-stable buckling beams. For this purpose, I wrote a second paper to show and explain a method to model bi-stable buckling beams in ANSYS$^{\text{TM}}$.

Finally, the main and most important part of this research (third paper) was to design a zero stiffness six degrees of freedom compliant precision stage.

I would like to thank all the students who helped me with new ideas and insights to realize this design: Lodewijk Kluit, Toon Lamers, Pieter Pluimers, Jos Lassooij. In particalur I want to thank Nima Tolou, my daily supervisor, and Just Herder to give me guidance and good reviews on my work during this graduation project. Furthermore, I would like to thank Jerry Peijster, my supervisor at Mapper Lithography, for his guidance and usefull remarks during the meetings and providing me the opportunity to do this work in collaboration with Mapper Lithography.

Delft, The Netherlands   A.G. Dunning
September, 2011

Contents

Mechanical
Sciences

Review Article: Inventory of platforms towards the design of a statically balanced six degrees of freedom compliant precision stage

A. G. Dunning, N. Tolou, and J. L. Herder

Faculty of Mechanical, Maritime and Materials Engineering, Department of Biomechanical Engineering,
Delft University of Technology, Delft, The Netherlands

Abstract. For many applications in precision engineering, a six degrees of freedom (DoF) compliant stage (CS) with zero stiffness is desirable, to deal with problems like backlash, friction, lubrication, and at the same time, reduce the actuation force. To this end, the compliant stage (also known as compliant mechanism) can be statically balanced with a stiffness compensation mechanism, to compensate the energy stored in the compliant parts, resulting in a statically balanced compliant stage (SBCS). Statically balanced compliant stages can be a breakthrough in precision engineering. This paper presents an inventory of platforms suitable for the design of a 6 DoF compliant stage for precision engineering. A literature review on 3–6 DoF compliant stages, static balancing strategies and statically balanced compliant mechanisms (SBCMs) has been performed. A classification from the inventory has been made and followed up by discussion. An obviously superior architecture for a 6 DoF compliant stage was not found. All the 6 DoF stages are either non-statically balanced compliant structures or statically balanced non-compliant structures. The statically balanced non-compliant structures can be transformed into compliant structures using lumped compliance, while all SBCMs had distributed compliance. A 6 DoF SBCS is a great scope for improvements in precision engineering stages.

1 Introduction

Many applications in precision engineering, including lithography, electron beam microscopy, micro assembly, aerospace, medical applications, require ultra precision positioning to manipulate an object in a vacuum or wet environment. For instance, in lithography the electrical circuits written on a wafer will have a resolution smaller than 20 nm (Willson and Roman, 2008). In the medical field, precise surgical tools with good force feedback are required to avoid tissue damage during operation (Sjoerdsma et al., 1997). All the named applications are situated inside a vacuum or wet environment. Therefore it is difficult to use conventional bearings, due to the need of lubrication. The backlash in conventional joints also has been an issue in high precision engineering. To overcome these problems, compliant mechanisms can be used.

A compliant mechanism is a mechanism that transfers force, motion or energy by using the elastic deformation of its flexible components rather than using rigid-body joints only. An advantage of compliant mechanisms is that it can easily be manufactured as a monolithic structure due to its hingeless nature of the design. This absence of movable joints reduces wear, friction and backlash in the mechanism and correspondingly increases precision, which is an important factor in the design of high-precision instrumentation. There is also no need for lubrication and the mechanism is insensitive to dust, which is an important advantage in instruments under vacuum (Howell, 2001).

However, the compliant mechanisms rely on the deflection of flexible members, which introduces positive stiffness and requires energy to deform. Therefore, the energy storage in the flexible members is distorting the input-output relationship and challenges the mechanical efficiency. When the deformation of the flexible members is large, non-linearities are introduced, which increases the complexity of the design (Herder and van den Berg, 2000; Morsch and Herder, 2010).

In many of the mentioned fields, it is required to manipulate an object in six degrees of freedom (DoF). In particular, in lithography and electron beam microscopy, the actuation of the 6 DoF positioning stage produces too much heat, mainly caused by the stiffness of the stage, which can affect the precision of the application (Nieuwenhuis, 2010). In medical instruments, the force feedback is not optimal, due to the stiffness and friction introduced in compliant and contact members (Sjoerdsma et al., 1997).

To overcome these problems a stiffness compensation mechanism can be added to the compliant mechanism, resulting in a statically balanced compliant mechanism (SBCM) with nearly zero stiffness. A statically balanced mechanism (SBM) is a mechanism on which the forces of one or more potential energy storage elements are acting, such that the mechanism is in static equilibrium and therefore has zero stiffness. The total potential energy should be constant in every position of the mechanism (Herder, 2001). To create static balancing a positive stiffness of the mechanism should be balanced with a negative stiffness compensation device. Therefore, it can be very advantageous to integrate a 6 DoF SBCM into an available application and replace the conventional positioning system.

The purpose of this literature survey consists of (1) to provide an overview of the state of the art of 6 DoF compliant stages. Interesting stages with less degrees of freedom, where translations are combined with rotations have also been investigated. A classification is made to compare the available stages to investigate whether there is a superior design for 6 DoF compliant stages. Thereafter, (2) an inventory on balancing strategies for compliant mechanisms is made. Finally, (3) possibilities to combine a 6 DoF compliant stage with static balancing will be investigated.

In Sect. 2, the method, including search method, search criteria, and the method to classify the results, is explained. The results of the literature survey are briefly described in Sect. 3. In Sect. 3.1 the results of the 6 DoF compliant stages are presented. It presents the type and classification of flexures, serial and planar positioning structures. Section 3.2 describes the balancing strategies with existing SBCMs and structures combining 6 DoF with static balancing. Section 4 interprets and discusses the results of each goal. Conclusions are presented in Sect. 5.

2   Method

2.1   Search method

The literature survey is separated into two parts. In the first part a literature search is conducted for 6 DoF compliant precision stages. This part also considers stages with fewer DoFs that may be converted into 6 DoF. These are stages with 3, 4 or 5 degrees of freedom, where translational degrees of freedom were combined with rotational degrees of freedom.

The second part is to examine the static balancing strategies for compliant mechanisms and make a classification.

By analyzing the topics a search plan was made. The key subjects and constraints were determined, particularly in the field of precision engineering. Only stages with a motion smaller than 1mm were searched for. Subsequently, key subjects were transformed into search terms, comprising synonyms and related terms. These search terms were used in the set of keywords in the search engines.

In total five different sets of keywords have been used, concerning keywords defining (1) compliant mechanisms, (2) the field of precision engineering, (3) 6 DoF stages, (4) static balancing and (5) zero stiffness.

In order to optimize the search, all sets of keywords were combined and narrowed. Also the references of the articles were checked for useful articles in the same subject. The results were first filtered by inspecting the article titles. Subsequently, the reduced results were filtered by reading the abstracts and looking to the images in the article. From the abstract or the images the working principle needed to be clear. Otherwise the papers were discarded.

The literature search was conducted using two search engines (Scopus; Espacenet). SCOPUS was used for journal articles and conference proceedings, while Espacenet was used to search for patents. All five sets of keywords were used in SCOPUS. Espacenet is the search engine of the European Patent Office and searches patents from all over the world. This engine is able to search patents with a set of keywords, instead of a classification system. Only patents of 6 DoF compliant stages and SBCMs were of interest for this literature survey, only specific combinations of sets of keywords were used. An overview of the sets of keywords can be found in Table 1.

2.2   Classification

A classification was made to compare the results of the compliant mechanisms within the field of 6 DoF stages and precision engineering. The following strategy and criteria have been used for classification.

The first and second level of classification, indicated the architecture of the mechanism. In the first level, a distinction was made between planar and spatial geometry of the structure. In a planar structure, in contrast to spatial structures, flexible elements to perform a 6 DoF motion are in the same plane, so for some motion out-of-plane motion is required. The second level described the configuration of the kinematic chain mechanism. This can be a parallel or a serial configuration (Lobontiu, 2003). In a parallel configuration, also called a closed-loop configuration, the fixed base is connected to the movable end-effector through multiple kinematic chains. A good example of a parallel mechanism is the Stewart platform (Stewart, 1965). Serial mechanisms use an open loop serial chain of links to connect the base with the end-effector. A robot arm is a good example of a serial mechanism.

Table 1. Overview of the sets of keywords used in SCOPUS (1–5) and Espacenet (1, 3, 4, 5).

Sets	Keywords
(1) Compliant mechanisms	– Compliant, flexible, flexure, monolithic – Mechanism, structure, design
(2) Precision engineering	– Precision, micro, nano, sensible – Stage
(3) 6 DoF stage	– Six degrees of freedom, six axis – Stage
(4) Static balancing	– Static balancing, neutral equilibrium
(5) Zero stiffness	– Zero/neutral/eliminate/remove/cancel stiffness – Constant potential energy, pre-stressed – Neutral stability – Gravity compensation
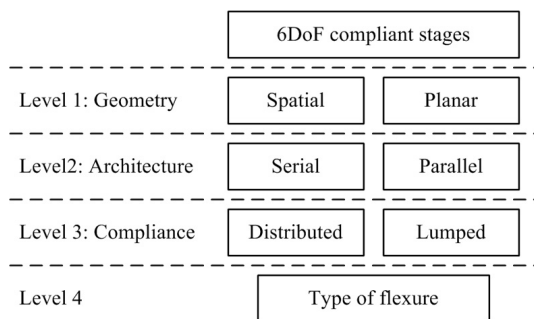
Figure 1. Schematic representation of the classification levels to compare the 6 DoF compliant stages.

The third level of classification described the types of stress distribution in the mechanism, which are lumped compliance and distributed compliance (Ananthasuresh and Kota, 1995).

In the fourth level the type of flexures used in the mechanism was distinguished.

In Fig. 1, a schematic representation of the classification is provided. Quantitative data found, involving size (S), working range (WR), will be noted.

To compare the stages, the ratios between translations, rotations and the size of the stages were investigated.

The SBCMs were classified according to the balancing principle, using (1) counterweights or (2) elastic elements, to compensate gravity forces or strain energy inside the mechanism (Herder, 2001). The mechanisms in these categories can be classified further according to the type of compensation mechanism. If reported in the article, the remaining stiffness after balancing, the statically balanced stroke and the size of the balancing mechanism is mentioned.

3   Results

3.1   State of the art in 6 DoF compliant stages

In the field of precision engineering the demand for 6 DoF stages is high. These stages have to be very accurate, with a resolution in the order of nanometers (Willson and Roman, 2008). In literature, precision compliant stages, which combine translations and rotations, with 3, 5 and 6 DoF were found. All the 6 DoF stages had three translational (x, y, z) and three rotational (θx, θy, θz) degrees of freedom. One 5 DoF stage (Wang et al., 2005) was found, which had no degree of freedom in rotation around the z-axis, and the 3 DoF stages had all two translational (x, y) and one rotational (θz) degrees of freedom. All the designs found in literature were fully compliant. In other words, no conventional joints were used for transferring motion. Besides, all the designs were highly symmetric, otherwise it is mentioned.

An overview of all the available results, including flexure type, size (S) and working range (WR) is shown in Table 2.

3.1.1   Type of flexures

Different flexures were found in the compliant mechanisms. Depending on the characteristics of the flexure it can have single or multiple deflection axes, which can be translational or rotational. Two rotational deflection axes in a joint create a universal joint and a combination of three rotational joints creates a spherical joint.

The flexible components could be classified in two groups, with flexures having (1) lumped compliance and (2) distributed compliance. With lumped compliance the flexion concentrates around a distinct number of flexures, causing high stress concentrations in the mechanism. These flexible elements have also low static and fatigue strength, usually undergoes small displacements, and manufacturing

www.mech-sci.net/2/157/2011/   Mech. Sci., 2, 157–168, 2011

- 3 -

Table 2. Overview of the results of the compliant stages, mentioned flexure type (mentioned with •), size and working range. Data not available identified with –.

	Leaf spring	Pin flexure	Small-length pin flexure	Small-length plate flexure	Corner filleted notch	Circular notch	Parabolic notch	Spherical notch	Monolithic	Size ΔX	Size ΔY	Size ΔZ	Trans ΔX	Trans ΔY	Trans ΔZ	Rot Δθx	Rot Δθy	Rot Δθz
Spatial parallel structures																		
Brouwer et al. (2010)	•									6.2	6.2	0.5	20	20	20	52.36	52.36	52.36
Seugling et al. (2002)	•									100	100	100	0.93	0.93	0.93	38e-3	38e-3	38e-3
Moon and Kota (2002)	•									–	–	–	–	–	–	–	–	–
Helmer et al. (2004)				•						164	147	255	4000	4000	4000	69.8	69.8	69.8
Hu et al. (2008b)					•					±Ø95.2		21.6	50	50	50	8.73	8.73	8.73
Liu et al. (2001)							•			–	–	–	–	–	–	–	–	–
Sun et al. (2003)							•			–	–	–	–	–	–	–	–	–
Wang et al. (2003)							•			Ø130		98.3	–	–	–	–	–	–
Wang et al. (2007)	•						•		•	–	–	–	5.8	5.7	1	–	–	–
Sun (2007)			•				•			–	–	–	1023	1023	1023	–	–	–
Yun and Li (2010)			•							250	250	250	9700	9700	9700	240	240	240
Spatial serial structures (2 parallel mechanisms in serie)																		
Choi and Lee (2005)	•								•	Ø258		10	–	–	–	–	–	–
Hu et al. (2008a)			•							Ø240		31.26	77.42	67.45	24.56	0.93	0.95	3.1
Chao et al. (2005)					•					–	–	–	130	140	18	–	–	–
Xiaohui et al. (2010)					•	•				–	–	–	–	–	–	–	–	–
Xuchu and Qianfeng (2009)			•		•					–	–	–	–	–	–	–	–	–
Liang et al. (2011)	•		•		•					–	–	–	0.034	0.034	0.034	–	–	–
Gao and Swei (1999)			•				•	•	•	–	–	–	–	–	–	–	–	–
Wang et al. (2005)									•	–	–	–	–	–	–	–	–	–
Chang et al. (1999a, b)	•								•	200	200	50	17.9	17.9	–	–	–	0.585
Planar parallel structures																		
Anderson (2003), Culpepper (2006), Culpepper and Anderson (2004)		•							•	±Ø180		3	100	100	100	4	4	4
Chen and Culpepper (2006)		•							•	Ø3		5.18	8.4	12.8	8.8	19.2	17.5	33.2
Zhang et al. (2005)			•						•	14	14	0.8	2	2	2	0.25	0.25	0.25
Park and Yang (2005)					•				•	–	–	–	7	7.1	10	0.25	0.23	0.26
Lu et al. (2004)					•				•	–	–	–	14	13	–	–	–	0.756
Ryu et al. (1997)					•				•	±Ø115		–	41.5	47.8	–	–	–	1.565
Tian et al. (2010)					•	•				–	–	–	–	–	–	–	–	–
Wang and Zhang (2008)					•				•	±Ø150		18.5	–	–	–	–	–	–
Yi et al. (2003)					•				•	±Ø120		–	100	100	–	–	–	17.5
Jong de, et al. (2010)	•								•	5.5	5.5	–	10	10	–	–	–	34.9
Lee and Kim (1997)					•				•	–	–	–	–	–	–	–	–	–

these elements can give difficulties, due to very thin sections (Ananthasuresh and Kota, 1995; Gallego and Herder, 2009). In this group, notch-type flexures and small-length plate and pin flexures could be found. The notch profile could be a (1) rectangular corner-filleted, (2) circular, (3) parabolic, or (4) spherical section (Fig. 2). The small-length plate flexure could bend in one degree of freedom and the pin flexure could bend in all three rotational degrees of freedom (Gallego and Herder, 2009).

For distributed compliant flexures, the flexibility is distributed equally over the entire flexible element. The flexible element has a constant cross-section, which prevent stress concentration around a point. Distributed compliance offers better performance and reliability compared to lumped compliance (Ananthasuresh and Kota, 1995). The pin flexure could bend in all three rotational degrees of freedom and
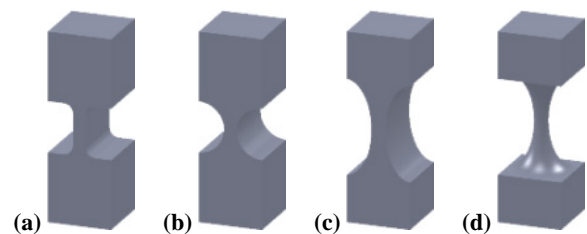

Figure 2. Notch-type flexures with lumped compliance. The notch profile is **(a)** rectangular corner-filleted, **(b)** circular, **(c)** parabolic, or **(d)** spherical.
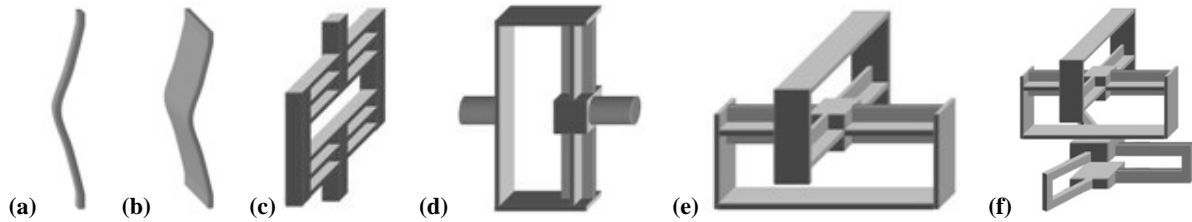
Mech. Sci., 2, 157–168, 2011   www.mech-sci.net/2/157/2011/

- 4 -

Figure 3. Flexures with distributed compliance. The flexures could be a **(a)** pin, **(b)** chevron, **(c)** translational, **(d)** rotational, **(e)** universal, or **(f)** spherical flexure. Reproduced from Gallego and Herder (2009).
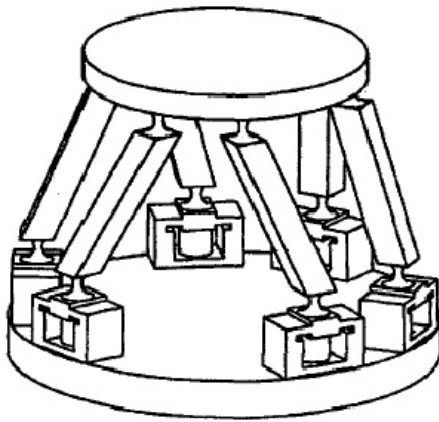

Figure 4. Typically example of a spatial parallel compliant stage (Liu et al., 2001). The platform is supported by legs, with compliant joints at both ends.

a chevron flexure, also called a leaf spring, could bend in one direction and take up torsion. Almost all of these flexures were built up from combining several chevron flexures in such a way that joints with different degrees of freedom are possible (Fig. 3) (Gallego and Herder, 2009).

3.1.2 Spatial compliant stages

The results for spatial compliant stages were separated into a group with a parallel and a serial kinematic chain. First the parallel designs will be described (Fig. 4).

In Brouwer et al. (2010) in-plane leaf springs form prismatic joints and three slanted leaf springs for out-of-plane motion form three universal joints. The flexures, arranged by 120°, create a monolithic spatial parallel platform stage. The same kind of flexures are used in Seugling et al. (2002) and Moon and Kota (2002). In the latter article, the leaf springs were combined such that they form a prismatic, rotational and spherical joint, respectively.

A large non-symmetric stage with corner-filled notches was developed in Helmer et al. (2004).

Circular notch-type flexures are used in Hu et al. (2008b). Here six slanted trapeziform displacement amplifiers form a

spatial stage. Each trapeziform amplifier can be modeled as two prismatic joints.

Spherical notches were found in mechanisms based on the Stewart platform. In Liu et al. (2001), Sun et al. (2003), and Wang et al. (2003) the platform is supported by 6 legs, that is the compliant equivalent of a 6-spherical-prismatic-spherical manipulator. In Wang et al. (2007) the platform is supported by 3 legs. Each leg is the compliant equivalent of a rotational-spherical manipulator. The legs are placed on small compliant mechanisms, which enables translational motion in 2 DoF with leaf springs and are placed 120° of each other.

Sun (2007) used a non-symmetric stage with spherical notch-type flexures in series with small-length plate flexures (prismatic joints) to create the desired degrees of freedom.

In Yun and Li (2010) small-length pin flexures on both sides of an actuator are used to move a platform. In total eight non-symmetrically placed actuators are used, which makes the stage the compliant equivalent of a 8-prismatic-spherical-spherical/spherical-prismatic-spherical manipulator.

All stages with a serial kinematic chain were constructed as two parallel mechanisms in series, a so-called serial-parallel mechanism (Fig. 5). All stages consist of a parallel monolithic mechanism, which could perform the motion in x, y and θz direction (further mentioned as in-plane motion), and a parallel mechanism performing motion in z, θx, θy direction (further mentioned as out-of-plane motion). The flexures are all arranged 120° of each other.

Choi and Lee (2005) designed a stage where the motion is enabled by leaf springs. The x, y and θz motions are transferred by six L-shaped leaf springs and the z, θx, θy motions are transferred by wide leaf springs.

In Hu et al. (2008a) the flexures are cornered-filleted notches. The in-plane mechanism is the compliant equivalent of a traditional 3-revolute-revolute-revolute manipulator. The out-of-plane mechanism is an equivalent of a traditional 3-universal-prismatic-universal manipulator.

Chao et al. (2005) used a 3-revolute-revolute-revolute compliant mechanism with circular notches for the in-plane motion. For the out-of-plane motion a 3-revolute-prismatic-spherical compliant mechanism with circular notches is used to form 3 legs, supporting the moving platform. The stage
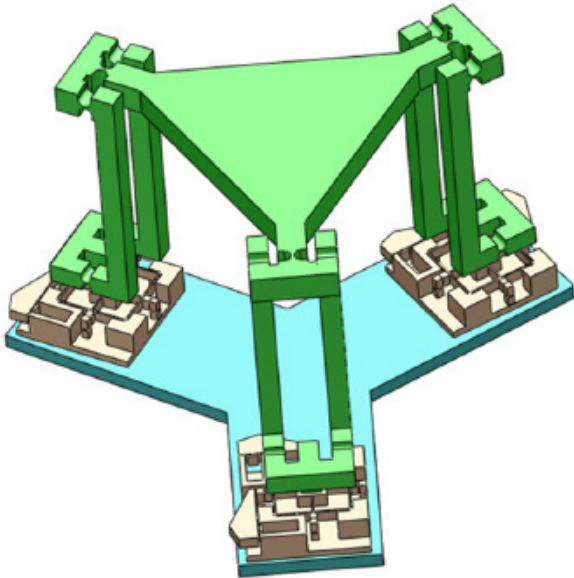
www.mech-sci.net/2/157/2011/   Mech. Sci., 2, 157–168, 2011

- 5 -

Figure 5. Typically example of a spatial serial compliant stage (Liang et al., 2011). Three legs forms a parallel compliant mechanism performing motion in z, θx, θy, θz. The legs are supported by parallel 2 DoF compliant mechanisms. Both parallel mechanisms in serie forms the spatial serial compliant stage.

Figure 6. Typically example of a planar compliant stage (Anderson, 2003; Culpepper, 2006; Culpepper and Anderson, 2004). The flexures to perfom motion are in the same plane.

3.1.3 Planar compliant stages

Only a few stages have a planar structure (Fig. 6). The main advantage of planar structures is that the whole mechanism can be manufactured monolithic and have a high stiffness, but usually a small workspace, compared to serial mechanisms. All the planar designs found in the articles were monolithic, and had a parallel kinematic chain. The differences in each design were the used flexure type.

In Anderson (2003), Culpepper (2006), and Culpepper and Anderson (2004) a nano-manipulator, called the HexFlex, which use 3 long pin flexures, placed 120° to each other, to enable 6 DoF is presented. Each flexure enables in-plane and out-of-plane motion. In Chen and Culpepper (2006) and Culpepper and Golda (2007) two different types of mirco-scaled versions of the HexFlex are made. In Zhang et al. (2005) the 6 DoF motion is enabled by four parallelograms. With small-length pin flexures the parallelograms can move in-plane and out-of-plane. In Park and Yang (2005) a set of circular notches arranged by 120° creates in-plane motion, and inclined circular notches placed 45° with respect to the plane enables out-of-plane motion.

Planar monolithic 3 DoF stages were found in Lu et al. (2004), Ryu et al. (1997), Tian et al. (2010), Wang and Zhang (2008), and Yi et al. (2003). The circular notch flexure groups are arranged 120° of each other. All the designs are modeled with a 3-revolute-revolute-revolute manipulator. Almost the same structure was found in a MEMS-based manipulator, produced by Jong de, et al. (2010), but the flexures are leaf springs and the compliant equivalent of a 3-prismatic-revolute-revolute manipulator is used. Lee and Kim (1997) designed an ultra-precision micro stage, with circular notch flexures, to correct the errors of a global stage.

from Xiaohui et al. (2010) has the same compliant equivalent structure as Chao et al. (2005) for in-plane motion. The out-of-plane motion is performed by 3 parabolic notch-type flexures. In Xuchu and Qianfeng (2009) a 3-revolute-revolute compliant mechanism with circular notches is used for in-plane motion. Small-length plate flexures are used for the out-of-plane motion.

Liang et al. (2011) used 3 legs, each consisting of two universal joints, supporting a platform for out-of-plane motion with 4 DoF (z, θx, θy, θz). These universal joints were manufactured with circular notch-type flexures. The in-plane motion (x, y) is provided by a spatial mechanism consisting of small-length plate flexures and leaf springs.

In Gao and Swei (1999) the compliant equivalent of a 3-revolute-prismatic-revolute manipulator is used for in-plane motion and a 3-revolute-prismatic-spherical manipulator for the out-of-plane motion. Three legs, with a parabolic and a spherical notch-type flexure, support the platform. The in-plane motion is provided by small-length plate flexures.

Wang et al. (2005) developed a 5 DoF compliant stage made with circular notch-type flexures, having a monolithic mechanism to provide translation along the x-axis and y-axis and a 4-revolute-revolute compliant mechanism to provide translation along the z-axis and rotations in all directions. The flexures in this stage are not arranged 120° of each other.

Chang et al. (1999a, b) designed a 3 DoF stage with leaf springs and small-length plate flexures, consisting of a 2 DoF (x, y) stage and a 1 DoF (θz) stage on top of it, which makes it also a serial-parallel structure.

Mech. Sci., 2, 157–168, 2011   www.mech-sci.net/2/157/2011/

- 6 -

Table 3. Overview of the results of the statically balanced compliant mechanisms (SBCM) and 6 DoF statically balanced mechanisms (SBM). The balancing mechanism is either with counterweights (C) or elastic elements, using springs (S), zero-free-length springs (ZFLS) or compliant flexures (CF), which are categorized into the use of buckling plates (BP), preloaded plates (PP), to balance strain energy (E) or gravity forces (G). Data not available identified with –.

	Reference	Flexure type					Balancing mechanism	Preloading	Category of SBCM	Stiffness/force compensation (%)	Compensated stiffness/force upper bound	Statically balanced stroke (mm)	Size of the balancing mechanism (mm³)
		Leaf spring	Circular notch	Parabolic notch	Spherical notch	Monolithic							
SBCM	Eijk van, and Dijksman (1979)	•					BP	E	–	100 %	–	–	–
	Herder and van den Berg (2000)	•					S	E	1	99.9 %	12.9 N	1	±49×10³
	Stapel and Herder (2004)	•				•	PP	E	3	100 %	±50 N mm⁻¹	0.3	±4280
	Tolou and Herder (2009)	•					PP	E	3	100 %	19 N	4.17	±720
	Lange de, et al. (2008)	•				•	BP	E	3	90 %	300 N	0.65	±980
	Powell and Frecker (2005)	•					S	E	1	100 %	–	–	–
	Hoetmer et al. (2009)	•				•	BP	E	3	120 %*	1 N mm⁻¹	1.7	±1850
	Morsch and Herder (2010)	•					PP	E	3	70 %	6.5 N**	23.6***	±4×10⁵
	Trease and Dede (2004)	•					CF	G	3	100 %	±5 N	–	–
	Tolou and Herder (2010) (case I)	•				•	BP	E	3	99 %	60 mN	0.05	9.6
	Tolou and Herder (2010) (case II)	•				•	BP	E	3	86 %	40 mN	0.06	1.6
6 DoF SBM	Streit (1991)				•		ZFLS	G					
	Ebert-Uphoff and Johnson (2002), Ebert-Uphoff et al. (2000)				•		S	G					
	Gosselin and Wang (2000)			•	•		C, S	G					
	Leblond and Gosselin (1998)						S	G					
	Shekarforoush et al. (2010)				•		ZFLS	G					

* This mechanism is overcompensated.
** Compensated force is calculated from given compensated moment.
*** Stroke is calculated from stroke given in radian.

3.2 Static balancing strategies for compliant mechanisms

Static balancing can be classified according to the balancing principle (Herder, 2001). These balancing principles are: (1) the addition of counterweights and (2) the use of elastic elements, to compensate gravity forces or strain energy inside the mechanism.

With the use of counterweights, the system is in equilibrium in any position. This method adds extra mass and inertia to the system, relative to springs or other elastic elements. The total potential energy of all gravity and elastic elements must be constant for perfect static balance.

There are several categories of SBCMs. These include (1) a compliant part balanced with a non-compliant compensation mechanism, (2) a compliant part with a compliant balancing mechanism, where the energy is stored in a separate spring, (3) the compensation energy is stored in a compliant part of the mechanism, rather than in a separate spring, and (4) adaptive balancing, taking into account that compliant mechanisms behave different under loaded and unloaded situations (Herder and van den Berg, 2000).

In Table 3 an overview of the results can be found.

3.2.1 Statically balanced compliant mechanisms

In literature, examples of SBCMs using elastic elements are very rare. In Eijk van, and Dijksman (1979) a mechanism with a constant negative stiffness, using a buckled plate spring, has been studied. Herder and van den Berg (2000) compensate the undesired stiffness in a laparoscopic grasper with a rolling-link mechanism and conventional helical springs (category 1). The reduced stiffness is in the order of 0.1 % of the stiffness of the gripper. In Stapel and Herder (2004) a fully compliant compensation device, based on a slider-rocker mechanism, for the laparoscopic grasper is developed (category 3). The total potential energy in the system is almost constant. In Tolou and Herder (2009), the gripper of Herder and van den Berg (2000) is balanced with a partially compliant mechanism, consisting of pairs of pre-stressed pinned-pinned initially curved beams, arranged perpendicular to the link driving the grasper and placed inside the tip of the grasper (category 3). This resulted in force of almost 0N to operate the grasper. Lange de, et al. (2008) used topology optimization to design a fully compliant grasper with a bistable balancing mechanism, with an actuation force reduction of 90 %, but due to calculated high stresses, a prototype is never fabricated (category 3). Powell and Frecker (2005) balanced a compliant forceps with a rigid link slider-crank

www.mech-sci.net/2/157/2011/   Mech. Sci., 2, 157–168, 2011

- 7 -

mechanism with a non-linear spring, optimized with potential energy analysis with finite element analysis (category 1).

Hoetmer et al. (2009) used the Building Block Approach to balance a gripper. With the use of a new balanced building block, consisting of buckling plates, the stiffness was reduced from 1 N mm^{-1} to -0.2 N mm^{-1} (category 3).

In Morsch and Herder (2010), the joint of a conventional balanced mechanism (Herder, 2001) is replaced by a cross-axis flexural pivot, and the zero-free-length springs by compliant leaf springs (category 3). This resulted in a fully compliant joint with a moment reduction of 70 %, measured from experiments.

Trease and Dede (2004) designed a partially compliant four bar mechanism with novel "open-cross" compliant joints to form a torsion-spring-based statically balanced gravity compensator (category 3). The potential energy of the system was balanced over ±45° from horizontal plane within a 3 % error.

In Tolou and Herder (2010), two different statically balanced compliant micro mechanisms were designed (category 3) where the preloading force and stroke are either perpendicular or collinear. The first type compensated the force for 99 % in the beginning of the travel path, due to external preloading force. But the collinear-type has been internally balanced without separated external preloading force, by using a bi-stable mechanism, compensating the force for 86 % at the end of the stroke.

All the above-mentioned SBCMs had one degree of freedom and had distributed compliance. The design methods may well be used to implement in a 6 DoF structure.

3.2.2   6 DoF statically balanced mechanisms

In literature 6 DoF SBCMs is not readily available. An investigation of the possibilities to combine compliant mechanisms with static balancing some 6 DoF SBMs found in literature are discussed here. All the structures discussed here are spatial parallel platform mechanisms.

Streit (1991) presented the first 6 DoF SBM. He presented a parallel platform mechanism consisting of three legs, where each leg has three degrees of freedom. The legs are parallelograms connected to the platform with spherical joints, and balanced with zero-free-length springs. Static balancing is only achieved when the centre of mass of the platform is close to the plane of the spherical joints. In Ebert-Uphoff and Johnson (2002) and Ebert-Uphoff et al. (2000) this condition is removed by introducing pulling and pushing legs connected to the platform with spherical joints. The mechanism has three active pushing legs, which tilt the platform upwards, and one passive pulling leg, attached in slightly off-centre of the platform and pulling the platform down to a static balanced condition.

Gosselin and Wang (2000) used six legs with revolute actuators to balance a platform, using both the counterweights method and the spring method.

Leblond and Gosselin (1998) showed different ways to balance existing spatial parallel mechanisms, such as the Gough-Stewart platform, with additional elements.

Shekarforoush et al. (2010) balanced two types of 6 DoF tensegrity systems, with passive zero-free-length springs and with an adjustable cable-spring combination. The connection between legs and the platform are all ball-socket joints, which could be represented as spherical joints.

In Table 3 the results are shown for balancing principle and which compliant flexure type could represent the joints in the mechanisms.

4   Discussion

In this part, the results are compared and discussed with each other based on criteria. Many articles did not mention size or working range, which makes it a challenge to compare all stages with each other. Besides, not every stage had the same structure to make a good comparison. Therefore, a comparison between all planar structures is made and finally the spatial stages are compared.

To make a good comparison, the ratios between translations, rotations and the size of the stages are compared. The ratios are normalized to the largest in the group, as shown in Fig. 7.

First, the ratios of translations (in µm) in the XY-plane relative to the size (in mm) of the XY-plane of planar structures (WRx·y/Sx·y) are compared. It is noteworthy, that in Chen and Culpepper (2006) the largest ratio is reached. Considering the ratios between rotations (in mrad) around the z-axis and the size (in mm) in the XY-plane (WRθz/Sx·y), again the largest ratio has been reached in Chen and Culpepper (2006). Also in Jong de, et al. (2010) and Ryu et al. (1997) a relative large ratio is found, compared to the other stages. The results showed that there is no clear relation between flexure type and translation/size or rotation/size ratio in XY-plane. Both Chen and Culpepper (2006) and Chang et al. (1999a) used leaf springs, but had the largest and the smallest ratios, respectively. Also the notch-type flexures did not showed ratios in the same order.

For the spatial stages the ratios of working range of the translations (in µm) relative to the size (in mm) of the stage (WRx·y·z/Sx·y·z) shows that the stage from Seugling et al. (2002) has a very small working range with respect to the size. In Brouwer et al. (2010), Culpepper and Anderson (2004), and Chen and Culpepper (2006) the ratios are high, due to the almost planar structure of the stages, which are able to perform 6 DoF motion. But the largest ratio is reached by a spatial structure (Yun and Li, 2010). Comparing the ratios between rotations (in mrad) and size (in mm) (WRθx·θy·θz/Sx·y·z) shows high ratios in Brouwer et al. (2010) and Chen and Culpepper (2006). This is also due to their planar structure. Remarkably, the ratio of the planar stage in Culpepper and Anderson (2004) is not as high as
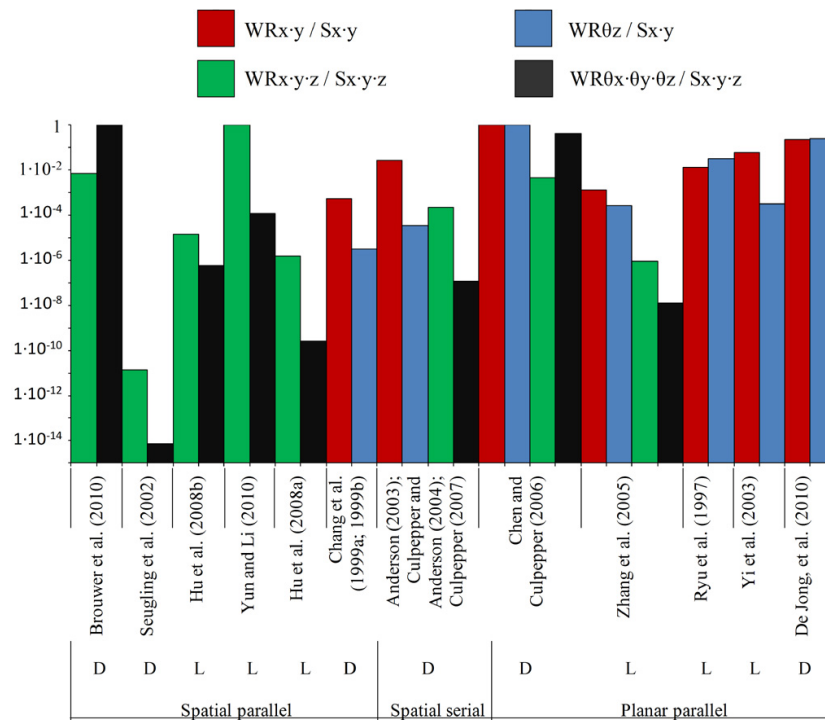
Figure 7. The ratios between translation, or rotation, and size for each compliant stage, if data was available. The ratios were normalized to the largest in the group, shown in logarithmic scale. The mechanisms use distributed compliance (D) or lumped compliance (L).

expected. Also in spatial structures there is no clear relation between working range and flexure type.

In theory, flexures with distributed compliance have a larger range of motion than flexures with lumped compliance. But also lumped compliant flexures were designed such that the complete stage had a large range of motion, using amplifiers in the stage (e.g. the legs in the spatial stages or the 3-revolute-revolute-revolute structure in planar stages act as amplifiers). Most of the stages with lumped compliance are based on these kinds of structures.

In many designs the groups of flexures are arranged 120° of each other. With a minimum of three equally distributed compliant structures, it is possible to create both translation and rotation of the whole stage, using only translation actuation. In other words, with minimal three 1 DoF compliant structures it is possible to create a 3 DoF stage. Due to this arrangement many stages were highly symmetric. This is to decrease the effect of the temperature gradient on accuracy of the design (Ryu et al., 1997).

From the results it appears that most of the 6 DoF spatial compliant structures are non-monolithic. Some 3 DoF planar structures are promising when implemented in a 6 DoF stage.

All the SBCMs, except one, have distributed compliance and use elastic elements to balance strain energy in the mechanism. The elastic elements (springs and compliant flexures) have been preloaded to store the strain energy, creating zero stiffness. However, pre-stressing of the elastic elements is

a challenge and gives difficulties in the design of statically balanced monolithic structures.

For further illustration, the ratios of the statically balanced stroke and compensated force relative to the size of the balancing mechanism is shown in Fig. 8. The compliant micro mechanisms (category 3 of SBCMs) have the largest ratios for statically balanced stroke relative to the size, while this ratio for compensated force relative to the size is still above the average of the other works. The largest ratio for compensated force relative to the size of the balancing mechanism is again for the category 3 of SBCMs. It may be concluded that a balancing mechanism based on buckling plates have great advantages to compensate relative large forces in a relative large stroke, compared to the size. The design with the non-compliant balancing mechanism (category 1 of SBCMs) has the smallest ratio for balanced stroke relative to the size. The preloaded plates shows less efficiency in terms of compensated force and balanced stroke relative to the average, however in all above case, further research is needed as only a few designs were available.

There are few examples of 6 DoF SBMs, but these are all spatial structures, which could be modeled with lumped compliance, balancing gravity forces. No example is available for SBCMs with lumped compliance. Combining SBCMs with lumped compliance, or redesigning an existing 6 DoF SBM, using distributed compliance and balancing strain energy, needs further research and will probably results in a complete new stage design.
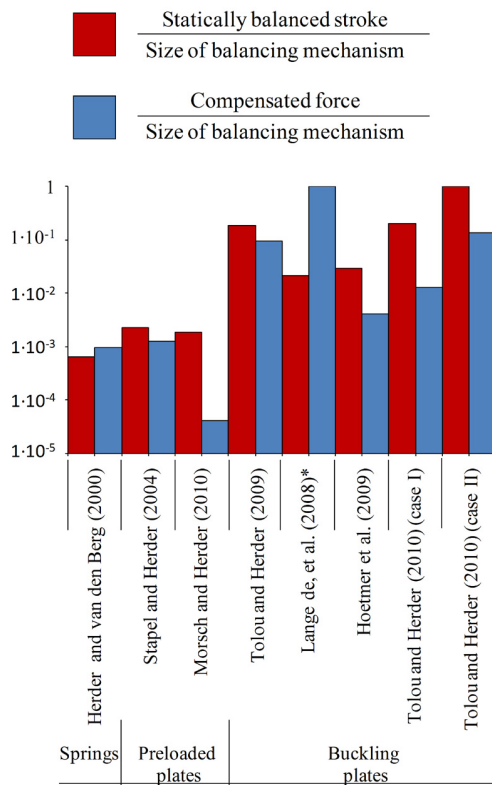
Figure 8. The ratios of statically balanced stroke and compensated force relative to the size of the balancing mechanism. Note that the ratios were normalized to the largest in the group and shown in logarithmic scale. The balancing mechanism used springs, preloaded plates or buckling plates to balance the mechanism.
* This design has an exceptionally high compensated force, but was never fabricated due to calculated high stresses.

5   Conclusions

An overview of existing compliant stages, combining translations and rotations (3–6 DoF), classification and discussion, comparing the ratios between translations, rotations and the size, has been made towards the design of 6 DOF statically balanced compliant stage.

It was found that different types of flexures are used in the planar and spatial stages. From the results there is no clear relation between the range of motion and the type of flexure. Where distributed compliance should have a larger range of motion, the lumped compliance stages use different kind of amplifiers to create a large range of motion. Consequently, it can be concluded that effectively each architecture for 6 DoF compliant stages performed equally well.

Different balancing strategies have been studied, as well as the possibilities to combine 6 DoF compliant stages with static balancing.

The compliant balancing mechanisms using buckling plates (either in micro- or mesoscale) shows the better per-

formance in terms of force compensation and stroke of static balancing relative to the size of the balancing mechanism.

It is shown that no 6 DoF statically balanced compliant stage is readily available. The existing statically balanced compliant mechanisms have 1 DoF, use pre-stressed elastic elements as balancing mechanism, and have distributed compliance, while all existing non-compliant 6 DoF statically balanced stages can be modeled with lumped compliance. Combining static balancing with a 6 DoF compliant stage needs either a new 6 DoF distributed compliant stage, balanced according to the method for balancing distributed compliance, or a new method to balance a lumped compliant 6 DoF stage.

A promising direction for future research would be to find a strategy to combine a 6 DoF monolithic compliant stage with static balancing.

References

Ananthasuresh, G. K. and Kota, S.: Designing compliant mechanisms, Mech. Eng., 117, 93–96, 1995.

Anderson, G. A. B.: A six degree of freedom flexural positioning stage, M.S. thesis, Massachusetts Institute of Technology, Cambridge, USA, 136 pp., 2003.

Brouwer, D. M., de Jong, B. R., and Soemers, H. M. J. R.: Design and modeling of a six DOFs MEMS-based precision manipulator, Precis. Eng., 34, 307–319, 2010.

Chang, S. H., Tseng, C. K., and Chien, H. C.: An ultra-precision XYθz piezo-micropositioner part I: Design and analysis, IEEE T. Ultrason. Ferr., 46, 897–905, 1999a.

Chang, S. H., Tseng, C. K., and Chien, H. C.: An ultra-precision XYθz piezo-micropositioner part II: Experiment and performance, IEEE T. Ultrason. Ferr., 46, 906–912, 1999b.

Chao, D., Zong, G., and Liu, R.: Design of a 6-DOF compliant manipulator based on serial-parallel architecture, in: Proceeding of the 2005 IEEE/ASME International Conference on Advanced Intelligent Mechatronics, Monterey, California, USA, 24–28 July 2005, 765–770, 2005.

Chen, S. C. and Culpepper, M. L.: Design of a six-axis micro-scale nanopositioner-μHexFlex, Precis. Eng., 30, 314–324, 2006.

Choi, K. B. and Lee, J. J.: Passive compliant wafer stage for single-step nano-imprint lithography, Rev. Sci. Instrum., 76, 075106, doi:10.1063/1.1948401, 2005.

Culpepper, M. L.: Multiple degree of freedom compliant mechanism, patent US2006252297, 2006.

Culpepper, M. L. and Anderson, G.: Design of a low-cost nanomanipulator which utilizes a monolithic, spatial compliant mechanism, Precis. Eng., 28, 469–482, 2004.

- 10 -

Culpepper, M. L. and Golda, D.: 6-Axis electromagnetically-actuated meso-scale nanopositioner, patent US2007220882, 2007.

Ebert-Uphoff, I. and Johnson, K.: Practical considerations for the static balancing of mechanisms of parallel architecture, P. I. Mech. Eng. K.-J. Mul., 216, 73–85, 2002.

Ebert-Uphoff, I., Gosselin, C. M., and Laliberté, T.: Static balancing of spatial parallel platform mechanisms – revisited, Mech. Des.-T. ASME, 122, 43–51, 2000.

Eijk van, J. A. and Dijksman, J. F.: Plate spring mechanism with constant negative stiffness, Mech. Mach. Theory, 14, 1–9, 1979.

Espacenet: http://www.espacenet.com/, last acces: 25 January 2011.

Gallego, J. A. and Herder, J. L.: Synthesis methods in compliant mechanisms: an overview, in: Proceedings of the ASME 2009 International Design Engineering Technical Conferences & Computers and Information in Engineering Conference, San Diego, California, USA, 30 August–2 September 2009, DETC2009-86845, 2009.

Gao, P. and Swei, S. M.: Six-degree-of-freedom micro-manipulator based on piezoelectric translators, Nanotechnology, 10, 447–452, 1999.

Gosselin, C. M. and Wang, J.: Static balancing of spatial six-degree-of-freedom parallel mechanisms with revolute actuators, J. Robotic Syst., 17, 159–170, 2000.

Helmer, P., Mabillard, Y., Clavel, R., and Bottinelli, S.: High precision apparatus for imposing or measuring a position or a force, patent US20040255696, 2004.

Herder, J. L.: Energy-free systems: theory, conception, and design of statically balanced spring mechanisms, Ph.D. thesis, Delft University of Technology, Delft, The Netherlands, 248 pp., 2001.

Herder, J. L. and van den Berg, F. P. A.: Statically balanced compliant mechanisms (SBCM's), an example and prospects, in: Proceedings of ASME 2000 Design Engineering Technical Conferences and Computers and Information in Engineering Conference, Baltimore, Maryland, USA, 10–13 September 2000, DETC2000/MECH-14144, 2000.

Hoetmer, K., Herder, J. L., and Kim, C. J.: A building block approach for the design of statically balanced compliant mechanisms, in: Proceedings of ASME 2009 International Design Engineering Technical Conferences & Computers and Information in Engineering Conference, San Diego, California, USA, 30 August–2 September 2009, DETC2009-87451, 2009.

Howell, L. L.: Compliant mechanisms, John Wiley & Sons, New York USA, 459 pp., 2001.

Hu, K., Kim, J. H., Schmiedeler, J., and Menq, C. H.: Design, implementation, and control of a six-axis compliant stage, Rev. Sci. Instrum., 79, 025105, doi:10.1063/1.2841804, 2008a.

Hu, Y. H., Lin, K. H., Chang, S. C., and Chang, M.: Design of a compliant micromechanism for optical-fiber alignment, Key Eng. Mat., 381–382, 141–144, 2008b.

Jong de, B. R., Brouwer, D. M., de Boer, M. J., Jansen, H. V., Soemers, H. M. J. R., and Krijnen, G. J. M.: Design and fabrication of a planar three-DOFs MEMS-based manipulator, J. Microelectromech. S., 19, 1116–1130, 2010.

Lange de, D. J. B. A., Langelaar, M., and Herder, J. L.: Towards the design of a statically balanced compliant laparoscopic grasper using topology optimization, in: Proceedings of the ASME 2008 International Design Engineering Technical Con-

ferences & Computers and Information in Engineering Conference, Brooklyn, New York, USA, 3–6 August 2008, DETC2008-49794, 2008.

Leblond, M. and Gosselin, C. M.: Static balancing of spatial and planar parallel manipulators with prismatic actuators, in: Proceedings of the 1998 ASME Design Engineering Technical Conferences, Atlanta, Georgia, USA, 13–16 September 1998, DETC98/MECH-5963, 1998.

Lee, C. W. and Kim, S. W.: An ultraprecision stage for alignment of wafers in advanced microlithography, Precis. Eng., 21, 113–122, 1997.

Liang, Q., Zhang, D., Chi, Z., Song, Q., Ge, Y., and Ge, Y.: Six-DOF micro-manipulator based on compliant parallel mechanism with integrated force sensor, Robot. CIM-Int. Manuf., 27, 124–134, 2011.

Liu, X. J., Wang, J., Gao, F., and Wang, L. P.: On the design of 6-DOF parallel micro-motion manipulators, in: Proceedings of the 2001 IEEE/RSJ International Conference on Intelligent Robots and Systems, Maul, Hawaii, USA, 29 October–3 November 2001, 343–348, 2001.

Lobontiu, N.: Compliant mechanisms: design of flexure hinges, CRC Press LLC, Boca Raton, Florida, USA, 447 pp., 2003.

Lu, T. F., Handley, D. C., Yong, Y. K., and Eales, C.: A three-DOF compliant micromotion stage with flexure hinges, Ind. Robot, 31, 355–361, 2004.

Moon, Y. M. and Kota, S.: Design of compliant parallel kinematic machines, in: Proceedings of the ASME 2002 Design Engineering Technical Conferences and Computer and Information in Engineering Conference, Montreal, Canada, 29 September–2 October 2002, DETC2002/MECH-34204, 2002.

Morsch, F. M. and Herder, J. L.: Design of a generic zero stiffness compliant joint, in: Proceedings of the ASME 2010 International Design Engineering Technical Conferences & Computers and Information in Engineering Conference, Montreal, Quebec, Canada, 15–18 August 2010, DETC2010-28351, 2010.

Nieuwenhuis, C.: Thermal behavior Mapper Short Stroke, restricted internal report, Demcon Advanced Mechatronics B.V., Oldenzaal, The Netherlands, 16 pp., 2010.

Park, S. R. and Yang, S. H.: A mathematical approach for analyzing ultra precision positioning system with compliant mechanism, J. Mater. Process. Tech., 164–165, 1584–1589, 2005.

Powell, K. M. and Frecker, M. I.: Method for optimization of a nonlinear static balance mechanism, with application to ophthalmic surgical forceps, in: Proceedings of the ASME 2005 International Design Engineering Technical Conferences & Computers and Information in Engineering Conference, Long Beach, California, USA, 24–28 September 2005, DETC2005-84759, 2005.

Ryu, J. W., Gweon, D. G., and Moon, K. S.: Optimal design of a flexure hinge based Xyθ wafer stage, Precis. Eng., 21, 18–28, 1997.

Scopus: http://www.scopus.com/, last acces: 25 January 2011.

Seugling, R. M., Lebrun, T., Smith, S. T., and Howard, L. P.: A six-degree-of-freedom precision motion stage, Rev. Sci. Instrum., 73, 2462–2468, 2002.

Shekarforoush, S. M. M., Eghtesad, M., and Farid, M.: Design of statically balanced six-degree-of-freedom parallel mechanisms based on tensegrity system, in: Proceedings of the ASME 2009 International Mechanical Engineering Congress & Exposition, Lake Buena Vista, Florida, USA, 13–19 November 2009,

IMECE2009-12625, 2010.

Sjoerdsma, W., Herder, J. L., Horward, M. J., Jansen, A., Bannenberg, J. J. G., and Grimbergen, C. A.: Force transmission of laparoscopic grasping instruments, Minim. Invasiv. Ther., 6, 274–278, 1997.

Stapel, A. and Herder, J. L.: Feasibility study of a fully compliant statically balanced laparoscopic grasper, in: Proceedings of the ASME 2004 Design Engineering Technical Conferences and Computers and Information in Engineering Conference, Salt Lake City, Utah, USA, 28 September–2 October, DETC2004-57242, 2004.

Stewart, D.: A platform with six degrees of freedom, Proceedings of the Institution of Mechanical Engineers, 180, 371–386, 1965.

Streit, D. A.: Spatial manipulator and six-degree-of-freedom platform spring equilibrator theory, in: Proceedings of the Second National Conference on Applied Mechanisms and Robotics, 1991.

Sun, L., Wang, J., and Wang, Z.: Six-freedom precision paralleled robot, patent CN2576434, 2003.

Sun, S.: Research of nanometer positioning stage with six degree of freedom based on binary actuation principle, in: Proceeding of MircoNanoChina07, Sanya, Hainan, China, 10–13 January 2007, 1639–1647, 2007.

Tian, Y., Shirinzadeh, B., and Zhang, D.: Design and dynamics of a 3-DOF flexure-based parallel mechanism for micro/nano manipulation, Microelectron. Eng., 87, 230–241, 2010.

Tolou, N. and Herder, J. L.: Concept and modeling of a statically balanced compliant laparoscopic grasper, in: Proceedings of ASME 2009 International Design Engineering Technical Conferences & Computers and Information in Engineering Conference, San Diego, California, USA, 30 August–2 September 2009, DETC2009-86694, 2009.

Tolou, N. and Herder, J. L.: Statically balanced compliant micro mechanisms (SM-MEMS): concepts and simulation, in: Proceedings of the ASME 2010 International Design Engineering Technical Conferences & Computers and Information in Engineering Conference, Montreal, Quebec, Canada, 15–18 August 2010, DETC2010-28406, 2010.

Trease, B. Dede, E.: Statically-balanced compliant four-bar mechanism for gravity compensation, in: 2004 ASME Student Mechanism Design Competition, 2004.

Wang, H. and Zhang, X.: Input coupling analysis and optimal design of a 3-DOF compliant micro-positioning stage, Mech. Mach. Theory, 43, 400–410, 2008.

Wang, L., Rong, W., Sun, L., and Jiao, J.: Analysis and design of a three-limb six degree-of-freedom parallel micromanipulator with flexure hinges, in: Proceeding of MircoNanoChina07, Sanya, Hainan, China, 10–13 January 2007, 1561–1566, 2007.

Wang, S. C., Hikita, H., Kubo, H., Zhao, Y. S., Huang, Z., and Ifukube, T.: Kinematics and dynamics of a 6 degree-of-freedom fully parallel manipulator with elastic joints, Mech. Mach. Theory, 38, 439–461, 2003.

Wang, Y., Liu, Z., Bo, F., and Zhu, J.: Design and research of 5-DOF Integrated nanopositioning stage, Zhongguo Jixie Gongcheng/China Mechanical Engineering, 16, 1317–1321, 2005.

Willson, C. G. and Roman, B. J.: The future of lithography: Sematech litho forum 2008, ACS Nano, 2, 1323–1328, 2008.

Xiaohui, J., Yanling, T., and Dawei, Z.: Six-freedom-degree precision positioning table for nano-imprint lithography system, patent CN101726997, 2010.

Xuchu, J. and Qianfeng, Q.: Precise positioning platform with six freedom of motion, patent CN101488371, 2009.

Yi, B. J., Chung, G. B., Na, H. Y., Kim, W. K., and Suh, I. H.: Design and experiment of a 3-DOF parallel micromechanism utilizing flexure hinges, IEEE T. Robotic. Autom., 19, 604–612, 2003.

Yun, Y. and Li, Y.: Design and analysis of a novel 6-DOF redundant actuated parallel robot with compliant hinges for high precision positioning, Nonlinear Dynam., 61, 829–845, 2010.

Zhang, D. Y., Ono, T., and Esashi, M.: Piezoactuator-integrated monolithic microstage with six degrees of freedom, Sensor. Actuat. A-Phys., 122, 301–306, 2005.

- 12 -

SHORT COMMUNICATION ON BI-STABLE COMPLIANT MECHANISMS: CORRECTION FOR FINITE ELEMENT MODELING, PRELOADING INCORPORATION AND TUNING THE STIFFNESS

A.G. Dunning, N. Tolou, L.F. Kluit, J.L. Herder
Faculty of Mechanical, Maritime and Materials Engineering, Department of Biomechanical Engineering,
Delft University of Technology, Delft, The Netherlands
Email: N.Tolou@tudelft.nl

ABSTRACT

Bi-stable straight-guided buckling beams are essential mechanisms for precision engineering, compliant mechanisms and MEMS, however a straightforward accurate numerical modeling was not yet available. When preloading effects must be included, numerical modeling becomes an even more challenging problem. The article presents a straightforward numerical model for bi-stable straight-guided buckling beams, which includes the preloading effects as well. Adjusting the bi-stable force-displacement characteristic by variation of design parameters and preloading are also investigated. In order to validate the model, measurements has been performed. It is shown, a subsequent transient analysis using ANSYS^{TM} can model the bi-stable straight-guided buckling beams incorporating preloading while at the same time the beams are slightly pre-curved in order to avoid converging into higher frequency buckling modes. Moreover, the bi-stable behavior can become more symmetric and more energy efficient by increasing the initial angle, preloading and thickness of the bi-stable buckling beams in the same order.

Keywords: Bi-stable mechanisms; buckling beam theory*;* large deflection; precision engineering; MEMS; compliant mechanisms; stiffness compensation; statically balancing.

1. INTRODUCTION

Compliant bi-stable mechanism, also called bi-stable straight-guided clamped buckling beams, has extensively been used in design of meso/micro mechanical systems due to their interesting force-displacement behavior: negative stiffness and two stable positions.

These mechanisms has been used in many applications where low actuation force and power, high cycle life, and predictable, repeatable motion are required, such as in latch-lock mechanisms (Hoffmann et al., 1999), relays (Sun et al., 1998), valves (Goll et al., 1996), clips (Jensen and Jenkins, 2011), multi-stable (Oh and Kota, 2009; Chen et al., 2010) and statically balanced mechanisms (Chen and Zhang, 2011; Tolou et al., 2010; Lassooij et al., 2011). These mechanisms mainly rely on buckling phenomena, therefore are highly nonlinear (Wang, 1997; Tolou et al., 2011b) and difficult to be analyzed (Jensen et al., 2001). Some interesting work has been done to investigate the force-displacement behavior of compliant bi-stable mechanisms using mathematical modeling (Qiu et al., 2004; Sönmez, 2008; Jensen and Howell, 2004; Todd et al., 2010; Kim, 2011; Zhao et al., 2008), numerical modeling (Oh and Kota, 2009; Qiu et al., 2004; Todd et al., 2010), or experiments were used (Qiu et al., 2004; Sönmez, 2008; Jensen and Howell, 2004; Todd et al., 2010; Kim, 2011; Zhao et al., 2008; Tolou et al., 2011a). Mathematical modeling mainly rely on linearization (Jensen et al., 2001), pseudo rigid-body modeling (Tolou et al., 2011b; Sönmez, 2008; Jensen and

Howell, 2004) or elastica solution ending to elliptic integrals and difficult to be implemented and of less accuracy for larger deflections (Todd et al., 2010; Kim, 2011; Zhao et al., 2008). Finite element modeling has been a promising straightforward method to evaluate the design before final production. However, it has been shown in literature, the available results from finite element modeling does not closely agree with those of experiments (Todd et al., 2010; Kim, 2011). The problem becomes even more challenging when preloading effects should also be incorporated. That could give rise to nonlinearity and no valid model has been presented so far for commercial finite element packages.

This work has been motivated to propose a correction for finite element modelling of compliant bi-stable buckling beams while at the same time preloading effects are incorporated. The effect of variation of initial angle and thickness of bi-stable beams and pre-loading on the force-displacement curve of bi-stable buckling beams is studied in this work.

The correction for finite element modelling of compliant mechanisms is presented in section 2.1, followed by preloading incorporation in section 2.2. The effects of changing parameters on the evaluation points of the force-displacement curve were studied in section 2.3. Measurements are presented in section 3. Results are presented in section 4 and discussed in section 5. Finally some conclusions are drawn in section 6.
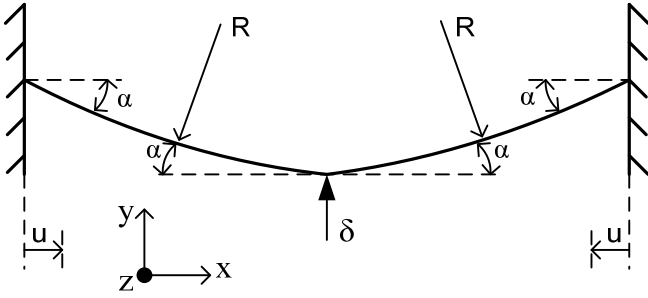
Fig. 1. Example of the straight-guided buckling beams with a very small curvature (1/R); the end tips are fixed; in the centre the beams are constraint in x-translation and rotation about z-axis; the initial angle (α) at the end tips and in the centre is equal; for preloading effects the beams are preloaded over a distance (u); the beams are loaded with a displacement (δ) in the centre.
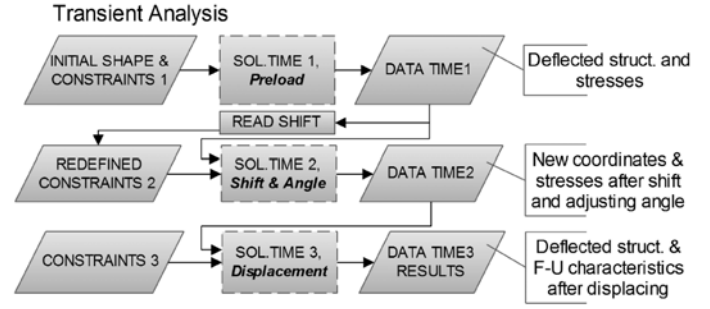

Fig. 2. Flow chart of the subsequent transient analysis; the data of the preloaded initial shape (time step 1) is used to solve the analysis for the deformed structure (time step 2); the data of the deformed structure together with the prescribed displacement gives the final results.

2. METHOD

2.1 Finite element modeling of the bi-stable mechanism

In this section, the correction for finite element modeling of the bi-stable straight-guided buckling beams is presented. The forces and displacements were analyzed using a commercially FEM package, ANSYS[TM] 10.0. Because of large deflections, a non-linear static analysis has been performed (ANSYS). All the elements were created using BEAM3 elements. This uni-axial element gives the shortest computation time while the actual out-of-plane properties can also be provided using the real constant capability of ANSYS[TM]. The BEAM3 element has three degrees of freedom at each node with tension, compression, and bending capabilities. The material is assumed to follow linear elastic stress-strain behavior and to be isotropic.

When initially straight beams are used to model the bi-stable straight-guided buckling beams, ANSYS[TM] tries to keep the beams as straight as possible during buckling. Due to this fact, the solution was converged into higher frequency buckling modes, forces and stresses becoming very high during buckling. Therefore, the beams were modeled with a very small initial curvature (1/R, with R=1000mm) (Fig. 1). With this approach, the higher frequency modes during buckling were avoided.

The bi-stable straight-guided buckling beams were fixed at the end tips in all directions. In the centre the beams were connected to each other, with only the y-translation as a degree of freedom. The x-translation and the rotation about z-axis were constraint. The bi-stable straight-guided buckling beams were loaded in the centre, where a vertical displacement δ was imposed.

2.2 Preloading incorporation

The analysis for preloading was performed using a subsequent transient analysis, at a fixed initial angle (Fig. 2). In the first time step of the analysis, the end tips of the beams were shifted inside, collinear to the motion of the mechanism (i.e. along the axis connecting the fixed ends of the beams), and

where only the vertical translation of the centre is free to move. After running the analysis the centre is shifted downwards. This shift was used in the second time step to achieve the correct constraints. In the third time step the initial constraints of the preloaded beams are correct and the centre was imposed by a vertical displacement.

2.3 Tuning the stiffness characteristics

In order the tune the stiffness characteristic of the bi-stable mechanism, the design variables angle and thickness of the straight-guided buckling beams, and preloading along the axis connecting the fixed ends of the beams were changing. Different ratios were analyzed to see how the force-displacement (i.e. stiffness) characteristic change by varying the initial angle, thicknesses and preloading. These evaluation ratios are listed below:

1) Unstable equilibrium position (c in Fig. 3) is compared to the second stable position (a) (Unst. Eq. pos. / 2nd stable pos.);
2) Ratio between the stroke of the positive force (a-c) and the stroke of the negative force (c-e) ($\Delta\delta_{Fpos} / \Delta\delta_{Fneg}$);
3) Ratio between the maximum force and the minimum force (F_{max} / F_{min});
4) Energy needed to put in the system divided by the energy delivered by the system (E_{in} / E_{out});
5) Stroke where the stiffness is negative (b-d) vs. full stroke (a-e) ($\Delta\delta_{Kneg} / \delta_{total}$)
6) Pre-buckling stroke (a-b) vs. full stroke (a-e) ($\Delta\delta_{pre-buckling} / \delta_{total}$).

where the corresponding evaluation points were depicted in Fig. 3. Moreover, the values of the negative stiffness and the pre-buckling stiffness were analyzed. The pre-buckling stiffness is calculated between point a and b (Fig. 3). The negative stiffness is calculated between point b and d (Fig. 3).
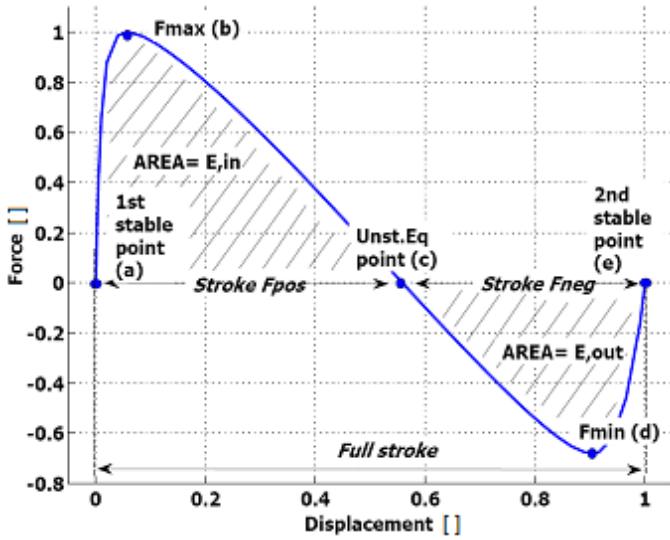
Fig. 3. Typical behavior of the force-displacement characteristic of a bi-stable mechanism; point a is the 1st stable point; at point b the force exerted on the mechanism is at its maximum; point c is the unstable equilibrium position, where the bi-stable mechanism snaps and produces a force in the same direction as the travel range; this force is the largest at point d; point e is the 2nd stable position of the beams; the area of the curve for F_{pos} and F_{neg} is the energy needed to put in the mechanism (E_{in}) or the energy produced by the mechanism (E_{out}), respectively.

3. MEASUREMENTS

A custom-built measurement set-up (Fig. 4) was used to determine the force-displacement characteristics of the bi-stable mechanism for different configurations: adjusting angle, thickness, and preloading at the end tips. As shown in Fig. 4, the bi-stable mechanism is decomposed into two straight-guided beams. The beams were mounted on rotational stages, with resolution of 0.004 degrees, at the fixed end tip, to adjust the angle for different configurations, and connected to each other with a revolute joint in the centre. This revolute joint is fixed during measurement, to have a rigid connection between the beams. The rotational stages were mounted on a sliding joint, with a resolution of 0.25mm, in order to allow preloading. The revolute joint in the centre was attached to the force sensor by a pulling/pushing rod. The mechanisms were slowly loaded from its relaxed position to its second stable position and then returned to the relaxed position to record the hysteresis.

The bi-stable buckling beams were made of AISI304 stainless steel, with a length of 70mm. The resolution of the test bench for the force sensor (FETE RIS components - B3G-C3-50kg-6B) is 0.6N with the range of [0 50] kg. The displacement was measured with a displacement sensor (mentioned as LVDT) (Positek – P101.200CL100) with the resolution of 0.045mm and travel range of [0 200] mm. An amplifier (Scaime CPJ 25) and data acquisition module (National Instruments USB6008) were used to read the data. The data was logged with the software Labview 8.2.1 and processed with MATLAB R14a.
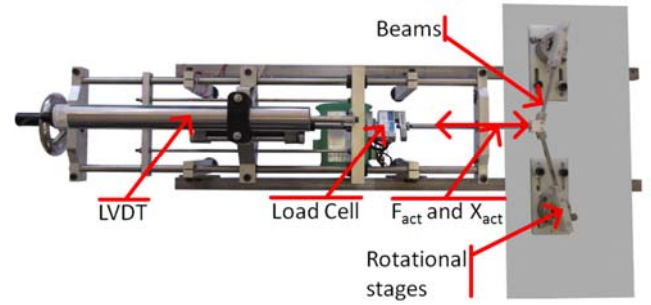

Fig. 4. Top view of the measurement set-up: the force-displacement characteristic of mechanisms was determined by measuring actuation force (Fact) and displacement (Xact) from relaxed position to second stable position and vice versa; the angle and preloading were adjusted by a rotational stage mounted on a sliding joint.

To investigate the force-displacement characteristic for the different configurations as mentioned in section 2.3, the following measurements were performed:

1) Change the initial angle from 5° to 30°, with steps of 5°.
2) Increase the preloading displacement from 0mm to 10mm, with steps of 2.5mm.
3) Employing the beams with different thicknesses of 0.15mm, 0.20mm and 0.25mm.

4. RESULTS

Fig. 5-7 show the effect of varying initial angle, preloading and thickness, on the bi-stable behavior of the mechanism, respectively. In Fig. 5a, 6a and 7a the results of the force-displacement characteristic for both the measurements and the ANSYS[TM] analysis are shown. For further illustration and discussion, the results of the ratios and values of stiffness are shown in detail in Fig. 5b, 6b and 7b. The values of the pre-buckling stiffness and the negative stiffness are normalized to the largest value.

5. DISCUSSION

In Fig. 5a-7a it is shown that the proposed finite element model using non-linear static or transient analysis performs well to model the bi-stable straight-guided beams with preloading effects: the maximum error is 2,5% compared to experimental results as the reference values.

As shown in Fig. 5b-7b, the negative stiffness is increasing from 0.6, 0.8 and 0.2 to 1 for an increase in initial angle, preloading and thickness, respectively. The ratio $\Delta\delta_{Kneg}/\delta_{total}$ is nearly constant for all above cases, i.e. the stroke with negative stiffness is a constant percentage ($\pm85\%$) of the complete stroke. The ratio $\Delta\delta_{pre-buckling}/\delta_{total}$ conversely decreases significant to 0.4 for increasing initial angle and decreasing less significant to 0.85 for increasing thickness, which means that the negative stiffness is introduced earlier compared to the full stroke. For increasing preloading this ratio shows an irregular behavior. This effect is due to the normalization: the measured
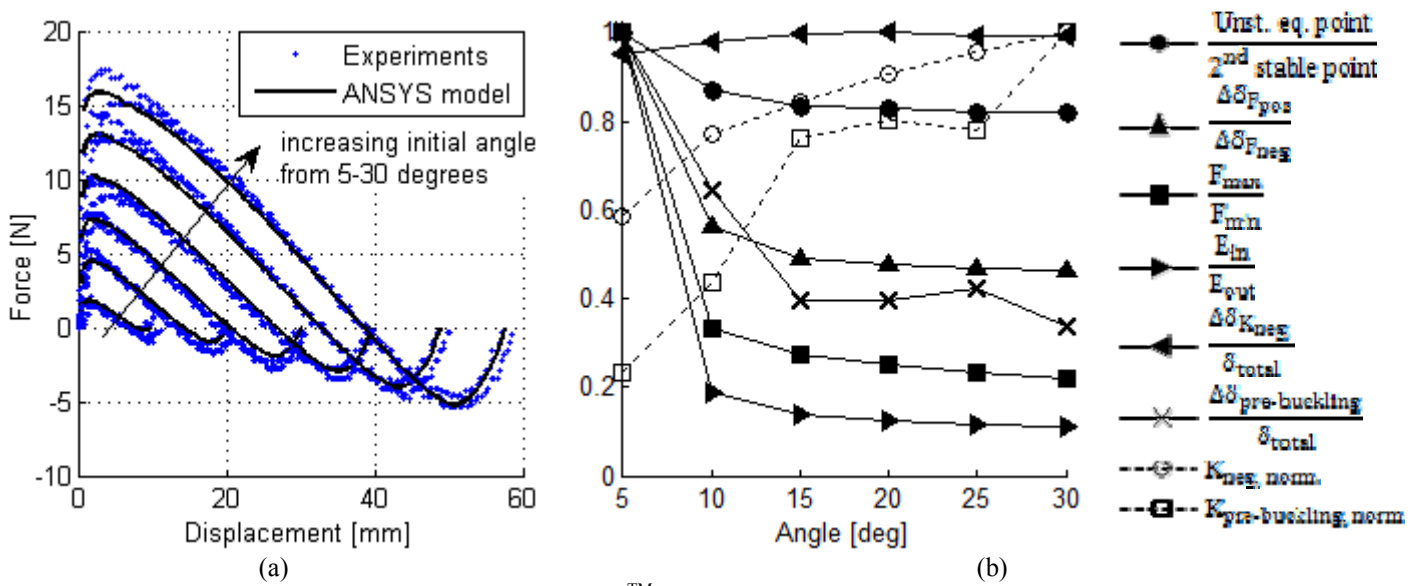
Fig. 5. (a) Results of the measurements and the ANSYS[TM] analysis and (b) ratios and values for increasing initial angle, with a thickness of 0.20mm and no preloading.
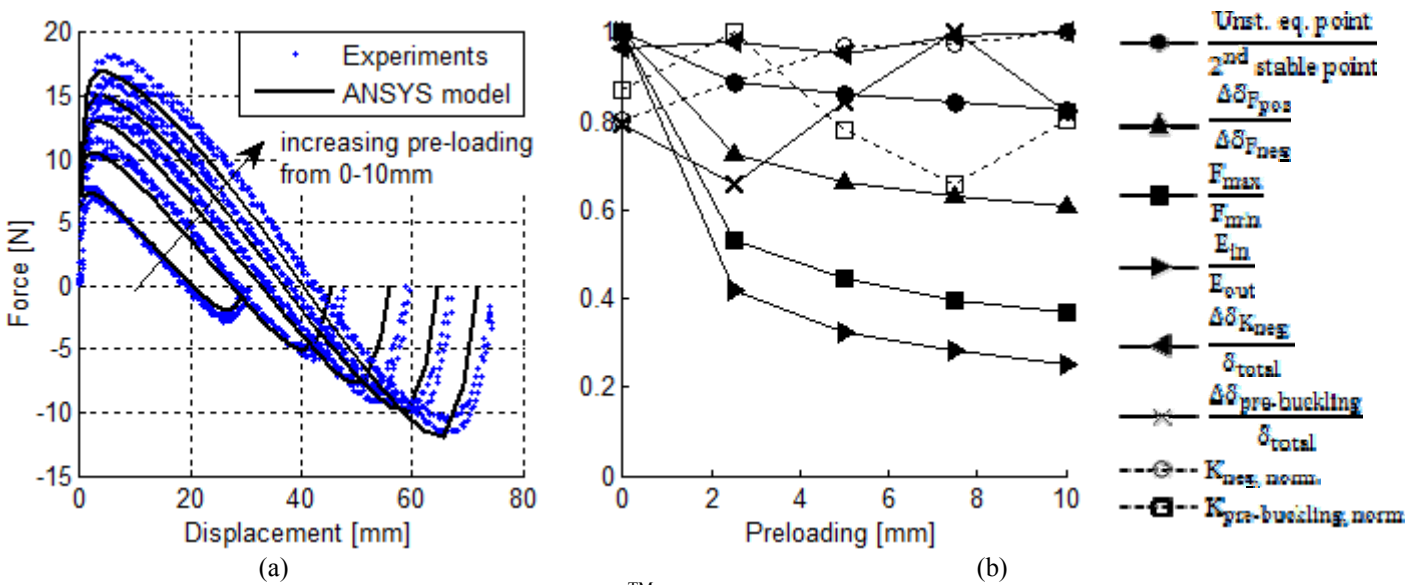

Fig. 6. (a) Results of the measurements and the ANSYS[TM] analysis and (b) ratios and values for increasing preloading, with an initial angle of 15° and a thickness of 0.20mm.
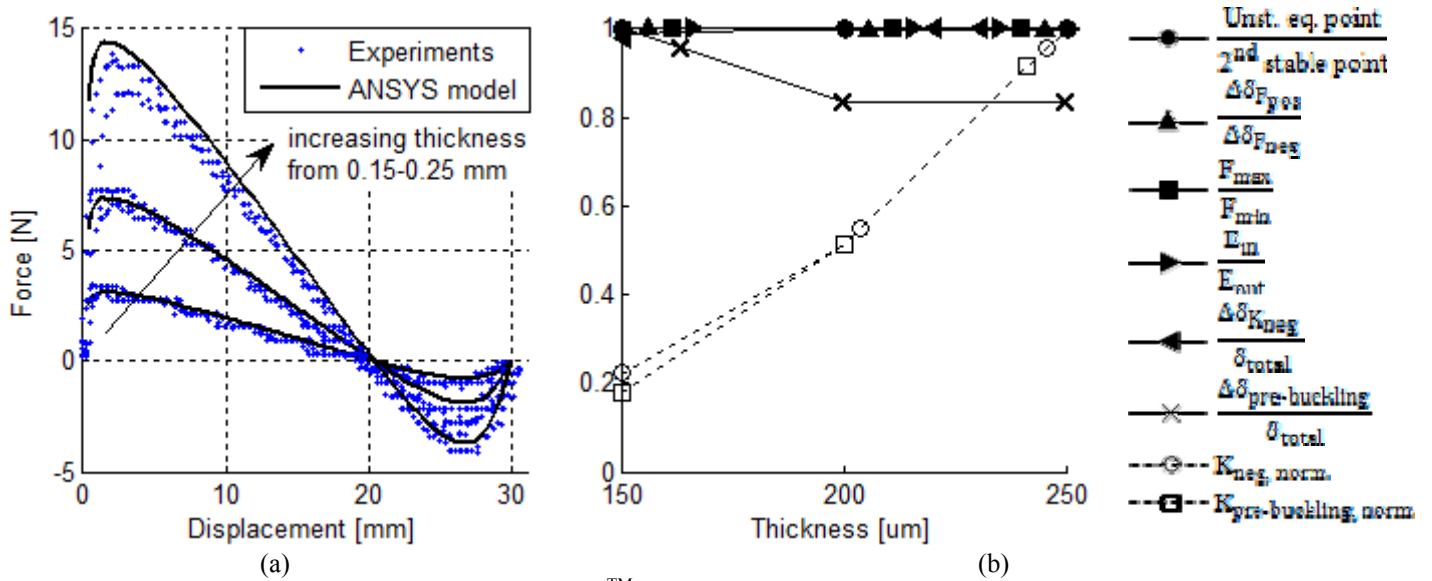
Fig. 7. (a) Results of the measurements and the ANSYS^{TM} analysis and (b) ratios and values for increasing thickness, with an initial angle of 15° and no preloading.

values of this ratio are much smaller than one, subsequently the small measurement errors are amplified.

For increasing the initial angle or preloading, the ratio $\Delta F_{pos}/\Delta F_{neg}$ reduce to 0.65 and 0.5, respectively; at the same time the ratio between F_{max}/F_{min} also reduces to 0.5 and 0.4, respectively, consequently the bi-stable behavior becomes more symmetric with respect to the x-axis (zero force). Moreover, the decrease in ratio E_{in}/E_{out} shows that the mechanism become more efficient in gaining energy from the mechanism after snap-through from the unstable equilibrium position. The change in initial angle from 5° to 15° and preloading from 0mm to 5mm has the most influence on the adjustment of the ratios, while from 15° to 30° and from 5mm to 10mm the changes are minor.

For increasing initial angle the pre-buckling stiffness is increasing significant from 0.2 to 1, while for increasing preloading this stiffness characteristic shows a different and irregular behavior: the pre-buckling stiffness is highly sensitive to small errors in the measurement for the position of the maximum force.

For increasing thickness almost all ratios are nearly one, while the stable and unstable positions of the beams remains the same. Only both the negative stiffness and the pre-buckling stiffness is increasing linear from 0.2 to 1 with increasing thickness.

6. CONCLUSIONS

An accurate finite element model (FEM) for bi-stable straight-guided buckling beams has been proposed. Preloading effects in the direction perpendicular to the motion of the mechanism has also been incorporated. The stiffness characteristics has been adjusted through tuning the dimensional and preloading properties. Experiments has been performed for validation purpose. It has been proposed to include a small initial curvature in FEM in order to avoid solution convergence into buckling modes of higher frequency.

In order to include the preloading effects, transient analysis including preloading, and motion displacement has been performed subsequently. The results shows the noticeable accuracy of the proposed modeling, with a maximum error of 2.5% compared to the measurements as reference values. The stiffness and ratio characteristics shows the largest adjustment for varying the angle between 5°-15°, and preloading between 0-5mm. An increase in initial angle and preloading of the bi-stable buckling beams can subsequently lead to a more symmetric bi-stable behavior with respect to the zero force axis, more energy efficiency, with a constant stroke of negative stiffness: ±85% of the full stroke, while for increasing the thickness only the values of stiffness increase.

The proposed modeling can extensively be employed in the design of mechanisms for precision engineering, MEMS and compliant mechanisms.

ACKNOWLEDGMENT

REFERENCES

ANSYS, Manual of ANSYS 10, ANSYS Inc., 2005.

Chen, G. and Zhang, S.: Fully-Compliant Statically-Balanced Mechanisms without Prestressing Assembly: Concepts and Case Studies, Mech. Sci., 2, 169-174, 2011.

Chen, G., Aten, Q.T., Zirbel, S., Jensen, B.D., and Howell, L.L.: A Tristable Mechanism Configuration Employing Orthogonal Compliant Mechanisms, J. Mechanisms Robotics 2, 014501 (2010).

Goll, C., Bacher, W., Buestgens, B., Maas, D., Menz, W., and Schomburg, W. K.: Microvalves With Bistable Buckled Polymer Diaphragms, J. Micromech. Microeng., 6, 77–79, 1996.

Hoffmann, M., Kopka, P., and Voges, E.: All-silicon bistable micromechanical fiber switch based on advanced bulk micromachining, IEEEJ. Select. Topics Quantum Electron., 5, 1, 46–51, 1999.

Jensen B.D., and Howell L.L.: Bistable Configurations of Compliant Mechanisms Modeled Using Four Links and Translational Joints, J. Mech. Des., 126, 4, 657-665, 2004.

Jensen, B.D., and Jenkins, C.H.: Design Of Small-Scale Statically Balanced Compliant Joints, in: Proceeding of ASME 2010 International Design Engineering Technical Conferences and Computers and Information in Engineering Conference, 28 – 31 August 2011, Washington DC, DETC2011-47482, 2011.

Jensen, B.D., Parkinson, M.B., Kurabayashi, K., Howell, L.L., and Baker, M.S.: Design Optimization Of A Fully-Compliant Bistable Micro-Mechanism, in: Proceedings of 2001 ASME International Mechanical Engineering Congress and Exposition, November 11–16 2001, New York, NY, 2001.

Kim, C.: Curve Decomposition Analysis For Fixed-Guided Beams With Application To Statically Balanced Compliant Mechanisms, in: Proceeding of ASME 2010 International Design Engineering Technical Conferences and Computers and Information in Engineering Conference, August 28 – 31, 2011, Washington DC, DETC2011-47482, 2011.

Lassooij, J., Tolou, N., Caccavaro, S., Tortora, G., Menciassi, A., Herder, J.L.: Laparoscopic 2DOF Robotic Arm with Statically Balanced Fully Compliant End Effector, Mech. Sci., In Press., 2011.

Oh, Y.S., Kota, S.: Synthesis of Multistable Equilibrium Compliant Mechanisms Using Combinations of Bistable Mechanisms, Journal of Mechanical Design, 131/2/021002, 2009.

Qiu, J. Lang, J.H., Slocum, A.H.: A curved-beam bistable mechanism, J. Of Microelectromechanical Systems, 13, 2, 137-146, 2004.

Sun, X., Farmer, K., and Carr, W.: A bistable microrelay based on twosegment multimorph cantilever actuators, in: Proc. IEEE MEMS 1998 Conference, 154–159, 1998.

Sönmez, Ü, Tutum, C.C.: A Compliant Bistable Mechanism Design Incorporating Elastica Buckling Beam Theory and Pseudo-Rigid-Body Model, Journal of Mechanical Design, 130/4/042304, 2008.

Todd, B., Jensen, B.D., Schultz, S.M., Hawkins, A.R.: Design and Testing of a Thin-Flexure Bistable Mechanism Suitable for Stamping From Metal Sheets, Journal of Mechanical Design, 132/7/071011, 2010.

Tolou, N., Henneken, V.A., Herder, J.L.: Statically Balanced Compliant Micro Mechanisms (Sb-Mems): Concepts And Simulation, in: Proceeding of ASME 2010 International Design Engineering Technical Conferences and Computers and Information in Engineering Conference, August 15 - 18, 2010, Montreal, Quebec, Canada, DETC2010-28406, 447-454, 2010.

Tolou, N., Estevez, P., Herder, J.L.: Collinear-Type Statically Balanced Compliant Micro Mechanism (Sb-Cmm): Experimental Comparision Between Pre-Curved And Straight Beams, in: Proceeding of the ASME 2011 International Design Engineering Technical Conferences and Computers and Information in Engineering Conference, Aug 28-31 2011, Washington DC, USA, 2011a.

Tolou, N., Khiat, A., Zhang, G.Q., Herder, J.L.: Analytical Method for Determination of Young's Modulus of Large Deflection Carbon Nanotube, International Journal of Nonlinear Sciences and Numerical Simulation, In Press, 2011b.

Wang, C. Y.: Post-buckling of a clamped-simply supported elastica, International Journal of Non-Linear Mechanics, 32, 6, 1115-1122, 1997.

Zhao, J., Jia, J., He, X., and Wang, H.: Post-buckling and snap-through behavior of inclined slender beams, J. Appl. Mech., 75/4/041020, 2008.

DESIGN OF A ZERO STIFFNESS SIX DEGREES OF FREEDOM COMPLIANT PRECISION STAGE

A.G. Dunning, N. Tolou, J.L. Herder
Faculty of Mechanical, Maritime and Materials Engineering, Department of Biomechanical Engineering,
Delft University of Technology, Delft, The Netherlands
Email: J.L.Herder@tudelft.nl

ABSTRACT

This paper presents the first zero stiffness six degrees of freedom (DoF) compliant precision stage. To deal with problems like backlash, friction and lubrication for performing ultra-precise positioning in a vacuum environment, a novel compliant structure is proposed. All six degrees of freedom are statically balanced (i.e. near zero stiffness) to balance the gravity force and cancel out the stiffness due to the compliant design of the structure. Cooperative action of post-buckling behavior of bi-stable beams and constant stiffness of v-shaped beams, arranged in three units in a triangular configuration, are proposed for out-of-the-horizontal-plane motions. The in-plane motions are achieved by three flexible rods loaded near their buckling load. An investigation on adjusting the design parameters to minimize the residual actuation force is also performed. A prototype was manufactured and finite element modeling was performed to evaluate the concept. Experimental evaluation showed that the design is successful: for the case study a gravity force of 34.4N was balanced with a residual stiffness of 1.75N/mm in a domain of 2mm for the out-of-plane translation, while the out-of-plane rotational stiffness was less than 18.5Nm/rad, caused by parasitic torsion of the bi-stable beams and v-shaped beams. The stiffness for in-plane translations and rotation was 0.4N/mm and 2Nm/rad, respectively. Near zero stiffness 6DoF positioning can thus be achieved. The novel mechanism or the principle may be extensively applied in several applications in precision engineering or in other relevant fields, such as vibration isolation.

Keywords: zero stiffness; six degrees of freedom; precision stage; gravity equilibrator; static balancing; compliant mechanism; flexible structure, vibration isolation.

1.   INTRODUCTION

Many applications in precision engineering require positioning of a heavy object in six degrees of freedom (DoF) with ultra high precision. These applications are very often situated inside a vacuum chamber. Particularly in vacuum, e.g. in lithography or electron beam microscopy, the actuation of positioning stages produces excessive level of heat, mainly caused by the stiffness of the stage and the heavy load. This can negatively affect the precision of the application (Nieuwenhuis, 2010). To deal with these challenges a monolithic compliant design is proposed, with the distinguishing feature that it is designed to have zero stiffness in all DoFs to reduce the actuation force.

A compliant mechanism (CM) is a monolithic mechanism that transfers force or motion (i.e. energy) by using the elastic deformation of its flexible segments rather than using rigid-body joints. Due to its hingeless design, compliant mechanisms can be fabricated out of one piece, reduces friction, wear and backlash, subsequently increasing the precision, which is an essential feature for high-precision applications. Lubrication is not needed, which resolve an essential problem for mechanism sensitive to dust or working in a vacuum environment (Howell, 2001).

A problem in compliant mechanisms is that the deformation of flexible segments introduces positive stiffness and requires energy. The energy storage in the flexible segments is distorting the input-output relationship and challenges the mechanical efficiency. When the deformation of the flexible members is large, non-linearities are introduced, which increases the complexity of the design. This adverse effect can be solved by introducing a stiffness compensation mechanism with negative stiffness, to compensate the positive stiffness of the compliant mechanism. This results in a statically balanced compliant mechanism (SBCM), having constant total potential energy in every position and therefore has zero stiffness (Herder and van den Berg, 2000; Herder, 2001; Morsch and Herder, 2010).

In Dunning et al. (2011a), an overview of the available 6 DoF compliant stages and 6 DoF statically balanced mechanism in literature is presented. Several 6 DoF compliant stages were found, none of which is statically balanced, while all of the 6 DoF statically balanced mechanisms that were found are not compliant. Furthermore, the possibilities to

combine a 6 DoF compliant stage with a static balancer were investigated. It was concluded that a 6 DoF statically balanced compliant stage (SBCS) would be a breakthrough in precision engineering.

The present work aims to solve all above mentioned problems at the same time: by proposing a design of a zero stiffness 6 DoF compliant precision stage, which at the same time is able to balance a gravity force applied on the stage.

This paper is structured as follows: in section 2 the design criteria of the compliant precision stage are given. In section 3 different concepts for each function of the mechanism are explained and discussed, followed by a final design. The dimensional design and the prototype are presented in section 4. Hereafter, the experimental evaluation of the prototype is presented and discussed in section 5 and section 6, respectively. Conclusions are drawn in section 7.

2. DESIGN CRITERIA

Towards the design of a zero stiffness 6 DoF compliant precision stage for precision engineering, some design criteria has been considered. A reference frame is used of which x and y are in the horizontal plane, while z is directed along the vertical axis, pointed downward. For convenience, the x-y plane is referred as the horizontal plane, or the plane for short.

The first criterion gives that the end-effector (i.e. moving platform) of the mechanism must be able to perform motion in 6 degrees of freedom, while being subject to a vertical force due to a mass that is supported. The motions are the out-of-plane motions: subdivided into translation along the vertical z-axis (Tz) while carrying a load, and rotations about the horizontal x-axis (Rx) and y-axis (Ry), and the in-plane motions: translation along the horizontal x-axis (Tx) and y-axis (Ty) and rotation about the vertical z-axis (Rz).

The second criterion involves the stiffness of the mechanism, while supporting a load. It is required that the stiffness for translations is less than 1N/mm in every direction, and the rotational stiffness about the three axes is less than 10Nm/rad, equivalent to a force of 1N at a characteristic length of 100mm for 10mrad of rotation.

3. CONCEPTUAL DESIGN

The design of a 6 DoF compliant precision stage was divided into three functions the mechanism has to perform. The first and second functions are distinguished according to the motions the 6 DoF compliant precision stage has to perform: (1) out-of-plane motions, subdivided into the Tz direction, to balance a load, and the rotations Rx and Ry, and (2) in-plane motions. The third function is tuning the mechanism to adjust the stiffness and the preload.

For each function solutions are proposed, assessed and finally the most promising solutions will be combined into a final conceptual design [Appendix A]. The solutions for each function are assessed according to the following criteria [Appendix A.1]:
- Residual stiffness for the statically balanced domain;
- Maximum stresses in the mechanism: this criterion is related to fatigue and lifetime of the mechanism;
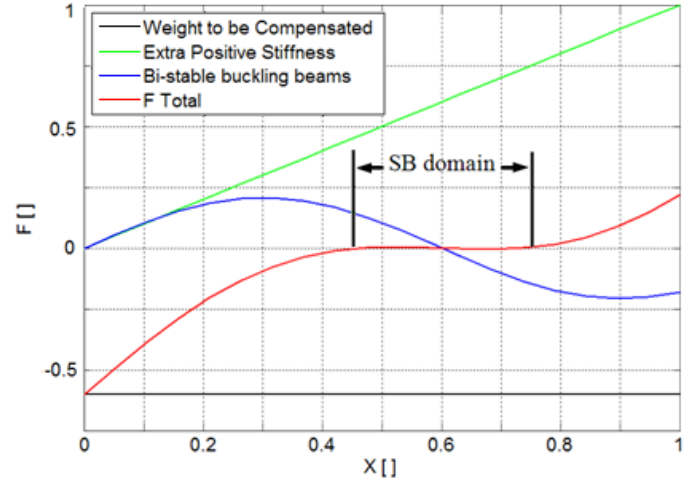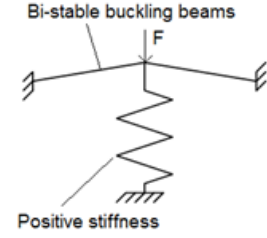- Parasitic motion in other directions than the balanced direction;

Fig. 1. Schematic force-displacement characteristic of a zero stiffness mechanism: bi-stable buckling beams with a negative stiffness domain combined with a linear positive stiffness create a statically balanced domain where a gravity force can be balanced.

- Tuning the mechanism: to have a design robust to fabrication errors;
- Ease of manufacturing;
- Required energy storage in the mechanism during assembly before it reaches the zero stiffness domain.

3.1 Out-of-plane motion

The out-of-plane motions were separated into solutions for balancing a gravity force in the Tz direction and solutions for the out-of-plane rotations (Rx, Ry).

3.1.1 *Tz* direction

In Dunning et al. (2011a), several concepts for balancing a force along the trajectory are discussed and it has been shown that a compliant balancing mechanism using bi-stable buckling beams shows the better performance in terms of force compensation and statically balanced domain relative to the size of the mechanism. In Fig. 1 a typical force-displacement characteristic of bi-stable buckling beams is shown. The domain of negative stiffness can be compensated by a linear positive stiffness, resulting in a force-displacement characteristic with zero stiffness at that domain. Units consisting of a combination of bi-stable buckling beams and a positive stiffness can be considered as building blocks for mechanisms with more degrees of freedom in different configurations. In Fig. 2 several of the more promising designs are shown [Appendix A.2].
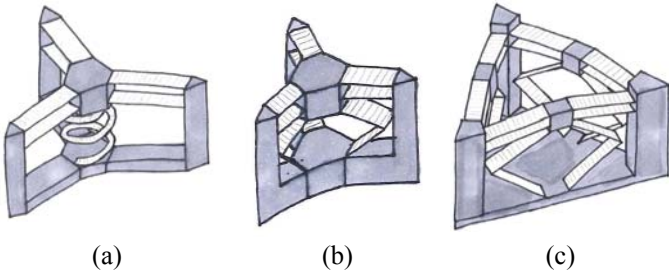
Fig. 2. Examples of solutions for balancing the translation in z-direction, while carrying a load: bi-stable buckling beams in different configurations are combined with a linear positive stiffness, provided by (a) a helical spring, (b, c) v-shaped beams.
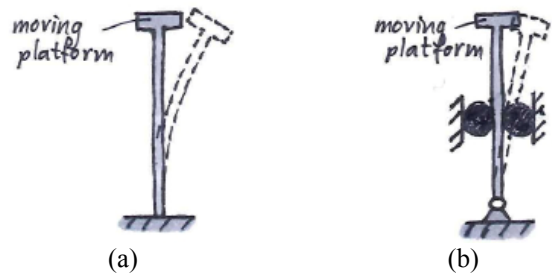

Fig. 3. Examples of solutions for out-of-plane rotations (*Rx*, *Ry*): (a) with a fully clamped rod loaded to its buckling load small rotations with low stiffness can be achieved, (b) the moment introduced by a vertical load on a stiff rod is compensated by a rubber ring.

All the solutions shown in Fig. 2 can balance a gravity force with zero stiffness behavior in the statically balanced domain. The bi-stable buckling beams can be arranged in different configurations: (1) connected in radial direction to a central platform (Fig. 2a, b), or (2) arranged in three units in triangular configuration (Fig. 2c). With the latter configuration, it is even possible to perform out-of-plane rotations *Rx* and *Ry*. Therefore this configuration was preferred. Using multiple bi-stable beams above each other reduces parasitic motion and stresses. As a positive stiffness mechanism, a helical spring (Fig. 2a) and a double v-shaped beam (Fig. 2b, c) were considered. The latter one, reduces parasitic motion about the axis perpendicular to the bi-stable beam, while it can be designed to have a linear stiffness characteristic for small deformations (similar to conventional linear springs) (Morsch and Herder, 2010). Therefore the double v-shaped beams were preferred. In combination with the previously selected configuration for bi-stable buckling beams, the complete mechanism can be manufactured out of three identical balanced mechanisms. Tuning the stiffness of the v-shaped beams is possible, as will be explained in Sect. 3.3.1.

3.1.2 *Rx, Ry* directions

For the out-of-plane rotations, one vertical flexible cantilever rod can be used (Fig. 3a). By deflection of the rod small rotations can be achieved. This solution is not balanced, but if the rod is loaded to its buckling load the stiffness of the rod for small transversal motion reaches nearly zero (Spiering and Grootenboer, 1993). Parasitic translation in the horizontal plane is introduced.

Another solution is to balance a vertical stiff rod, connected to the ground with a spherical joint, with a rubber ring around the rod (Fig. 3b). The gravity load introduces a moment about the spherical joint; the reaction force of the rubber ring should compensate this moment. Adjusting the stiffness is possible by changing the rubber ring. Due to damping and the backlash in the system the precision is affected negatively.

The most promising solution is the use of the configuration selected in Sect. 3.1.1 (Fig. 2c), where a combination of three statically balanced compliant mechanisms, arranged in triangular configuration, consisting of bi-stable buckling beams and v-shaped beams, can achieve balancing the *Tz* direction and the out-of-plane rotations *Rx* and *Ry*, while carrying a load.

3.2 In-plane motions (*Tx, Ty, Rz*)

To perform the in-plane motions three main solutions were proposed [Appendix A.3]. In the first main solution the moving platform is suspended by cables (Fig. 4a). The cables have a preferred lowest position, which requires energy to move the platform.

The second main solution is the use of rods supporting the moving platform. This can be done using different configurations: the moving platform can be supported by (1) flexible rods, fixed to the platform and the ground (Fig. 4b), (2) stiff rods, connected to the platform and the ground with spherical joints and balanced with a rubber ring, (3) a combination of straight rods and preloaded rods (Fig. 4c), resulting in a balanced mechanism (Tolou and Herder, 2010). The platform can also be suspended by tension rods, requiring energy to deform the rods while the stiffness is difficult to tune.

The third main solution is the use of compliant structures in different configurations. These solutions are not balanced. The moving platform is supported by three L-shaped beams (Fig. 4d). These L-shaped beams are subjected to torsion when loaded by a gravity force. This torsion can be reduced by increasing the height of the L-shaped beams or by supporting the platform with some flexible rods.

A combination of 3 flexible rods (Fig. 4b), placed in a triangular configuration, can perform the in-plane translations and rotation. Loaded to its buckling load, the rods can reach a nearly zero stiffness for small in-plane motions (Spiering and Grootenboer, 1993). This solution is easy to manufacture, the parasitic motion is small and the stiffness can be tuned by changing the length of the rods. For these reasons, the use of flexible rods supporting the moving platform was considered to be the most promising solution.

3.3 Tuning

Due to fabrication errors in the mechanism, variations in the stiffness or the balanced force of the mechanism can occur. To adjust the stiffness and the balanced force a tuning mechanism is required [Appendix A.4].

3.3.1 Tuning the stiffness

To adjust the stiffness of the mechanism it is possible to tune the stiffness of the bi-stable buckling beams or the stiffness of the v-shaped beams. In Dunning et al. (2011b) was found that varying the initial angle or preloading of bi-stable
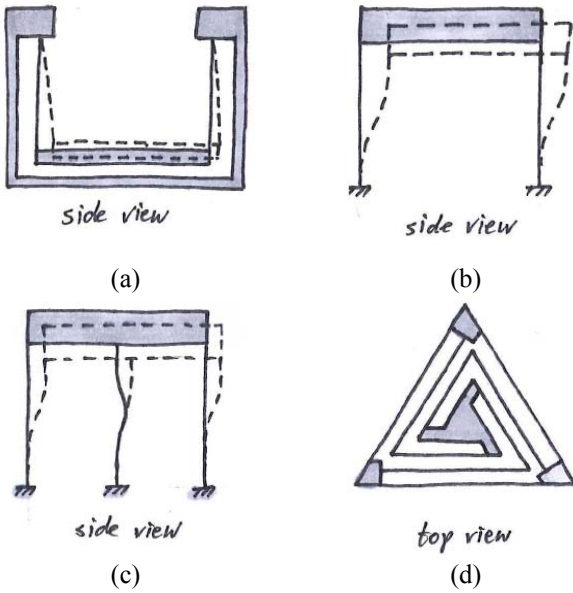
(a) (b)

(c) (d)

Fig. 4. Examples of solutions for in-plane motions (*Tx*, *Ty*, *Rz*) with low stiffness: the moving platform is (a) suspended by cables, (b) supported by flexible rods, loaded to their buckling load(c) supported by a combination of straight rods and preloaded rods (balanced), (d) supported by three L-shaped beams.
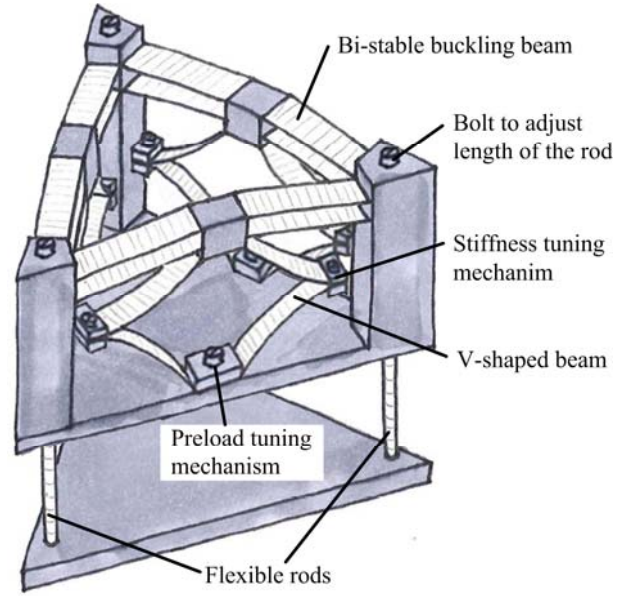

Fig. 5. Sketch of the conceptual design: the top part consists of three statically balanced compliant mechanisms, each consisting of a pair of bi-stable buckling beams and a pair of v-shaped beams, to balance the out-of-plane motions (*Tz*, *Rx*, *Ry*); the bottom part consists of three flexible rods, which have nearly zero stiffness for the in-plane motions (*Tx, Ty, Rz*) when loaded to the buckling load.

buckling beams can change the stiffness. This requires small complex components to be manufactured.

The stiffness of the v-shaped beam can be adjusted by a horizontal motion of the lowest end tip of the beam. Tuning is very difficult, because simulations showed that the stiffness characteristic becomes non-linear.

The most promising solution is changing the length of the v-shaped beam, which can be assumed as two beams, fixed at one end where they connect and straight guided perpendicular to the beam at the other end, in series. The stiffness of a simple beam, fixed at one end and straight guided at the other end, is calculated according to Eq. 1 (Gere, 2002):

$$K = \frac{F}{x} = \frac{12\,EI}{L^3} \rightarrow \left(I = \frac{wt^3}{12} \right) \rightarrow \frac{Ewt^3}{L^3} \quad (1)$$

where E is Young´s modulus, w is the width, t is the thickness and L is the length of the beam.

To adjust the stiffness of a beam the length is the only parameter that can be changed. For the v-shaped beam the length can be adjusted by clamping the two parts of the v-shaped beam together. Tuning is easy and simulations showed that the stresses in the mechanism are not exceptionally high and the stiffness keeps its linear characteristic.

3.3.2 Tuning the preload

In every design the gravity force to be balanced can vary. By tuning the preload of the v-shaped beam the force that can be balanced can be adjusted.

Tuning this preload is possible by pulling the end tips of the v-shaped beam together or pushing them away from each other.

Due to small and complex components this solution is not easy to manufacture and tuning is not easy.

The most promising solution is moving the lowest end tip of the v-shaped beam up or down to tune the preload. This is easy to manufacture, simulations showed that the stresses in the mechanism are not becoming exceptionally high and it is easy to be implemented.

3.3 Final concept for 6 DoF precision stage

To perform 6 DoF motions the most promising solutions were integrated into one final conceptual design (Fig. 5), which is a combination of the mechanism for the out-of-plane motions (*Tz, Rx, Ry*) supported by three flexible rods, fixed at both ends, in triangular configuration, able to perform the in-plane motions (*Tx, Ty, Rz*). The tuning mechanism for stiffness and preload were positioned on the v-shaped beams of the out-of-plane mechanism. The length of the flexible rods can be tuned with bolts on top of the out-of-plane mechanism, to adjust the stiffness for in-plane motion.

4. DIMENSIONAL DESIGN

To design a prototype, the dimensions of the conceptual design need to be determined and optimized. In the next section an investigation is performed to optimize the dimension parameters of the components of the 6 DoF compliant precision stage [Appendix B].
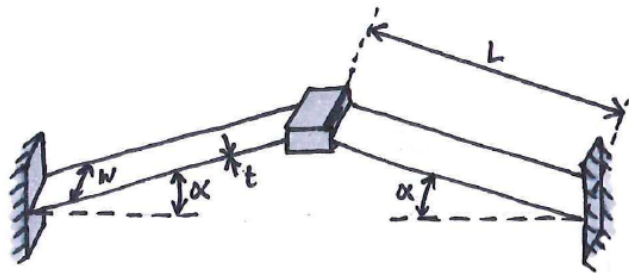
Fig. 6. Sketch of bi-stable buckling beams with the initial angle (α), a thickness (t), width (w) and length (L). The mechanism buckles when the middle platform is translated downwards.
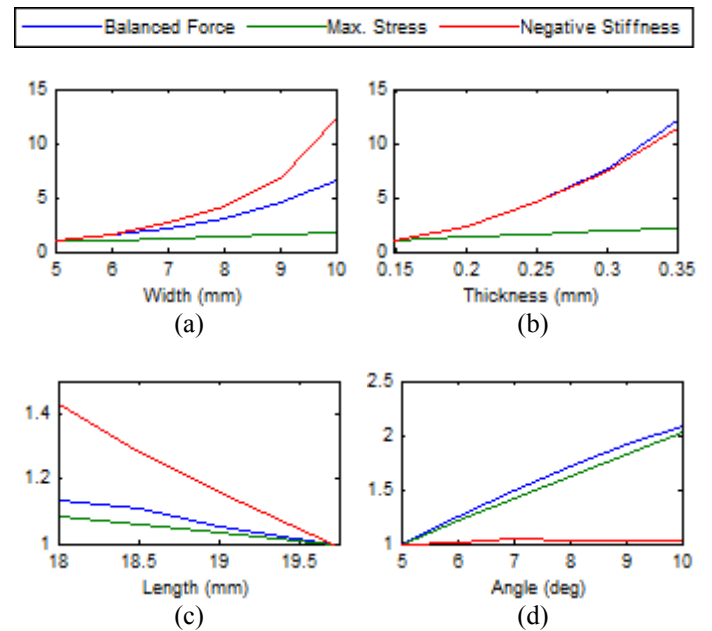

Fig. 7. Behavior of the balanced force, maximum stress and negative stiffness of the bi-stable buckling beams, for varying design parameters (a) width, (b) thickness, (c) length or (d) initial angle of the bi-stable buckling beams. When the dimension parameter width, thickness or initial angle was varying, the length was optimized to fit in a triangular space with edges of 62mm, while the others were kept constant. The balanced force was calculated by adding a positive stiffness equal to the negative stiffness. The values were normalized to the smallest in the group.

4.1 Out-of-plane balancing

The out-of-plane motions are proposed to be performed by the mechanism described in Sect. 3.3 (Fig. 5). The objective for the final design is to balance a gravity force, while minimizing the negative stiffness of the bi-stable beams and the positive stiffness of the v-shaped beams, in order to reduce the stresses in the mechanism and have better tuning possibilities. Therefore, both components have to be optimized in terms of stresses, balanced force and stiffness [Appendix B.1].

4.1.1 Bi-stable buckling beams

In Dunning et al. (2011b) it was found that decreasing the initial angle, preloading and thickness of the bi-stable buckling beams decreases the negative stiffness of the bi-stable buckling beams. However, the stresses in the bi-stable beams and the gravity force that can be balanced with the mechanism were not investigated. In this section the relation between the maximum stress, potentially balanced force and negative stiffness of the bi-stable buckling beams for dimension parameters width, thickness, length and initial angle (Fig. 6) are investigated. The simulations were done in ANSYS[TM] using the approach described in Dunning et al. (2011b). The potentially balanced force was calculated by adding a positive stiffness equal to the negative stiffness. The values of the balanced force, negative stiffness and stresses were normalized to the smallest in the group, to have dimensionless results.

When the dimension parameter width, thickness or initial angle was varying, the length was optimized to fit in a triangular space with edges of 62mm, while the others were kept constant.

Width

The width was increased from 5mm to 10mm, with steps of 1mm. In Fig. 7a it is shown that both the negative stiffness and the balanced force are increasing parabolic, where the negative stiffness increases approximately to 12 and the balanced force to 7. The maximum stress linearly increases to 2. For increasing width and optimizing the length of the bi-stable beams the negative stiffness becomes highly sensitive to fabrication errors.

Thickness

The thickness was increased from 0.15mm to 0.35mm, with steps of 0.05mm. Fig. 7b shows that the balanced force is increasing parabolic to 11.5. The domain between the first stable position and the second stable position does not change for increasing thickness; consequently the negative stiffness is increasing the same as the balanced force. The maximum stress linearly increases to 2.

Length

Decreasing the length of the bi-stable beams resulted in a linear increase of the negative stiffness to 1.4, where the balanced force and the maximum stress are nearly constant (Fig. 7c). Decreasing the length has a negative influence on the relation between balanced force and negative stiffness: the negatives stiffness is increasing more than the balanced force.

Initial angle

The initial angle was increased from 5° to 10°, with steps of 1°. Both balanced force and maximum stress are increasing linearly to approximately 2, where the negative stiffness is constant (Fig. 7d). In Dunning et al. (2011b) the negative stiffness is increasing when the length of the bi-stable buckling beams are constant. When the length is optimized to a certain space, the negative stiffness is constant. Increasing the initial angle, with the length optimized, results in a mechanism which can balance a larger gravity force with a constant negative stiffness.

From the behavior of the balanced force, maximum stress and negative stiffness it can be concluded that maximizing the length and minimizing the width of the bi-stable buckling beams has a positive effect on the relation between balanced force and negative stiffness. At the same time, the negative stiffness becomes less sensitive to fabrication errors.

For decreasing thickness, the relation between balanced force and negative stiffness is kept constant. The negative stiffness becomes less sensitive to fabrication errors.

For increasing initial angle, a larger gravity force could be balanced over a larger domain, while the negative stiffness is kept constant. Variations in the initial angle have no influence on the negative stiffness.

Summarizing, for the objective to balance a gravity force with a low negative stiffness of the bi-stable mechanism, the initial angle should be as large as possible, considering the allowed stresses. Subsequently, the thickness and width should be as small as possible, and the length should be maximized to the available space.

4.1.2 V-shaped beams

The dimensions of the v-shaped beam, with constant stiffness for small deformations, are depending on the stiffness and the balanced domain of the bi-stable buckling beams and the allowable stresses. In Eq. 1 it has been shown that the stiffness of the v-shaped beam is highly sensitive for variations in thickness and length of the beams.

4.2 In-plane balancing

The in-plane motions are performed by three flexible rods, which have zero stiffness when loaded to the buckling load (Spiering and Grootenboer, 1993). The buckling load of a rod with circular cross section, fixed at one end and straight guided at the other end, can be calculated according to Eq. 2 (Gere, 2002):

$$F_b = \frac{\pi^2 EI}{L^2} \rightarrow \left(I = \frac{\pi\, d^4}{64} \right) \rightarrow \frac{\pi^3 E d^4}{64\, L^2} \qquad (2)$$

The buckling load, and consequently the stiffness for in-plane motions, is highly depending on the diameter of the rod.

4.3 Prototype

For experimental evaluation of the balancing principle a prototype was fabricated (Fig. 8). To provide a basis for evaluation of the concept, the prototype was dimensioned to balance a gravity force of 40N [Appendix C].

The bi-stable buckling beams were manufactured with wire electrical discharge machining. The dimensions of the bi-stable buckling beams were determined according to critical dimensions given by the manufacturer of the prototype (Optimum draadvonktechniek b.v.). The material of the bi-stable buckling beams is titanium Grade 5 (Ti6Al4V), which can resist high stresses without plastic deformation due to the high yield stress (830MPa) compared to the Young's modulus (113GPa) (Salomon's Metalen).
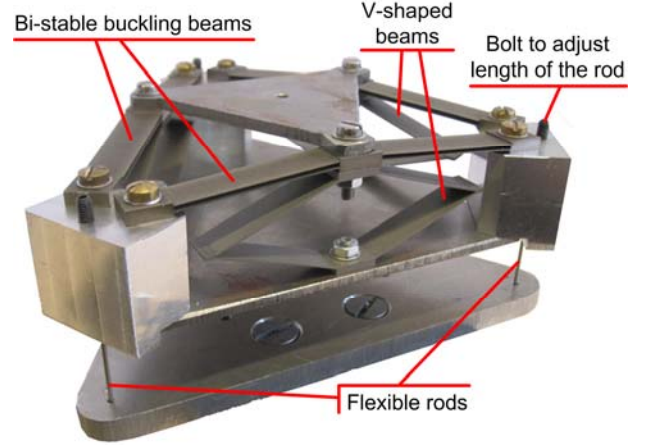

Fig 8. The assembled prototype. It shows the bi-stable buckling beams and the v-shaped beams for out-of-plane motions, and flexible rods for in-plane motions. The length of the rods can be tuned with the bolts.

Table 1. Overview of the dimensions and material of the different components of the prototype.

Component	Length (mm)	Width (mm)	Thickness (mm)	Initial angle	Material
Bi-stable buckling beams	35	9	0.25	5°	Titanium Grade 5 (Ti6Al4V)
V-shaped beams	29.3	9	0.45	20° with ground	Titanium Grade 5 (Ti6Al4V)
Rods	50	-	Ø1	-	Brass (CuZn39Pb3)

Taking the stiffness of the bi-stable buckling beams into account, the dimensions of the v-shaped beams were calculated.

The mechanism for out-of-plane motions was modeled with the finite element software package ANSYS[TM] using the approach described in Dunning et al. (2011b) (ANSYS). The results are shown in Fig. 10.

Extra simulations were done to investigate the influence of fabrication errors on the stiffness of the mechanism in its statically balanced domain. The stiffness of the worst scenarios was calculated, and it resulted that the maximum error must be smaller than 5μm to fulfill the design criterion of a stiffness lower than 1N/mm in the *Tz* direction.

For several reasons, the tuning mechanisms for the v-shaped beams were left out of the prototype.

Rods of brass (CuZn39Pb3), with a Young's modulus of 97GPa (Matweb), and 1mm diameter, perform the in-plane motions. The length of the rods, with a buckling load of 40N, should be 50mm. Due to fabrication errors both the diameter and the length of the rods can vary. With a maximum error of 0.08mm the stiffness for in-plane motions of the rods is smaller than 1N/mm, and still fulfills the design criteria. An overview of the dimensions and material of the prototype is given in Table 1.

5. EXPERIMENTAL EVALUATION

This section describes the measurement setup for experimental evaluation, the measurement protocol and the results obtained from the measurements.

5.1 Measurement setup

A setup was built for experimental evaluation of the prototype (Fig. 9) [Appendix D.1]. For every degree of freedom a displacement was applied on the prototype and the force was measured. The derivative of the force-displacement characteristic is equal to the stiffness.

The prototype was mounted on two linear stages (Thorlabs PT3A/M, resolution: 1μm, travel range: 25mm) for x and y-translation. The displacement was performed and measured by a linear motor stage (Physik Instrumente M-505.4DG, resolution: 0.05μm, travel range: 100mm), connected to the prototype through a force sensor (FUTEK LSB200, resolution: 10mV, range: 0-44.5N). The data was read using an amplifier (ICP DAS 3016) and a data acquisition module (National Instruments USB6008). The data was logged with the software Labview 10 and processed with MATLAB R14a.

Two microscope cameras (Dino-Lite AM-4013TL, frame rate: 30fps, magnification rate: 20-90x; BW1008, magnification rate: 5-500x) were used to align the force sensor to the prototype.

5.2 Measurement protocol

Five experiments were done to analyze the stiffness of the mechanism. In the three experiments to analyze the stiffness for out-of-plane motions the linear motor stage was mounted vertically on a frame. First, a vertical displacement of 4.5mm was applied at the centre of the platform, connected to the bi-stable buckling beams. With the measured force the stiffness in Tz direction was analyzed [Appendix D.2]. In the second and third experiment the stiffness in Rx direction, where the x-axis is parallel to a pair of bi-stable buckling beams, and Ry direction, where the y-axis is perpendicular to a pair of bi-stable beams, was analyzed, respectively. A weight, which is the result of the balanced force determined in the first experiment, was put on top of the platform to bring the mechanism in the balanced domain. A vertical displacement of 2mm was applied 80mm right from the centre of the platform (Fig. 9). To determine the rotation of the mechanism, the vertical displacement on the other side (80mm left from the centre of the platform) was measured with a laser displacement sensor (Micro-epsilon optoNCDT1401, range: 10mm, resolution: 1μm). The moment was determined by multiplying the measured force with the characteristic length from the rotation point, adding the moment produced by the weight, with an increasing moment arm for increasing rotation and
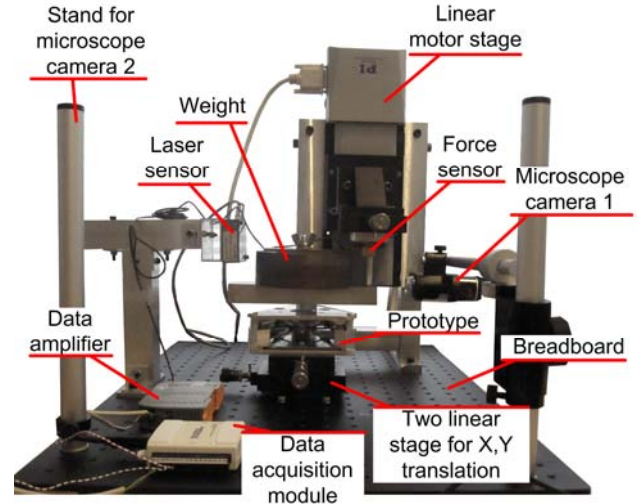

Fig. 9. The measurement setup to analyze the stiffness of the prototype. For the stiffness for out-of-plane motions the linear motor stage is mounted vertically on a frame. To analyze the stiffness for in-plane motions the linear motor stage is mounted horizontal on the breadboard.

extracting the moment produced by the vertical deformation of each of the three units of the out-of-plane mechanism [Appendix D.3].

In the third and fourth experiment the linear motor stage was mounted horizontal, and the prototype was loaded with a weight, corresponding to the balanced force determined in the first experiment. In the third experiment a horizontal displacement of 2mm was applied in the centre of the mechanism, to analyze the stiffness in Tx direction, which is equivalent to the stiffness in Ty direction [Appendix D.4]. Finally, to analyze the stiffness in Rz direction, the mechanism was made to rotate about a ball bearing in the centre of the bottom plate of the out-of-plane mechanism. A horizontal displacement, parallel to a pair of bi-stable beams, of 1mm was applied 65mm from the rotation point of the mechanism, corresponding to 15mrad [Appendix D.5]. The moment was determined by multiplying the measured force with the characteristic length of 65mm, which slightly decreases for increasing rotation [Appendix D.5].

During the experiments an extra plate was mounted on top of the prototype, to avoid bending of the bottom plate due to large horizontal reaction forces of the bi-stable buckling beams, which can negatively affect the bi-stable behavior of the buckling beams. During the design phase this should be taken into account, which is explained in the discussion.

5.3 Results

In Fig. 10 the results of the force-displacement characteristic of the bi-stable buckling beams, v-shaped beams and the complete prototype in Tz direction for both the finite element simulations and the measurements are shown. The maximum force of the bi-stable buckling beams from the measurements is lower than expected from simulations. Also the stiffness of both the bi-stable buckling beams and the v-shaped beams is lower. This results in a nearly balanced
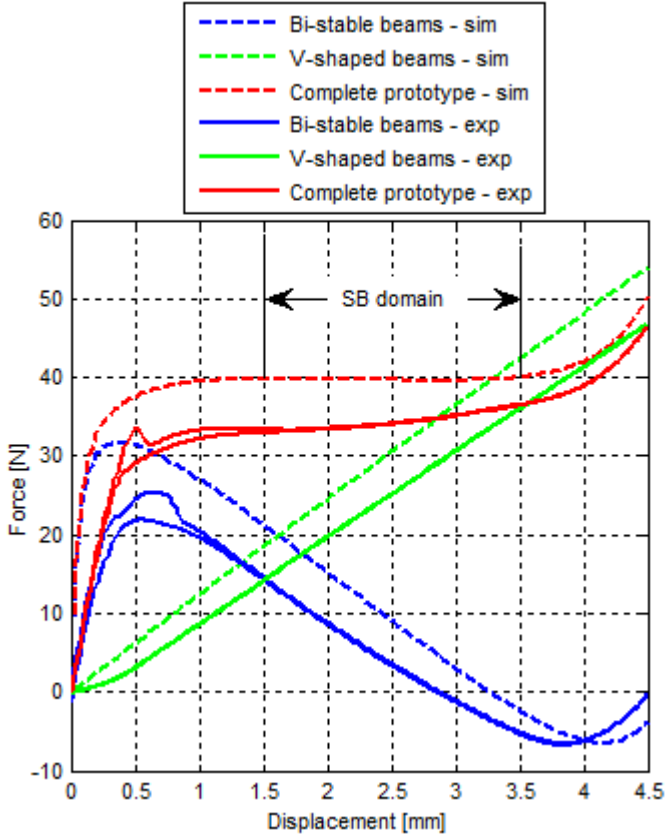
Fig. 10. Results of the force-displacement characteristic of the bi-stable buckling beams, v-shaped beams and the complete prototype, for simulations in ANSYS^{TM} (dashed) and experiments (solid) in Tz direction. The residual stiffness in the balanced domain of the prototype is 1.75N/mm, from 1.5-3.5mm displacement.

complete prototype, with a stiffness of 1.75N/mm from 1.5-3.5mm displacement and a balanced force of 34.4N.

The results of the moment-rotation characteristic for the out-of-plane rotations are shown in Fig. 11a. The stiffness induced by torsion of the beams in Rx and Ry direction is 12Nm/rad and 18.5Nm/rad, respectively, for rotations to 10mrad.

In Fig. 11b and Fig. 11c the results for the in-plane motions are shown. When the load on the rods is increased from 435g to 3508g the stiffness in Tx and Ty direction is reduced from 1.1N/mm to 0.4N/mm, for translation to 2mm. The rotational stiffness in Rz direction is reduced from 4.6Nm/rad to 2Nm/rad, for rotation to 15mrad.

6. DISCUSSION

The goal of this study was to design a zero stiffness 6 DoF compliant precision stage, able to balance a gravity force applied on the stage. As a result, the prototype uses three statically balanced compliant mechanisms, arranged in a triangular configuration, consisting of bi-stable buckling beams and v-shaped beams for balancing the out-of-plane motions (Tz, Rx, Ry), supported by three flexible rods, clamped at one end to the ground and the other end clamped to the moving platform, for in-plane motions (Tx, Ty, Rz).

The stiffness in Tz direction is 1.75N/mm in a domain of 2mm, from 1.5-3.5mm displacement (Fig. 10). The negative stiffness of the bi-stable buckling beams and the positive stiffness of the v-shaped beams is smaller than the results of the simulations, which is caused by fabrication errors: the error in thickness for the bi-stable beams and the v-shaped beams is ±0.05mm and ±0.1mm, respectively; the error in width for the bi-stable beams and the v-shaped beams is ±0.05mm. The stiffness is highly sensitive to variations in width and thickness of the beams. This explains the residual stiffness and the lower balanced force. Tuning the stiffness of the v-shaped beams can result in a lower residual stiffness. However, the negative stiffness of the bi-stable buckling beams is not perfectly linear. Therefore, the smallest residual stiffness in the balanced domain that can be achieved for this prototype is 0.4N/mm [Appendix F.1].

The hysteresis in the force-displacement characteristic of the bi-stable buckling beams, and therefore also in the characteristic of the complete prototype is due to the asymmetric buckling behavior of the bi-stable beams in the beginning of the negative stiffness domain, caused by small variations in dimensions between the bi-stable beams. Consequently, the bi-stable buckling beams are forced into different buckling modes at the beginning of the negative stiffness domain. On the other hand, in the return motion the bi-stable buckling beams all have the same buckling mode, resulting in a smoother buckling behavior.

The sum of the separate force-displacement characteristics in Tz direction of the bi-stable buckling beams and the v-shaped beams is not equivalent to the force-displacement characteristic of the complete mechanism (Fig 10). Once the bi-stable beams and v-shaped beams are connected with the moving platform, parasitic torsion and bending of the beams is reduced, resulting in a different force-displacement characteristic of the complete mechanism.

During out-of-plane rotations (Rx, Ry) the three balanced mechanisms of the out-of-plane mechanism were subjected to vertical displacement and torsion. To determine the rotational stiffness induced by the torsion of the bi-stable buckling beams and the v-shaped beams, the moment produced by the three balanced mechanisms was extracted from the moment produced by the linear motor stage and the weight [Appendix D.3]. The rotational stiffness induced by torsion of the out-of-plane mechanism is 12Nm/rad and 18.5Nm/rad for Rx and Ry direction, respectively, for rotations to 10mrad (Fig. 11a). The stiffness in Ry direction is larger, due to torsion of the bi-stable buckling beams parallel to the stiff beam about the y-axis [Appendix F.2]. A recommendation for improvement of the design is to increase the robustness to torsion using a different connection between the bi-stable buckling beams and the moving platform. When this is achieved, the design for out-of-plane mechanism shows high potential to perform zero stiffness out-of-plane motions.

The in-plane motions are performed by three flexible rods, loaded with a load close to the buckling load. The results for stiffness in Tx and Ty direction and the rotational stiffness in Rz direction show a large decrease of the stiffness when the load on the rods is increased (Fig. 11b, c). The required stiffness for
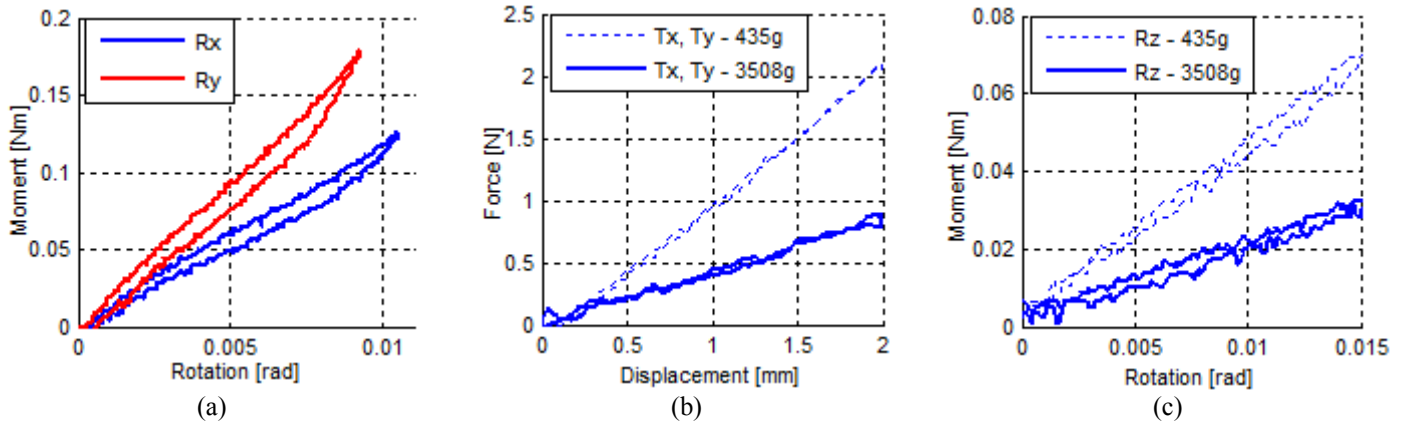
Fig. 11. Results of the measurement for (a) rotational stiffness for out-of-plane motions (K_{Rx}=12Nm/rad, K_{Ry}=18.5Nm/rad), (b) stiffness in *Tx* and *Ty* direction (K_{Tx}=K_{Ty}=0.4N/mm), (c) rotational stiffness in *Rz* direction (K_{Rz}=2Nm/rad).

in-plane motions is reached. An essential remark is the limited range of motion of the rods. The higher the load on the rods and the larger the motion of the rods, the more sensitive the rods are for buckling. To avoid buckling a safety factor on the load applied on the rods should always be taken into account.

Another important remark is the large horizontal reaction forces of the bi-stable buckling beams. Simulations showed a maximum horizontal reaction force of 76N for a pair of bi-stable buckling beams. A future design should be able to withstand these forces without horizontal motion of the end-tips of the bi-stable buckling beams, otherwise the bi-stable behavior of the buckling beams, and consequently the zero stiffness behavior of the complete mechanism is negatively affected.

7. CONCLUSIONS

The first near zero stiffness 6 DoF compliant precision stage, which is able to balance a gravity force, is presented. Out-of-the-horizontal-plane motions are performed by three statically balanced compliant mechanisms, arranged in a triangular configuration, consisting of bi-stable buckling beams with a negative stiffness domain, compensated by v-shaped beams with positive stiffness. The out-of-plane mechanism is supported by three flexible rods, arranged in a triangular configuration, performing the in-plane motions. To determine the optimal dimensions for the out-of-plane mechanism an investigation on the design parameters was made, in order to balance a gravity force with low negative and positive stiffness of the bi-stable beams and v-shaped beams, respectively. It was shown that the initial angle of the bi-stable buckling beams is the most important design parameter to balance a gravity force with low negative stiffness. The stiffness of the mechanism is highly sensitive to variations in width and thickness of the beams. A prototype was made and evaluated, resulting in a statically balanced domain of 2mm in vertical direction, where a gravity force of 34.4N was balanced and the smallest residual stiffness that can be achieved is 0.4N/mm. Parasitic torsion during out-of-plane rotations induced a rotational stiffness of 12Nm/rad and 18.5Nm/rad for rotation to 10mrad around the x-axis and y-axis, respectively. Nevertheless, the out-of-plane

mechanism showed high potential for (near) zero stiffness out-of-plane motions. The stiffness for in-plane translations to 2mm (*Tx, Ty*) and rotation to 15mrad (*Rz*) was reduced from 1.1N/mm to 0.4N/mm and from 4.6Nm/rad to 2Nm/rad, respectively, when the load on the flexible rods is increased from 435g to 3508g. The flexible rods are sensitive to buckling, and dimensioning the rods for near zero stiffness is challenging. It was found that the internal reaction forces are great and can significantly affect the near zero stiffness behavior of the mechanism.

REFERENCES

ANSYS, Manual of ANSYS 10, ANSYS Inc., 2005.

Dunning A.G., Tolou, N., Herder, J.L.: Review article: Inventory of platforms toward the design of a statically balanced six degrees of freedom compliant precision stage, Mech. Sci., 2, 157-168, 2011a.

Dunning, A.G., Tolou, N., Kluit, L.F., Herder, J.L.: Short communication on bi-stable compliant mechanisms: correction for finite elements modeling, preloading incorporation and tuning the stiffness, 2011b.

Gere, J.M.: Mechanics of Materials, 5th SI edition, Nelson Thornes Ltd, Cheltenham UK, 922pp., 2002.

Herder, J.L.: Energy-free systems: theory, conception, and design of statically balanced spring mechanisms, Ph.D. thesis, Delft University of Technology, Delft, The Netherlands, 248pp., 2001.

Herder , J.L., and van den Berg, F.P.A.: Statically balanced compliant mechanisms (SBCM's), an example and prospects, in: Proceedings of ASME 2000 Design Engineering Technical Conferences and Computers and Information in Engineering Conference, Baltimore,

Maryland, USA, 10-13 September 2000, DETC2000/MECH-14144, 2000.

Howell L.L.: Compliant mechanisms, John Wiley & Sons, New York USA, 459pp., 2001.

Matweb: http://www.matweb.com/, last access: 15 August 2011.

Morsch, F.M., and Herder J.L.: Design of a generic zero stiffness compliant joint, in: Proceedings of the ASME 2010 Internal Design Engineering Technical Conferences & Computers and Information in Engineering Conference, Montreal, Quebec, Canada, 15-18 August 2010, DETC2010-28351, 2010.

Nieuwenhuis, C.: Thermal behavior Mapper Short Stroke, restricted internal report, Demcon Advanced Mechatronics B.V., Oldenzaal, The Netherlands, 16pp., 2010.

Optimum draadvonktechniek b.v.: http://www.draadvonk.nl, last acces: 15 August 2011.

Salomon's Metalen: http://www.salomons-metalen.nl/pdf/ austenitische_martensitische_roestvrijstalen.pdf, last acces: 15 August 2011.

Spiering, R.M.E.J. and Grootenboer, H.J.: Eindige elementen methode in de werktuigbouwkunde, Technical report, University of Twente, The Netherlands, 1993(in Dutch)

Tolou, N. and Herder, J.L.: Statically balanced compliant micro mechanisms (SM-MEMS): concepts and simulation, in: Proceedings of the ASME 2010 International Design Engineering Technical Conferences & Computers and Information in Engineering Conference, Montreal, Quebec, Canada, 15-18 August 2010, DETC2010-28406, 2010.

Appendix A

Conceptual Design

The phase of conceptual design was done according to three functions the zero stiffness 6 DoF compliant precision stage have to perform (Fig. A.1). The first and second function were distinguished according to the motions the mechanism have to perform: the motions in vertical Z-direction (*Tz*) and the rotations about the horizontal X-axis (*Rx*) and Y-axis (*Ry*) are called out-of-plane motions, which are motions out of the horizontal plane. The horizontal translations in X (*Tx*) and Y direction (*Ty*) and horizontal rotation about Z-axis (*Rz*) are called in-plane motions. In the *Tz* direction a gravity force has to be balanced.

To correct some errors in the fabrication process, the mechanisms must be tunable.
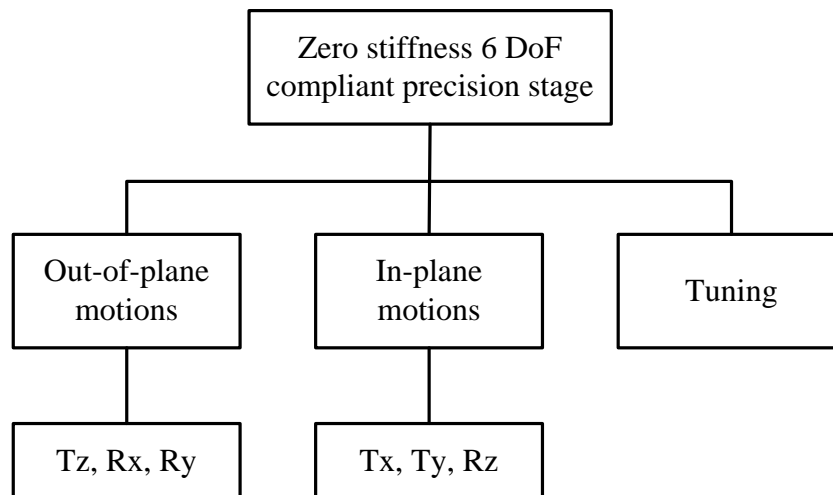
Fig. A.1. Function diagram of the zero stiffness 6 DoF compliant precision stage. The motions in the horizontal plane (x-axis and y-axis) are called in-plane motions. Tx means translation in the x-direction, Rx means rotation in about the x-axis.

For each function, concepts are created and assessed. The most promising solution for each function are combined to a conceptual design.

A.1 Assessment of concepts

The following criteria were used to assess the solutions. Each concept was assessed according to these criteria, and given scores of +, 0 or -.

Remaining stiffness – the remaining stiffness or force needed to actuate the mechanism after balancing. A + means that the remaining stiffness is lower than 1N/mm. A 0 was given when the remaining stiffness is between 1 and 10N/mm. A – means that the remaining stiffness is higher than 10N/mm.

Maximum stresses – the maximum stresses in the mechanism for the statically balanced domain. This criterion is related to the lifetime of the mechanism and the fatigue in the materials. The score + was given when the max. stresses are below 30% of the yield strength of the material. A 0 means that the max. stresses are between 30% and 60% of the yield strength, while a – was given when the stresses are higher than 60% of the yield stress.

Parasitic motion – undesired motion in other directions than the required balanced direction. If the parasitic motion is small, and it can be solved by the balanced motion, the score is a +. If the parasitic motion is small, but it cannot be solved by the balanced motion, the score is 0. A – means that the parasitic motion is large, and cannot be solved by the balanced motion.

Tuning – this is related to the robustness to fabrication errors. The stiffness of the mechanism must be tunable, to correct these errors. If this is possible, and the tuning mechanism is easy to use and to manufacture, the score is +. If tuning is possible, but it is difficult to adjust the stiffness, a 0 was given. When tuning is impossible, the score is -.

Ease of manufacturing – this criterion concerns the ease of manufacturing, fabrication method, amount of components and ease of assembling. A + says that the mechanism is easy to manufacture, and (if applicable) easy to assemble. A 0 means that the mechanism is difficult to manufacture (e.g. difficult components), but easy to assemble. Or the other way around, easy to manufacture and difficult to assemble. A – was given when it is difficult to manufacture and difficult to assemble.

Energy storage during assembly– the required energy stored into the mechanism before it is balanced. This criterion is related to safety during assembly. When there is no preloading (energy storage) needed, the score is +. When preloading is needed, but the stresses are not very high, a 0 was given. A – means that the stresses during preloading are exceptionally high.

These criteria were assessed to their importance. The criteria were given scores from 1-5, where 5 is the most important. Because zero stiffness in 6 DoF is the most important design criterion, the remaining stiffness is the most important assessment criterion (score 5). To reach this design criterion parasitic motion must be avoided (score 4) and the stiffness must be

tunable (score 4). Plastic deformation of the material is not allowed (score 3). The energy storage during assembly (score 2) and the ease of manufacturing (score 1) are the least important criteria.

The total score of each solution was calculated by multiplying each score with the importance factor of the criterion. A + is given the value 5, 0 has the value 3, and – has the value 1.

A.2   Out-of-plane motions

The out-of-plane function was divided into two subfunctions. First, the concepts for a T_Z direction, balancing a gravity force, are discussed. In the section A.2.2, the concepts for the out-of-plane rotations are discussed.

A.2.1 T_Z direction

In Dunning et al. (2011a) it is shown that the use of bi-stable buckling beams is the most suitable to balance a high force over a large range in a relative small volume. These beams were used as the components which produces negative stiffness, and must be balanced with a positive stiffness. In Fig. A.2 the characteristic of this principle is shown. The negative stiffness of the bi-stable characteristic is balanced with a positive stiffness, resulting in a system which can balance a gravity force. Units consisting of a combination of bi-stable buckling beams and a positive stiffness are used as building blocks for mechanisms with more degrees of freedom.
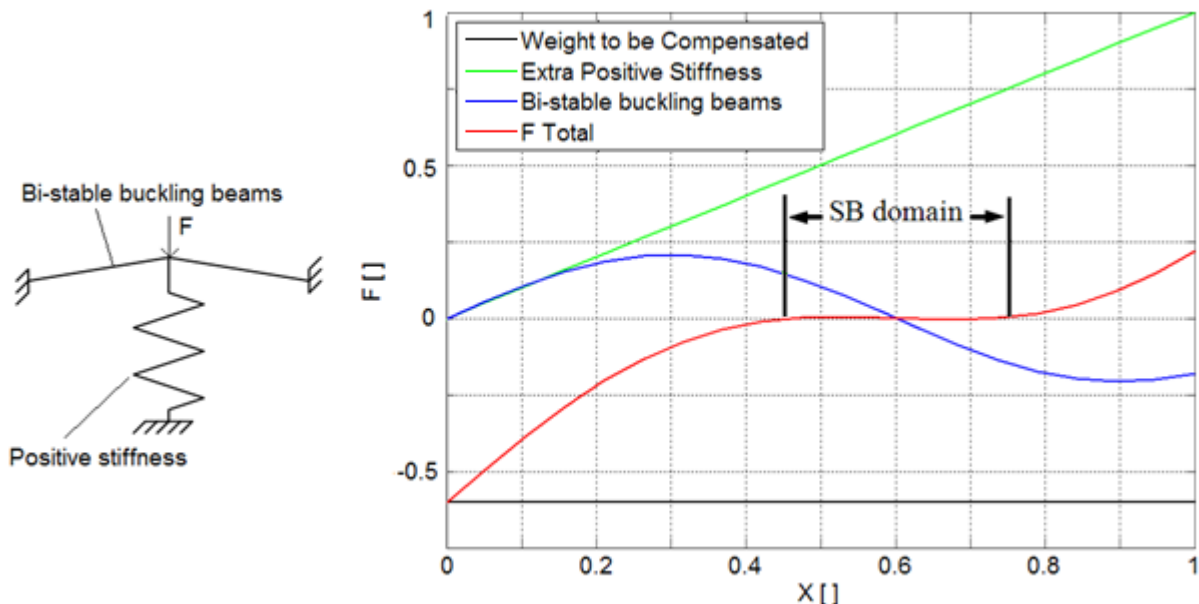
Fig. A.2. Schematic force-displacement characteristic of a zero stiffness mechanism: bi-stable buckling beams with a negative stiffness domain combined with a linear positive stiffness create a statically balanced domain where a gravity force can be balanced.

The different configurations for the balanced mechanism are shown in Table A.1

(a) Three pairs of bi-stable buckling beams, connected in radial direction to the central moving platform. The positive stiffness consist of 3 v-shaped beams, which has linear stiffness for small deformations (Morsch and Herder, 2010).

(b) The moving platform is supported by three balanced mechanisms, consisting of multiple bi-stable buckling beams and a positive stiffness, arranged in a triangular configuration. Different configurations for the positive stiffness are:
   1. A single v-shaped beam. Rotations of the bi-stable buckling beams are easily introduced.
   2. Double v-shaped beams, connected close to the mid-line of the bi-stable beam. With this the rotations are cancelled out more than with (b.1).
   3. Double v-shaped beams, connected far from the mid-line of the bi-stable beam. With this the rotations are cancelled out more than with (b.2), but it also requires more space.

Because the three balanced mechanisms can act independently of each other, this concept can also balance the out-of-plane rotations.

(c) This concept is almost equal to concept a. But here, the moving platform in the centre is supported by six beams, so multiple beams above each other are not needed.

(d) The negative stiffness of the bi-stable buckling beams is balanced with a simple helical spring.

(e) Two pairs of bi-stable buckling beams, with different initial angle can balance the mechanism (Tolou et al., 2010). An example of the characteristic is shown in Fig. A.3.
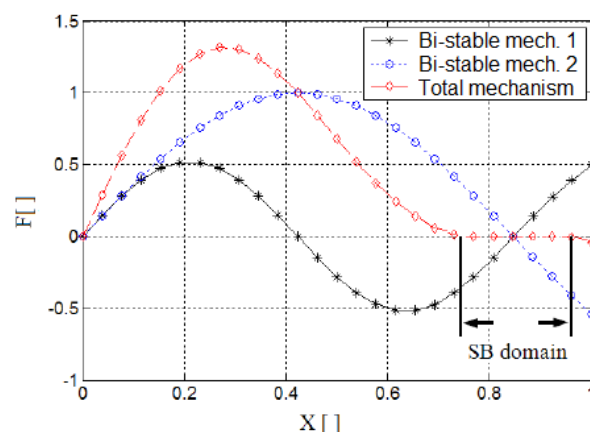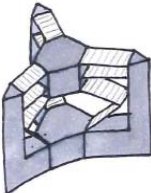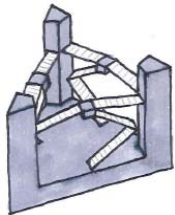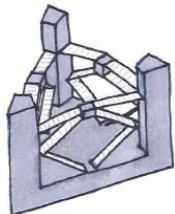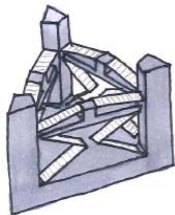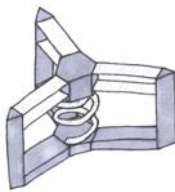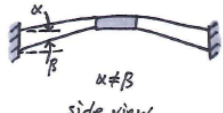

Fig. A.3. Typical characteristic of two bi-stable buckling mechanisms: at a certain domain the stiffness of both mechanisms cancel out each other (reproduced from Tolou et al. (2010).

Table A.1. Overview and assessment of the solutions for balancing the translation in Z-direction (Tz): – is poor, 0 is normal and + is good. Bold values are based on simulations in ANSYS.
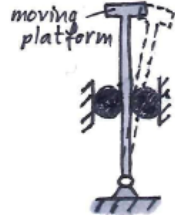
Solution		Remaining stiffness	Maximum stresses	Parasitic motion	Tuning	Ease of manufacturing	Energy storage during assembly	Total score
(a)		+	**0**	+	+	+	+	89
(b.1)		+	+	-	+	+	+	79
(b.2)		+	+	+	+	+	+	95
(b.3)		+	+	+	+	+	+	95
(c)		+	-	+	+	+	+	83
(d)		+	+	0	-	+	+	71
(e)		+	**0**	0	-	+	+	65

A.2.2 *Rx*, *Ry* directions

For the out-of-plane rotations concept (b) for the balanced *Tz* direction can be used. Two extra concepts are discussed (see Table A.2).

(a) A single vertical flexible cantilever rod supports the platform. This concept is not balanced, but can have a low stiffness for transversal motion when the rod is loaded with the buckling load (Spiering and Grootenboer, 1993).

(b) A vertical stiff rod with a spherical joint at the ground supports the platform. A rubber ring around the rod can balance the gravity force. Rubber has linear stiffness for small deformations [1]. Damping and backlash affect the precision of the solution.

Table A.2. Overview and assessment of the solutions for balancing the out-of-plane rotations (Rx, Ry): – is poor, 0 is normal and + is good. Bold values are based on simulations in ANSYS.

Solution	Remaining stiffness	Maximum stresses	Parasitic motion	Tuning	Ease of manufacturing	Energy storage during assembly	Total score
(a)	+	0	0	+	+	+	81
(b)	+	0	0	0	+	+	73

A.2.3 Conclusions

The most promising solution is the use of three identical balanced mechanisms, consisting of two v-shaped beams beneath the bi-stable buckling beams, arranged in triangular configuration (concept b.2). The negative stiffness of the bi-stable buckling beams are balanced with the positive stiffness of the v-shaped beams. The stiffness of the v-shaped
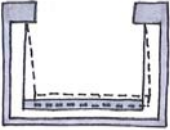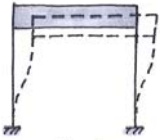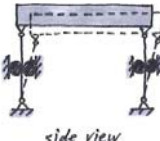
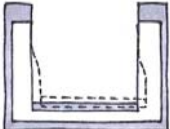[1] http://www.sonus.nl/dutch/begrippen/toelichtingen/trillingsd.html, last access: August 31, 2011
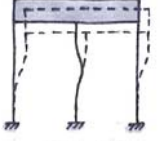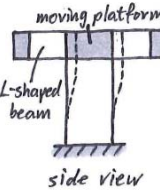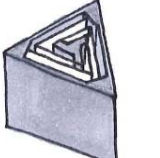
beams can easily be tuned, as explained in section A.4.1. At the same time, the three balanced mechanisms can perform out-of-plane rotations. During assembly of the complete prototype no energy is stored inside the mechanism. Parasitic motion is decreased by using multiple bi-stable buckling beams above each other. The stresses in the bi-stable buckling beams and v-shaped beams are highly depending on the dimensions of the beams and can be decreased by using multiple bi-stable buckling beams and v-shaped beams, placed above each other.

A.3 In-plane motions

In all concepts for in-plane motions the *Tx*, *Tz* and *Rz* directions were combined into one solution. An overview of the solutions with the assessment is shown in Table A.3.

(a) The platform is connected to the ground with cables. These cables have no stiffness, but have a preferred position at the lowest position. The force needed to swing a cable is dependent on the length of the cable.

(b) A combination of three flexible rods fixed to the platform in triangular configuration. If the rods are loaded with the buckling load, the rods have a near zero stiffness for in-plane motions (Spiering and Grootenboer, 1993).

(c) A combination of three stiff rods connected to the platform with spherical joints. A rubber ring around each rod can balance the gravity force.

(d) The platform is connected to the ground with tension rods (like concept a). The rods have an unbalanced stiffness. They also produce torsion in the bi-stable buckling beams.

(e) A combination of straight rods and preloaded rods. When the rods in the middle are preloaded, they will produce some force in the same direction as the actuation force. With this the stiffness of the straight rods is compensated.

(f) The platform is supported by a combination of 3 L-shaped beams. The beams could have distributed or lumped compliance. The mechanism is not balanced. Loading the platform with a gravity force induces torsion in the beams.

(g) To prevent the torsion in concept (g) some flexible rods are placed under the platform.

(h) To prevent the torsion in concept (g) the height of the L-shaped beams is enlarged. With this solution still there is some torsion left when the platform is loaded with a gravity force.

Table A.3. Overview and assessment of the solutions for balancing the in-plane motions (Tx, Ty, Rz): – is poor, 0 is normal and + is good. Bold values are based on simulations in ANSYS.

Solution	Remaining stiffness	Maximum stresses	Parasitic motion	Tuning	Ease of manufacturing	Energy storage during assembly	Total score
(a)	**0**	+	0	+	+	+	77
(b)	**+**	**0**	0	+	+	+	81
(c)	+	0	0	0	+	+	73
(d)	0	+	0	0	0	+	67
(e)	**+**	**0**	0	+	0	+	79
(f)	**0**	+	-	-	+	+	53
(g)	0	+	0	-	-	+	57
(h)	-	+	0	+	0	+	51

A.3.1   Conclusions

The most promising solution is the use of flexible rods, fixed to the ground and the moving platform (concept b). A combination of three rods, in triangular configuration, can perform the in-plane translations and the in-plane rotation. When the rods are loaded with the buckling load the stiffness for in-plane motions is reduced to zero (Spiering and Grootenboer, 1993). Of course, a safety margin is needed, because the rods are sensitive to buckling. There is a small parasitic motion in the Tz-direction, but this can easily be compensated by the mechanism for balancing the Tz direction. Tuning is possible by changing the length of the rods.

A.4   Tuning

To correct fabrication errors, adjusting the stiffness, and adjusting the balanced force of the mechanism a tuning mechanism is necessary. First, the concepts to adjust the stiffness are discussed. After that, the concepts for adjusting the balanced force, which can be changed by adjusting the preload, are discussed. To assess the concepts the importance factor for the tuning criteria was changed to 5. In Table A.4 an overview of the solutions for adjusting the stiffness and in Table A.5 the solutions of balancing the preloading is shown.

A.4.1   Tuning the stiffness

Tuning the stiffness is needed, because the residual stiffness in the balanced domain can vary due to fabrication errors.

(a) By changing the initial angle and preloading of the bi-stable buckling beams the stiffness is adjusted (Dunning et al., 2011b).

(b) The v-shaped beam can be assumed as two simple beams, fixed at one end where they connect and straight guided perpendicular to the beam at the other end. The stiffness of a simple beam, fixed at one end and straight guided at the other end, can be calculated according to equation A.2 (Gere, 2002).
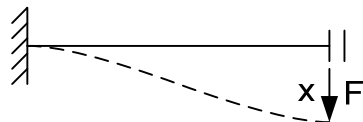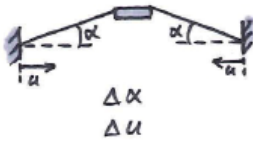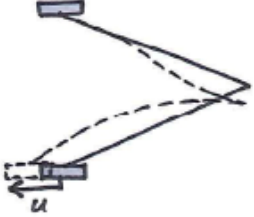
$$F = \frac{12EI}{L^3} x \qquad (A.1)$$

$$K = \frac{F}{x} = \frac{12EI}{L^3} \qquad (A.2)$$

In the concept the Young's modulus E and the moment of inertia I are constant. To adjust the stiffness of the beam the length must be changed. The length of the v-shaped beam can be changed by tighten two small plates together at the right position.

(c) The lowest end tip of the v-shaped beams can be moved slightly left or right. Simulations showed that the stiffness characteristic becomes non-linear.

Table A.4. Overview and assessment of the solutions for tuning the stiffness of the mechanism: – is poor, 0 is normal and + is good. Bold values are based on simulations in ANSYS.
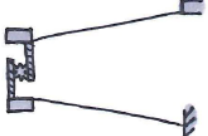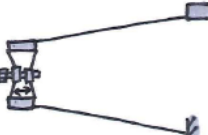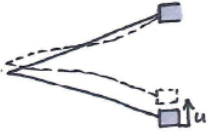
Solution		Maximum stresses	Tuning	Ease of manufacturing	Energy storage during assembly	Total score
(a)		-	**0**	0	0	27
(b)		+	+	+	+	55
(c)		+	-	+	+	35

A.4.2 Tuning the preload

Tuning the preload is needed because the total mass which must be balanced can vary.

(a) A worm gear is connected to the beam ends. With the worm gear the end tips of the beams can be pulled to each other or pushed away from each other. This solution requires small and complex components to be manufactured.

(b) The worm gear from concept (a) is replaced by a compliant mechanism. The challenge in this design is that it must be very small, while the loads are high. This solutions requires small and complex components to be manufactured.

(c) The end tip of the lowest beam can be moved up or down to adjust the preload.

Table A.5. Overview and assessment of the solutions for tuning the preloading of the mechanism: – is poor, 0 is normal and + is good. Bold values are based on simulations in ANSYS.

Solution	Maximum stresses	Tuning	Ease of manufacturing	Energy storage during assembly	Total score
(a)	0	-	-	+	25
(b)	0	-	-	+	25
(c)	+	**0**	+	+	45

A.4.3   Conclusions

The most promising solution for tuning the stiffness is changing the length of the v-shaped beams with two small plates, tightening the two parts of the v-shaped beams together (concept b). This solution can be combined with the solution for balancing the out-of-plane motions. Another important factor is that during the stiffness adjustment the stiffness keeps its linear characteristic, in opposite of concept c, where the stiffness characteristic will become non-linear.

The most promising solutions for adjusting the preload is the vertical translation of the lowest end tip of the v-shaped beam (concept c). This is very easy to manufacture and to operate.

A.5 Final concept for 6 DoF precision stage

The final conceptual design consist of a combination of the most promising solutions for each function. The solutions of each function do not coincide, which makes it very easy to combine these solutions. In Fig. A.5 a sketch of the final conceptual design is shown. The mechanism for balancing the out-of-plane motions, three balanced mechanisms with bi-stable buckling beams and v-shaped beams, is supported by three flexible rods which can perform the in-plane motions with nearly zero stiffness. The tuning mechanisms for adjusting the stiffness and preload are positioned on the v-shaped beams. The length of the rods can be adjusted by the bolts on top of the out-of-plane mechanism.
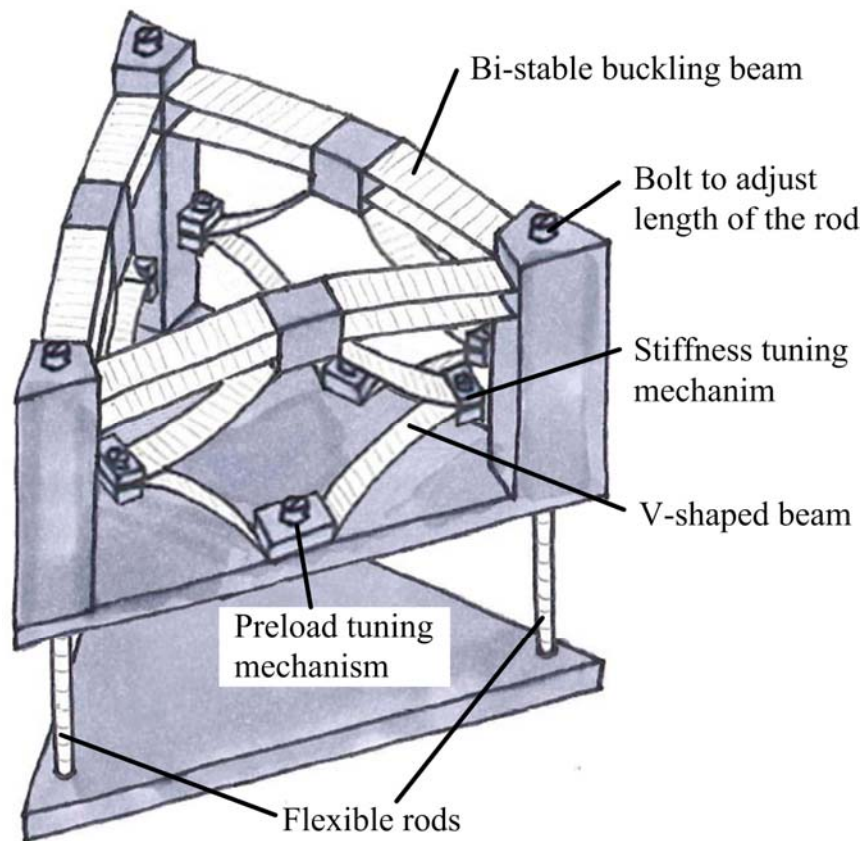

Fig. A.5. Drawing of the final conceptual design. The out-of-plane mechanism (three identical balanced mechanisms, consisting of multiple bi-stable buckling beams and v-shaped beams) is supported by the in-plane mechanism (three flexible rods), in triangular configuration.

Appendix B

Dimensional Design

To come to a final prototype, the dimensions of the conceptual design needs to be determined and optimized. In this appendix the dimensions of the different components of the design, the bi-stable buckling beams and the v-shaped beams for out-of-plane motions and flexible rods for in-plane motions, are optimized to perform zero stiffness 6 DoF motions.

B.1 Out-of-plane balancing

The objective of the final design is to balance a gravity force, while minimizing the negative stiffness of the bi-stable buckling beams and the positive stiffness of the v-shaped beams, in order to have better tuning possibilities and reduce the stresses in the mechanism.

B.1.1 Bi-stable buckling beams

The bi-stable buckling beams introduce the negative stiffness. In Dunning et al. (2011b) it has been shown that the negative stiffness of the bi-stable buckling beams can be changed by varying the preloading, the initial angle and the thickness of the beams. When increasing the initial angle or preloading the negative stiffness can be increased, while simultaneously the ratio "stroke of pre-buckling/full stroke" can be decreased. For the conceptual design this is beneficial, because the stroke before the balanced domain is shorter.

However, the stresses and the forces that could be balanced were not investigated in Dunning et al. (2011b). Therefore, in this section the relation between the maximum stresses in the bi-stable buckling beams, the potentially balanced force and the negative stiffness for different dimension parameters is investigated . Simulation in ANSYS^{TM} were done, using varying dimension parameters width, thickness, length and initial angle of the bi-stable buckling beams (Fig. B.1). The bi-stable buckling beams were loaded to the second stable position of the beams.
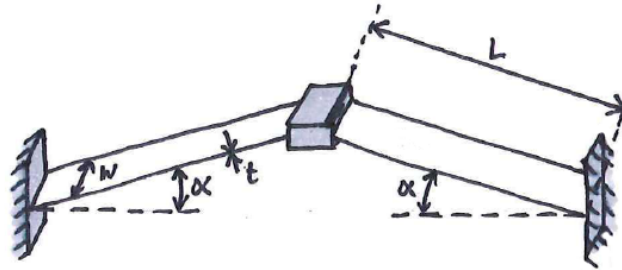
Fig. B.1. Bi-stable buckling beams with the initial angle (α), thickness (t), width (w) and length (L). The mechanism buckles when the middle platform is translated downwards.

Width

The width of the bi-stable buckling beams was increased from 5mm to 10mm, with steps of 1mm. Table B.1 shows the results of two different configurations, with an initial angle of 5° and 10°. In both configurations the thickness was 0.15mm and the length was optimized to fit in a triangular space with edges of 62mm.

Table B.1. Results of simulations for increasing width of the bi-stable buckling beams for two different configurations.

Width (mm)	Length (mm)	Stroke (mm)	Balanced force (N)	Max.Stress (MPa)	Negative Stiffness (N/mm)
Initial angle: 5°, thickness: 0.15mm					
5	19.72	2.1	2.4	265	1.33
6	17.98	1.9	3.5	288	2.11
7	16.24	1.8	5	315	3.17
8	14.50	1.6	7.5	347	5.31
9	12.76	1.4	10.5	388	8.57
10	11.02	1.2	16	440	15.00
Initial angle: 10°, thickness: 0.15mm					
5	19.95	4.5	5	536	1.38
6	18.19	4	7.5	585	2.25
7	16.43	3.6	11	645	3.61
8	14.67	3.3	15	717	5.68
9	12.91	2.9	23	808	9.31
10	11.15	2.4	33	925	17.08

To compare the balanced force, maximum stress and the negative stiffness with each other, the values were normalized to the smallest in the group. Fig. B.2 shows the results of the normalized values. The negative stiffness increases parabolic, from 1 to approximately 12. The balanced force increases parabolic, from 1 to approximately 7. The maximum stress in the beams increases linear, from 1 to 2. This shows that increasing the width, with optimizing the length of the bi-stable buckling beams is unfavorable: the negative stiffness is increasing more than the balanced force.

The behavior of the negative stiffness and the balanced force is parabolic because both the width and the length is changed. The formula for calculating the stiffness of straight bi-stable buckling beams was not found in literature, but probably deal with the term EI/L^3. If only the width is changing the negative stiffness and the balanced force is expected to increase linear. But in this case also the length is changing, which results in a parabolic behavior of the negative stiffness and the balanced force.

For increasing the width, the bi-stable buckling beams becomes highly sensitive for variations in the width.
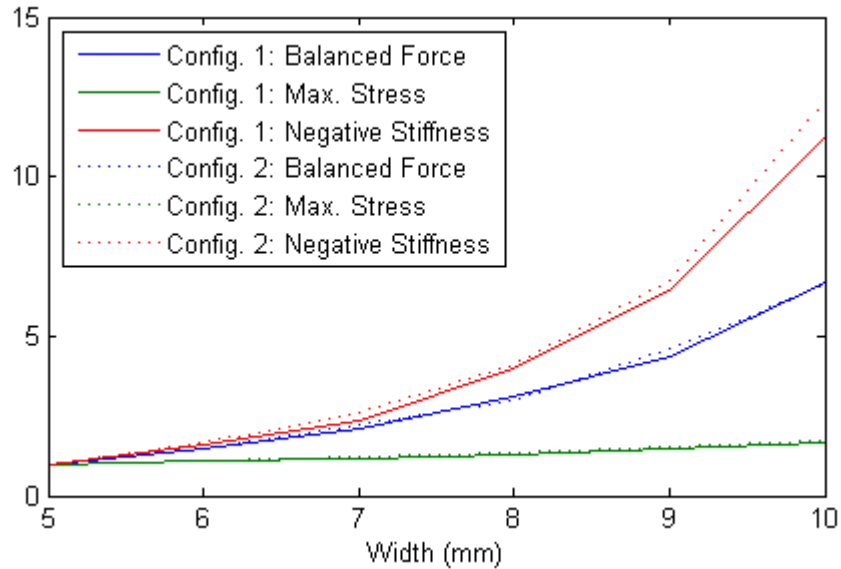

Fig. B.2. Results of the normalized values for balanced force, maximum stress and negative stiffness for increasing width and optimizing the length of the bi-stable buckling beams for two configurations.

Thickness

The thickness was increased from 0.15mm to 0.35mm, with steps of 0.05mm. Table B.1 shows the results of two different configurations, with a width of 5mm and 6mm, respectively. In both configurations the initial angle was 5° and the length was optimized to the maximum.

Table B.2. Results of simulations for increasing thickness of the bi-stable buckling beams for two different configurations.

Thickness (mm)	Length (mm)	Stroke (mm)	Balanced force (N)	Max.Stress (MPa)	Negative Stiffness (N/mm)
Width: 5mm, initial angle: 5°					
0.15	19.72	2.1	2.4	265	1.33
0.2	19.72	2.1	5.6	345	3.00
0.25	19.72	2	11	421	6.00
0.3	19.72	2	18	495	9.75
0.35	19.72	1.9	29	570	15.26
Width: 6mm, initial angle: 5°					
0.15	17.98	1.9	3.5	288	2.11
0.2	17.98	1.9	8	373	4.84
0.25	17.98	1.8	16	455	9.44
0.3	17.98	1.8	27	536	15.28
0.35	17.98	1.7	40	621	23.53

Fig. B.3 shows the results of the normalized values of the balanced force, maximum stress and negative stiffness. Both the negative stiffness and the balanced force are increasing simultaneously and parabolic from 1 to approximately 12. The maximum stress in the beams increases linear, from 1 to 2. Increasing the thickness of the bi-stable buckling beams results in an increase of both the balanced force and the negative stiffness. At the same time, the bi-stable buckling beams become more sensitive to fabrication errors on the thickness.
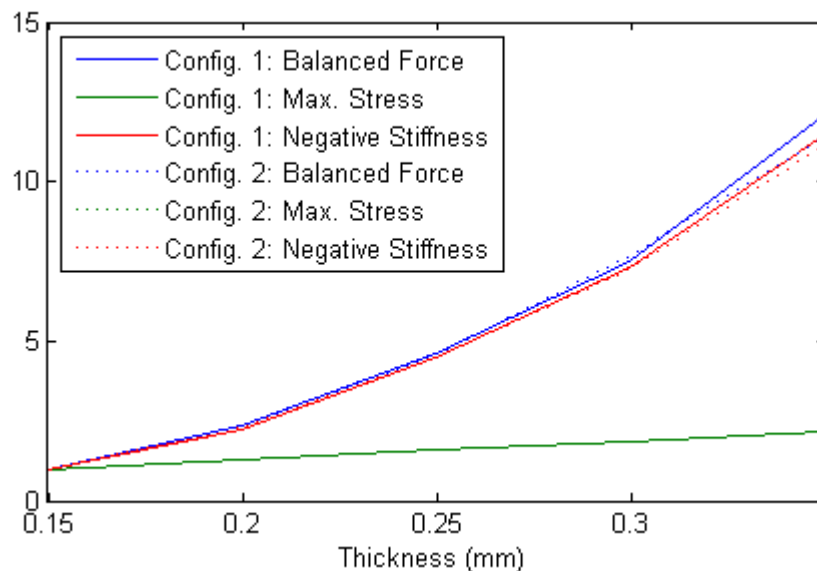

Fig. B.3. Results of the normalized values for balanced force, maximum stress and negative stiffness for increasing thickness of the bi-stable buckling beams for two configurations.

Length

For two different configurations (initial angle is 5° and 6°, respectively, the width is 5mm and the thickness is 0.3mm) the length was decreased from the maximum length for the configuration to 18mm. Table B.3 shows the results of the simulations.

Table B.3. Results of simulations for decreasing length of the bi-stable buckling beams for two different configurations.

Length (mm)	Stroke (mm)	Balanced force (N)	Max.Stress (MPa)	Negative Stiffness (N/mm)
initial angle: 5°, width: 5mm, thickness:0.3mm				
19.72	2.1	19	495	9.29
19	1.95	20	511	10.77
18.5	1.85	21	523	11.89
18	1.75	21.5	536	13.29
Initial angle: 6°, width: 5mm, thickness: 0.3mm				
19.75	2.5	25	601	10.20
19	2.4	26.5	621	11.46
18.5	2.3	28	636	12.61
18	2.2	29	651	14.09

In Fig. B.4 the results of the normalized values are shown. Immediately it can be seen that decreasing the length has a negative influence on the balanced force-negative stiffness relation. The negative stiffness increase linear to almost 1.4, where the balanced force and the maximum stress in the beams are nearly constant.
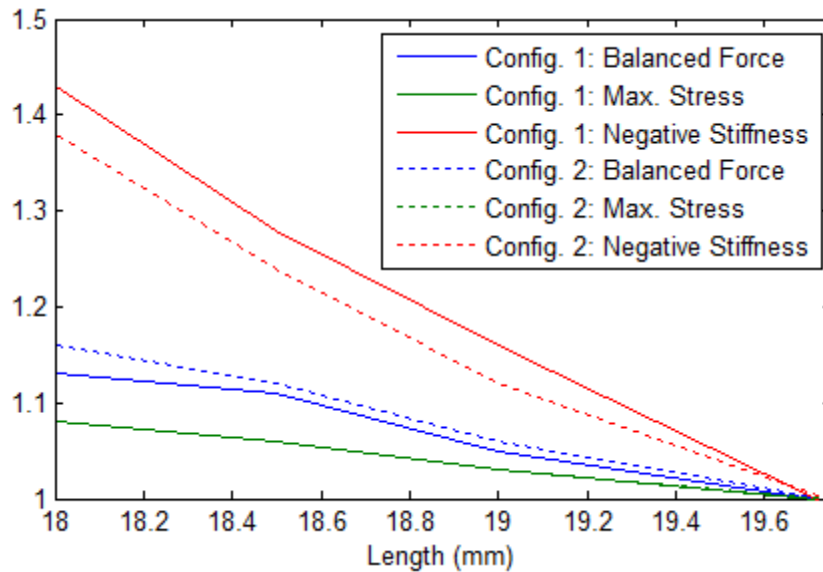

Fig. B.4. Results of the normalized values for balanced force, maximum stress and negative stiffness for decreasing length of the bi-stable buckling beams for two configurations.

Initial angle

The initial angle was increased from 5° to 10°, with steps of 1°. Table B.4 shows the results of two different configurations, with a width of 5mm and 7mm. In both configurations the thickness was 0.15mm and the length was optimized to fit in a triangular space with edges of 62mm.

Table B.4. Results of simulations for increasing initial angle of the bi-stable buckling beams for two different configurations.

Initial angle (^{o})	Length (mm)	Stroke (mm)	Balanced force (N)	Max.Stress (MPa)	Negative Stiffness (N/mm)
Width: 5mm, thickness:0.15mm					
5	19.72	2.1	2.4	265	1.33
6	19.75	2.6	3	320	1.35
7	19.79	3	3.6	375	1.40
8	19.84	3.5	4.1	429	1.37
9	19.89	4	4.6	483	1.38
10	19.95	4.5	5	536	1.38
Width: 7mm. thickness:0.15mm					
5	16.24	1.6	37	588	24.06
6	16.27	2	48	710	26.00
7	16.30	2.4	57	838	26.67
8	16.34	2.8	66	986	27.14
9	16.38	3.2	76	1100	27.81
10	16.43	3.5	87	1230	28.57

Fig. B.5 shows the results of the normalized values. The balanced force and the maximum stress increase simultaneously and linear to approximately 2. Conversely, the negative stiffness is almost constant. Increasing the initial angle has a positive effect on the balanced force-negative stiffness relation: the balanced force increases, while the negatives stiffness is constant. Increasing the initial angle increases the robustness to fabrication errors for the negative stiffness.
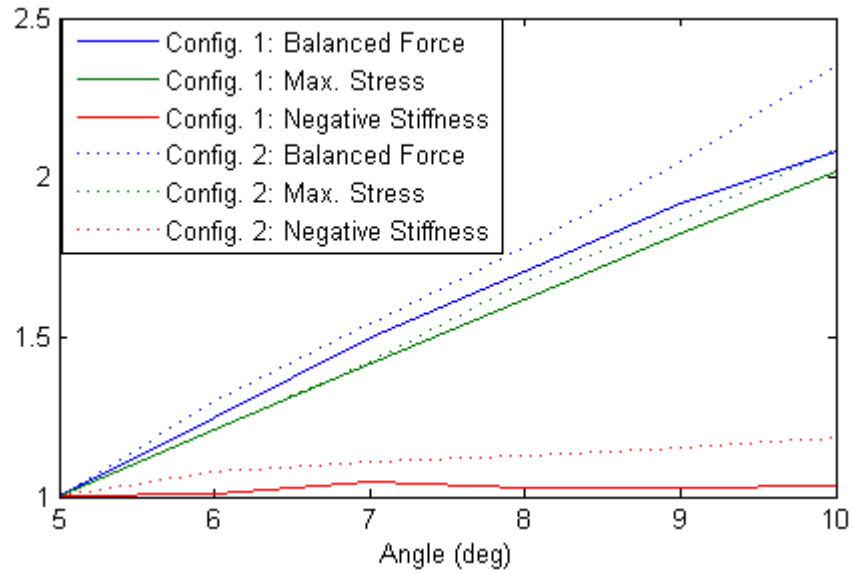
Fig. B.5. Results of the normalized values for balanced force, maximum stress and negative stiffness for increasing initial angle and optimizing the length of the bi-stable buckling beams for two configurations.

The objective of the final design is to balance a gravity force with low negative stiffness of the bi-stable beams. Increasing the width and the length has a negative influence on the force-negative stiffness relation. The length should be as large as possible, maximized to the available space. To cancel out the influence of fabrication errors on the negative stiffness both the width and the thickness should be as small as possible.

The initial angle of the bi-stable buckling beams should be as large as possible, considering the allowed stresses in the mechanism.

B 1.2 V-shaped beams

The V-shaped beam can be assumed as two beams, fixed at one end where the connect and straight guided perpendicular to the beam at the other end (Fig B.6), in series. The stiffness of the v-shaped beam can be approached by considering Eq. A.2 under an angle (Eq. B.1-B.3) (Gere, 2002).
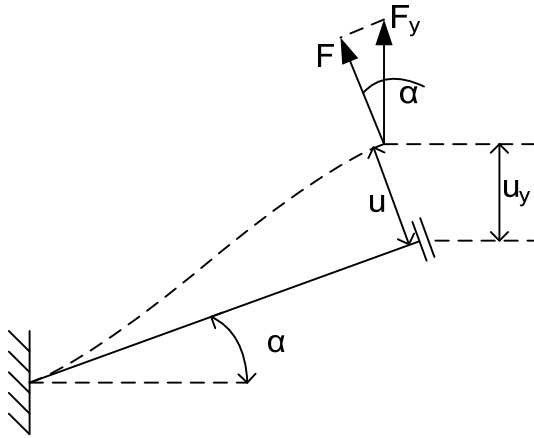

$$K_{\substack{v-shaped \\ beam}} = \cfrac{1}{\cfrac{1}{K_{beam}} + \cfrac{1}{K_{beam}}} \quad \text{(B.1)}$$

$$= \frac{K_{beam}}{2}$$

$$K_{beam} = \frac{F_v}{x_v} = \frac{F/cos(\alpha)}{x \cdot cos(\alpha)}$$

$$= \frac{12EI}{L^3 \cdot cos^2(\alpha)} \quad \text{(B.2)}$$

Fig. B.6. The V-shaped beam can be assumed as two beams, fixed at one end where they connect and straight guided at the other end, in series.

$$K_{\substack{v-shaped \\ beam}} = \frac{6Ewt^3}{L^3 \cdot cos^2(\alpha)} \quad \text{(B.3)}$$

The dimensions of the v-shaped beams can be optimized when the total negative stiffness of the bi-stable buckling beams is known. The v-shaped beams should have the same stiffness as the negative stiffness of the bi-stable buckling beams. The number of the v-shaped beams depends on the required stroke and the allowable stresses in the material. An important remark is that the stiffness of the v-shaped beams is highly sensitive for variations in thickness and length of the beams.

B.2 In-plane balancing

The stiffness of the flexible rods performing the in-plane motions is a result of the force applied on the rods. If this force is the same as the buckling load of the rods the stiffness is zero for transversal (Spiering and Grootenboer, 1993). The buckling force can be calculated according to Eq B.4 (Gere, 2002).

$$F_b = \frac{\pi^2 EI}{L^2} \rightarrow \left(I = \frac{\pi d^4}{64} \right) \rightarrow F_b = \frac{\pi^3 E d^4}{64 L^2} \quad \text{(B.4)}$$

The buckling force is highly depending on the diameter of the rods. For safety reasons it is not recommended to load the rods with the buckling load, but with a slightly smaller force.

B.3   Conclusions

In the investigation to the relation between balanced force, maximum stress and negative stiffness of the bi-stable buckling beams it has been shown that the width and the thickness of the bi-stable buckling beams should be as small as possible, to increase the robustness to fabrication errors, the length should be optimized to the maximum for the available space, in order to balance a gravity force with low negative stiffness of the bi-stable beams. The most important design parameter for bi-stable beams is the initial angle. Increasing the initial angle does not affect the sensitivity of the negative stiffness to fabrication errors for initial angle.

The stiffness of the v-shaped beam are highly depending on the thickness and length of the beams. The dimensions are determined according to the negative stiffness of the bi-stable buckling beams.

The buckling force, and consequently the stiffness for in-plane motions of the flexible rods is highly depending on the diameter of the rods. For safety reasons, it is recommended to load the rods with a slightly smaller force than the buckling force.

Appendix C

Prototype

A prototype was made to evaluate the model and the balancing principle (Fig. C.1). In this section the detailed dimensions of the different components and materials are presented. Furthermore, the drawings and some photos of the prototype are included.
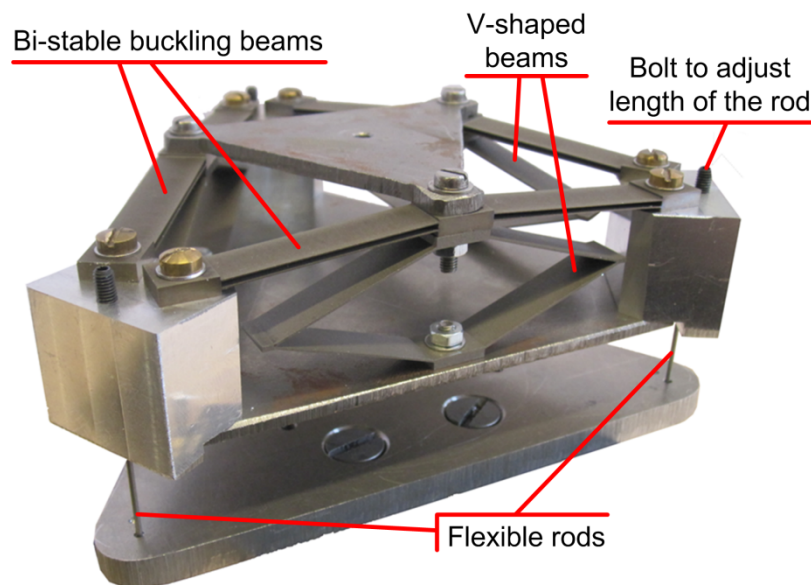

Fig C.1. The assembled prototype with the different components and tuning possibilities.

C.1 Detailed dimensions

C.1.1 Bi-stable buckling beams

Due to the specifications of the measurements setup (see Appendix D) the prototype was optimized to balance a gravity force of 40N.
The bi-stable buckling beams were manufactured using wire electrical discharge machining (wire-EDM). This production method has some limitations. In collaboration with the manufacturer (Optimum draadvonktechniek b.v.) the limitations were discussed and the critical dimensions were determined. The most important limitation of wire-EDM was that the thickness of a beam cannot be smaller than 0.15mm. If the thickness is larger, the influence of heat on the dimensions is smaller and it was guaranteed that the thickness would be closer to

the specified dimensions. Therefore, in this prototype the bi-stable buckling beams are 0.25mm. With an initial angle of 5° and a width of 9mm, the length of the beams should be 35mm.

The material of the bi-stable buckling beams is titanium Grade 5 (Ti6Al4V). This material is a special type of titanium with a high yield strength (830 MPa) compared to the Young's modulus (113 GPa). This material can resist high stresses without plastic deformation.

Two pairs of bi-stable buckling beams are placed above each other, to reduce the parasitic rotation during buckling.

The bi-stable beams were modeled in ANSYS^{TM} using the approach described in Dunning et al. (2011b) (see Appendix E). In Fig. C.2 the results of the simulation are shown. The negative stiffness of the bi-stable beams is 11.90 N/mm in *Tz* direction.

C.1.2   V-shaped beams

The v-shaped beams were made by the same manufacturer as the bi-stable buckling beams. They were also made out of the same material, with the same width, so it could be manufactured monolithic.

Knowing the stiffness of the bi-stable beams, 11.90N/mm, the dimensions of the v-shaped beams can be calculated. It was chosen to have an angle with the ground of 20°. With a thickness of 0.45mm, a length of 29.3mm is needed.

The results of the simulation of the v-shaped beams is shown in Fig. C.2.

Extra simulations were done to determine the max. fabrication errors. The two worst scenarios were simulated. In the first scenario the stiffness of the bi-stable buckling beams is lower, and the stiffness of the v-shaped beams is larger than modeled, resulting in a mechanism with a low positive stiffness in the balanced domain. In the second scenario the stiffness of the bi-stable buckling beams is larger and the stiffness of the v-shaped beams is lower than modeled, resulting in a mechanism with a low negative stiffness in the balanced domain. The maximum fabrication error on the dimensions must be smaller than 5µm to fulfill the design criterion of a stiffness lower than 1N/mm in *Tz* direction. Due to several reasons, including the cost item, it is decided to leave the tuning mechanisms for the stiffness and preload out of the prototype.

Table C.1. Overview of the dimensions and material for the mechanism for out-of-plane balancing.

Bi-stable buckling beams	
Length	35mm
Width	9mm
Thickness	0.25mm
Initial angle	5°
Material	Titanium Grade 5 (Ti6Al4V)

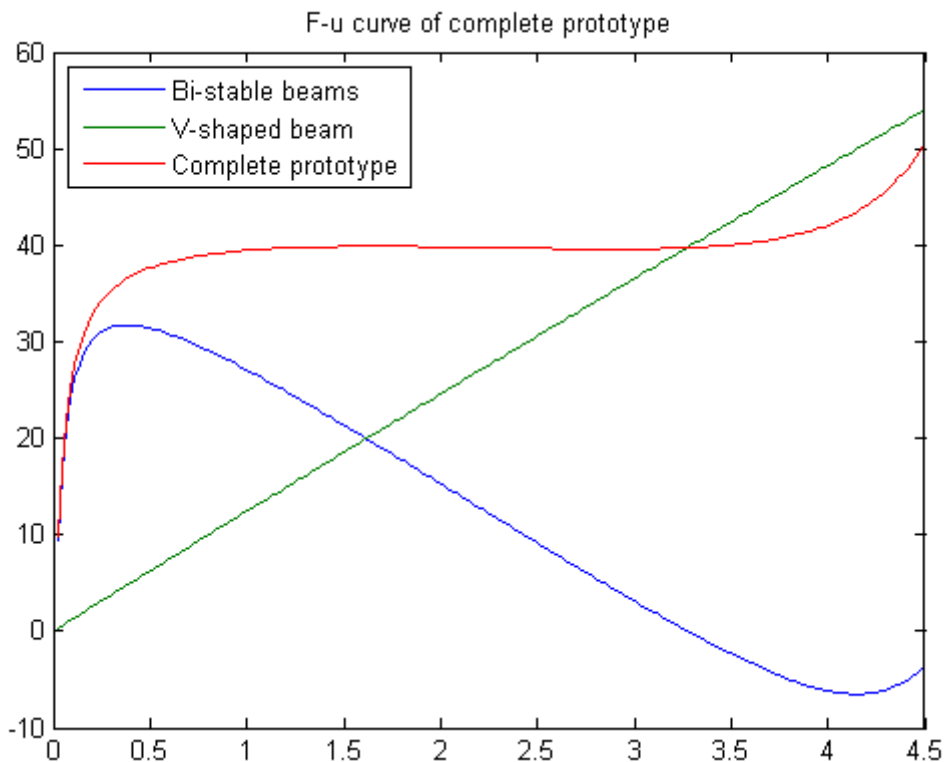| **V-shaped beams**	
Length	29.3mm
Width	9mm
Thickness	0.45mm
Angle with ground	20°
Material	Titanium Grade 5 (Ti6Al4V)

Fig. C.2. Results of the simulation of the mechanism for out-of-plane motion in Tz direction. The negative stiffness of the bi-stable buckling beams is compensated by a positive stiffness, resulting in a statically balanced domain with constant force and zero stiffness.

C.1.3   Rods for in-plane balancing

The flexible rods for in-plane motions were dimensioned to have a buckling force of 40N. Due to some manufacturing and cost issues, and to prevent that the beams will not be exceptionally long, the beams have a diameter of 1mm, made of brass (CuZn39Pb3). This material has a Young's modulus of 97 MPa (MATWEB). With these properties, the length of the rods should be 50mm.

Due to fabrication errors both the diameter and the length can vary. Extracting the error from the diameter and adding to the length ('worst-case 2') decrease the buckling force. In this case the rods should balance 40N (=13,33N per rod). In table C.2 the buckling force of the three cases is shown, with a fabrication error of 0.08mm.

Table C.2. The calculated buckling force of one flexible rod for three different cases. In the middle the normal case is shown. The other cases are the limits for an error of 0,08mm.

Length Diameter	'worst-case 1': 49.92mm	50mm	'worst-case 2': 50.08mm
0.92mm			13.42N
1mm		18.98N	
1.08mm	26.65N		

A simulation is done using the length and diameter of 'worst-case 1' with the buckling load of 'worst-case 2'. In Fig. C.3 the result is shown. The stiffness of one rod will be 0.30N/mm for in-plane translations. The complete in-plane balancing mechanism will have a stiffness less than 1N/mm in the worst case.
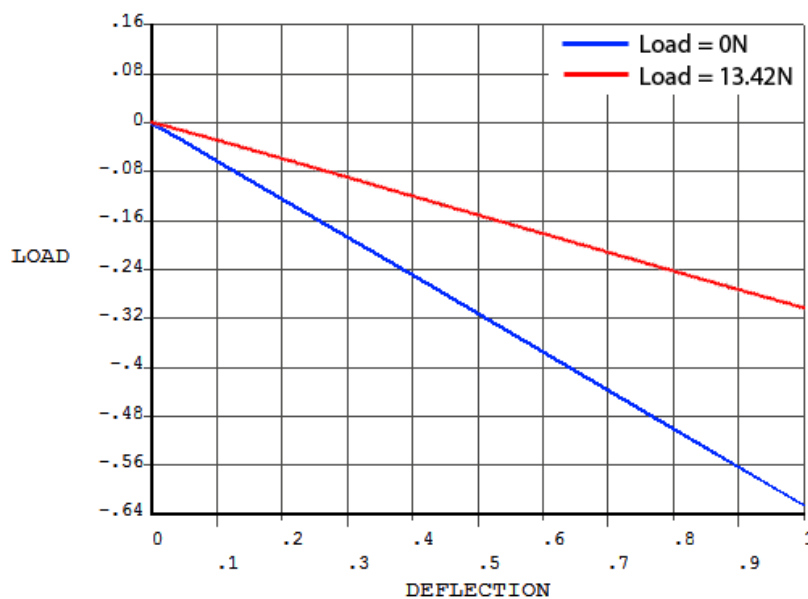

Fig. C.3. Force-displacement curve of one flexible rod, where 'worst-case 1' is loaded with the buckling load of 'worst-case 2', compared to a load of 0N. (see Table C.2).

Table C.3. Overview of the dimensions for the rods for in-plane balancing.

Length	50mm
Diameter	1mm
Material	Brass (CuZn39Pb3)

C.2   Assembling

The bi-stable beams were mounted on three blocks, flat on top, with M3 bolts. The blocks were mounted on the bottom plate. It is important to mount the bi-stable buckling beams without stresses inside the beams. The v-shaped beams were mounted beneath the bi-stable buckling beams, and together with the top plate fixed to the bi-stable beams with bolt and nut. The v-shaped beams were also fixed to the bottom plate.

The rods were inserted in the blocks. With a wire-end the length of the beams could be adjusted. At the other end the rods were inserted in the mounting plate (ground). This mounting plate is mounted on the XY-stage (see Appendix D).
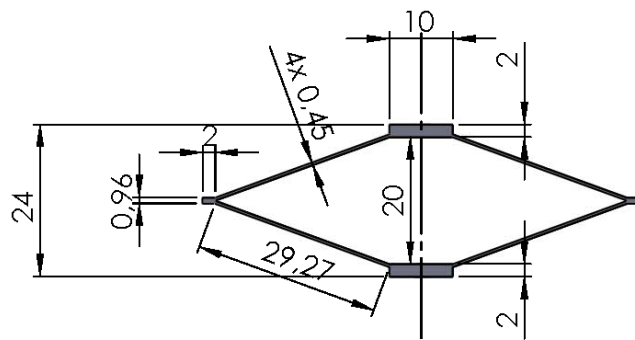
C.3   Drawings and photos

On the next pages the following drawings for manufacturing the prototype and photos are shown:

- Bi-stable buckling beams
- V-shaped beams
- Blocks
- Top plate
- Bottom plate
- Mounting plate
- Perspective view of the prototype
- Side view of the prototype
- Top view of the prototype

Drawing of a bi-stable buckling beam
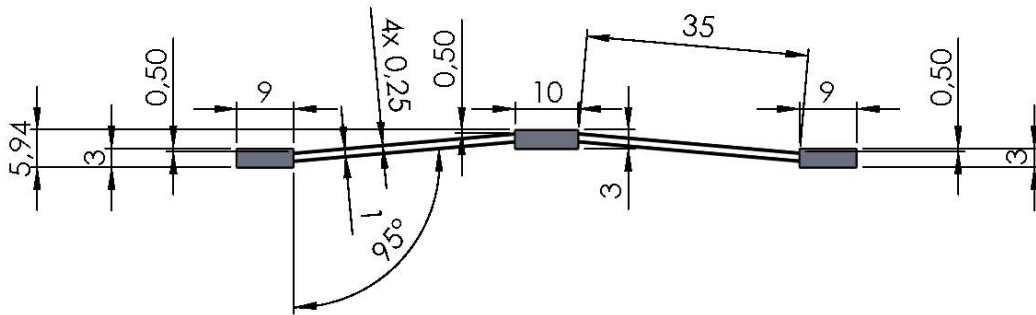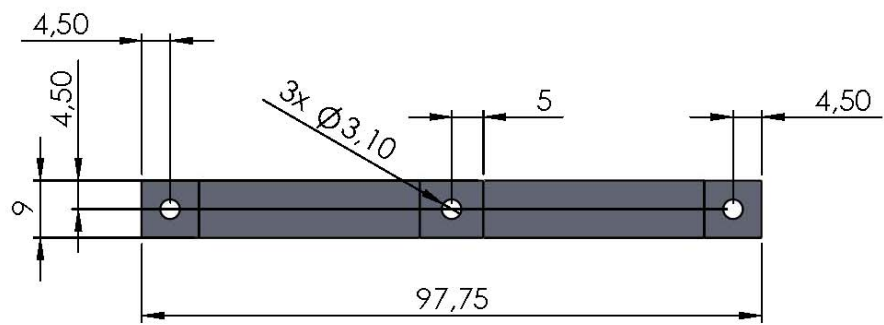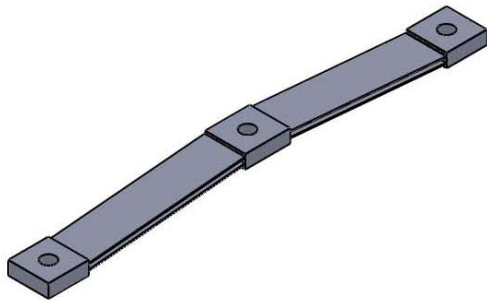
Drawing of a v-shaped beam
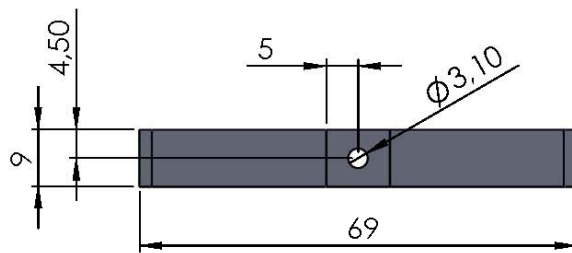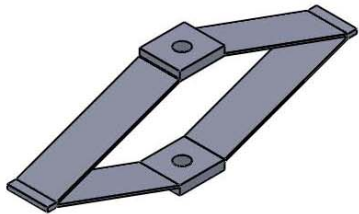
Drawing of the blocks (to mount the bi-stable buckling beams)
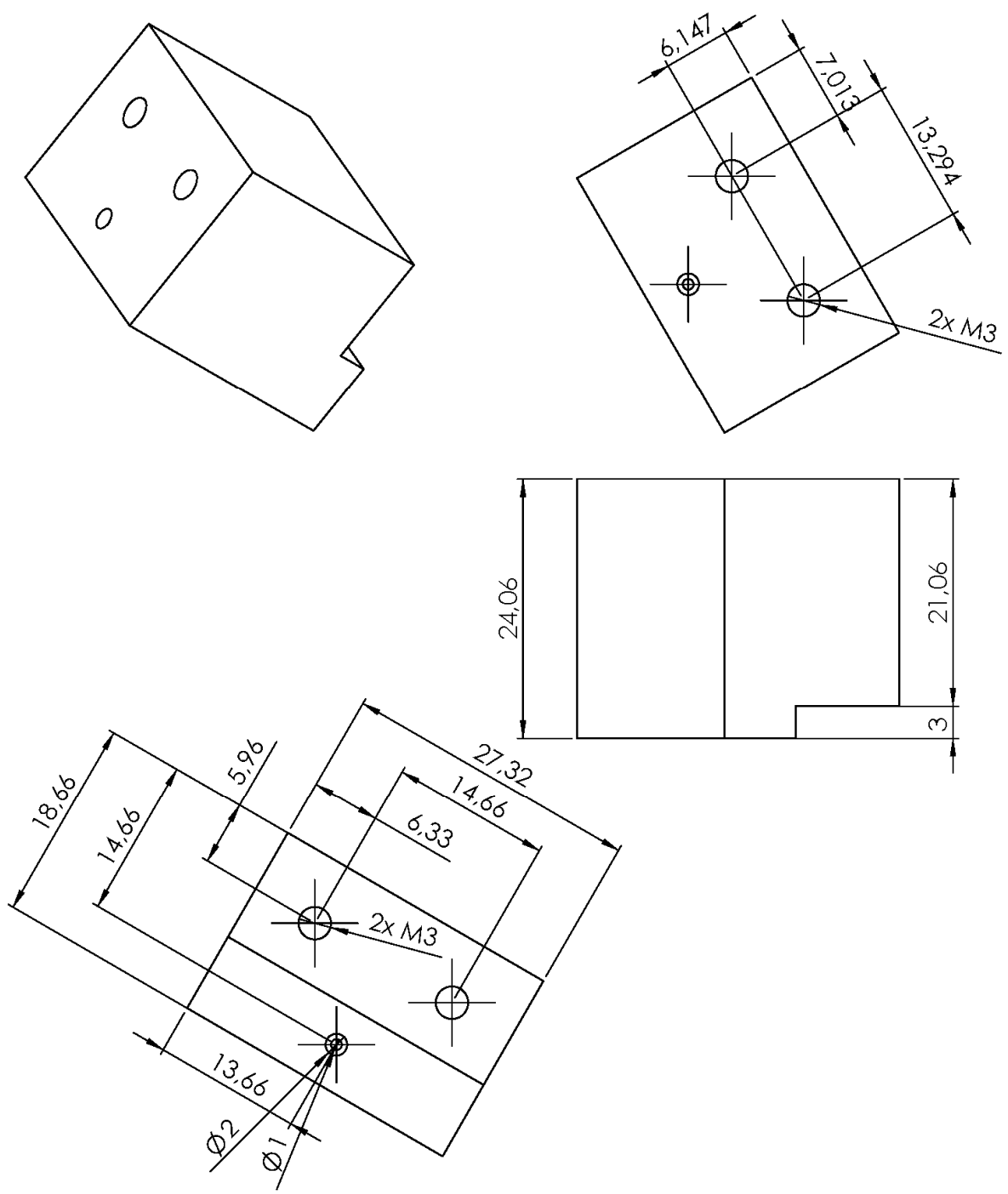
Drawing of the top plate

Drawing of the bottom plate

Drawing of the mounting plate (ground)
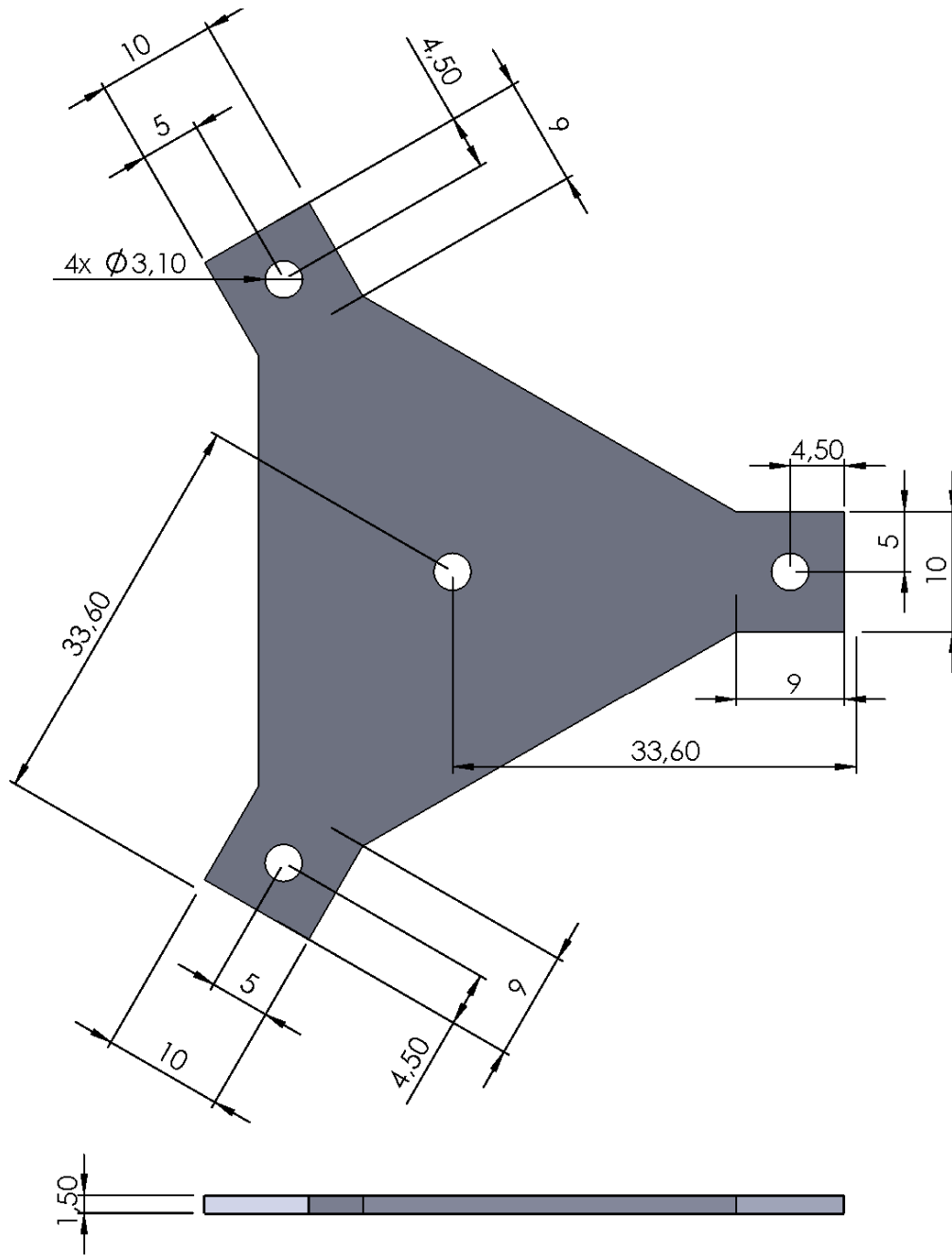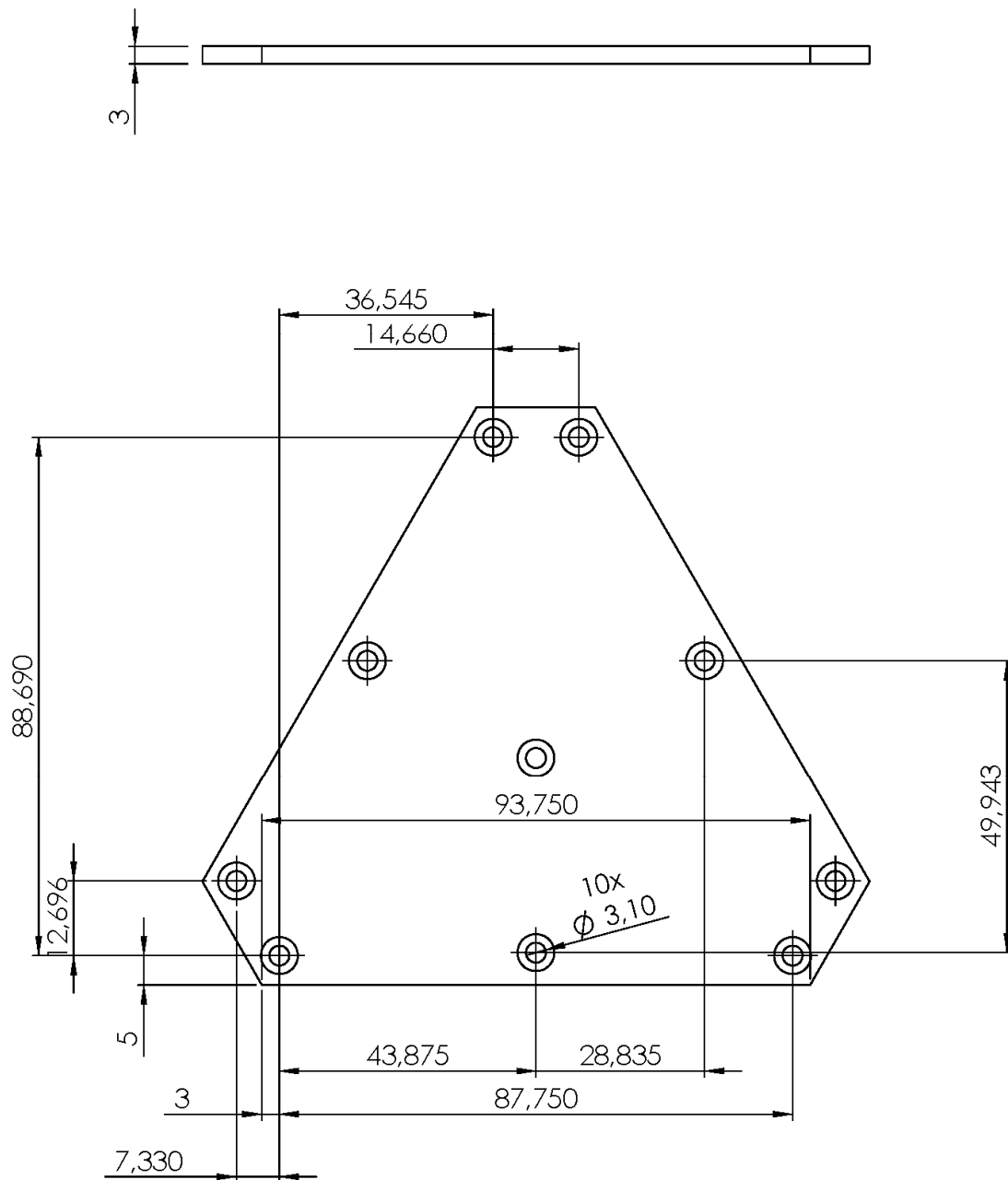
Photos of the prototype

Perspective view

Bi-stable buckling beams

Top plate

V-shaped beams

Bolt to adjust length of the rod

Rod

Block

Bottom plate

Mounting plate
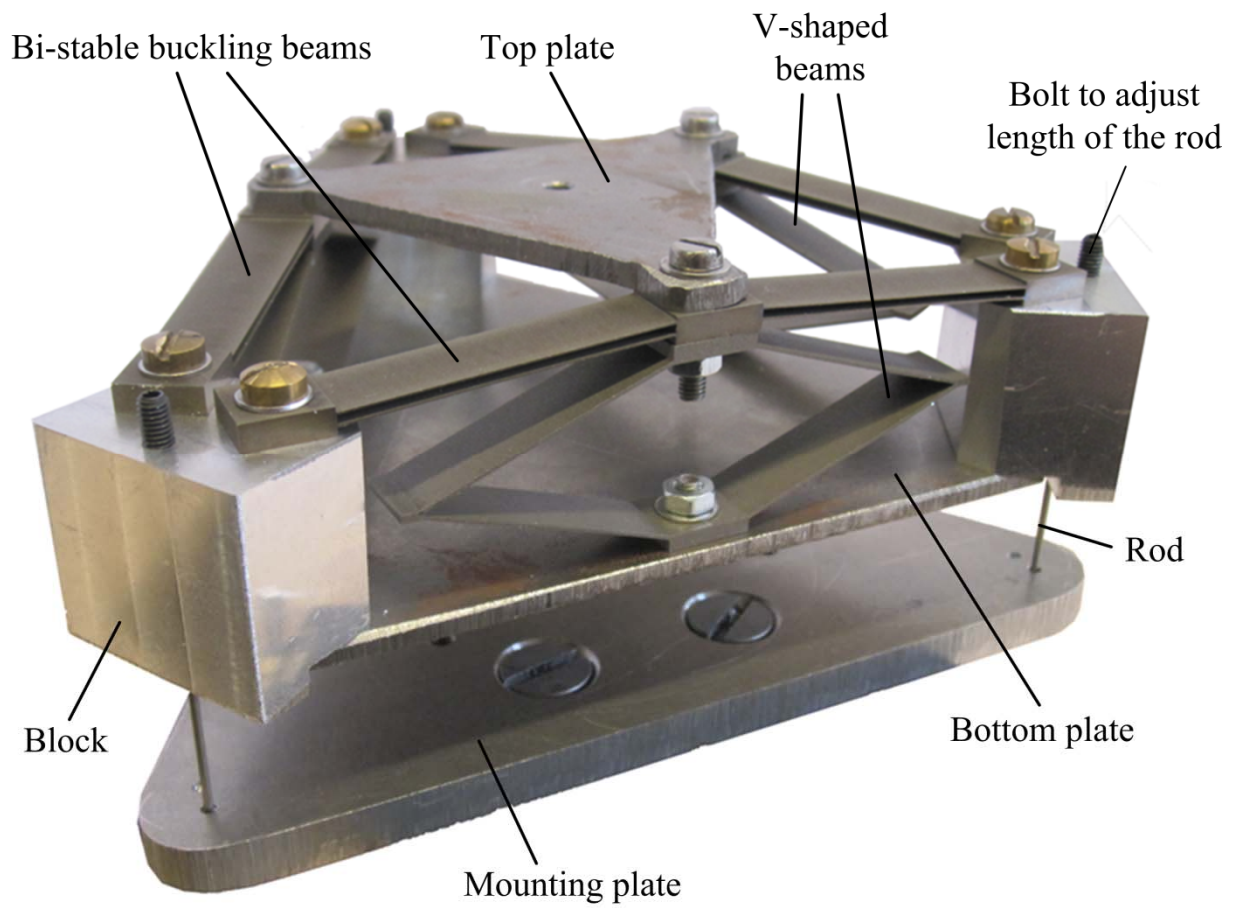
Side view
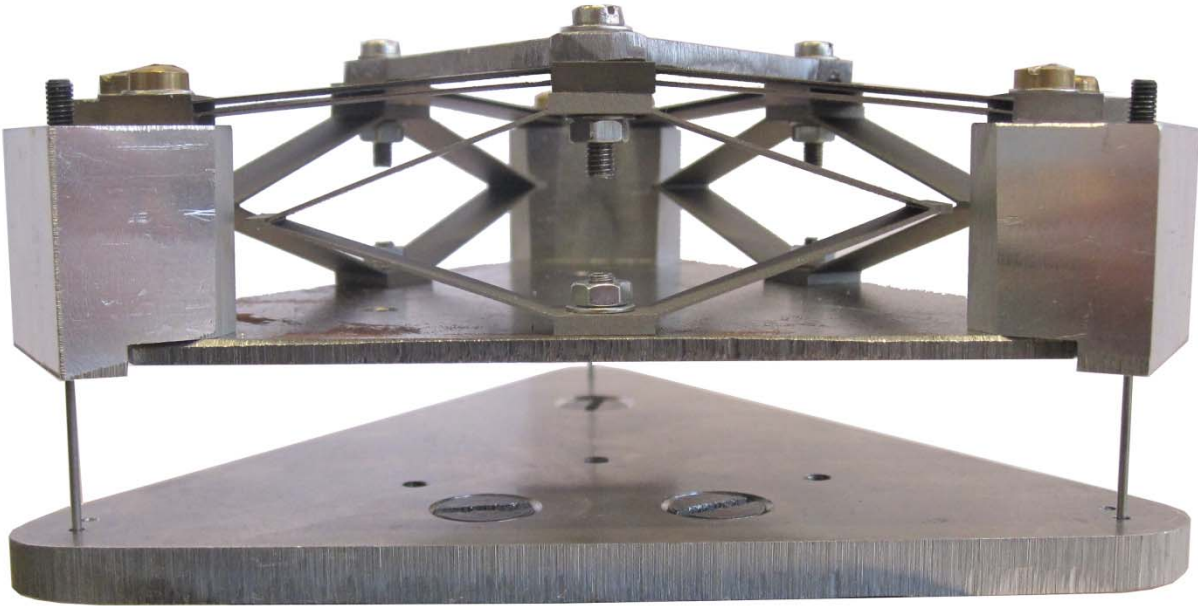
Top view
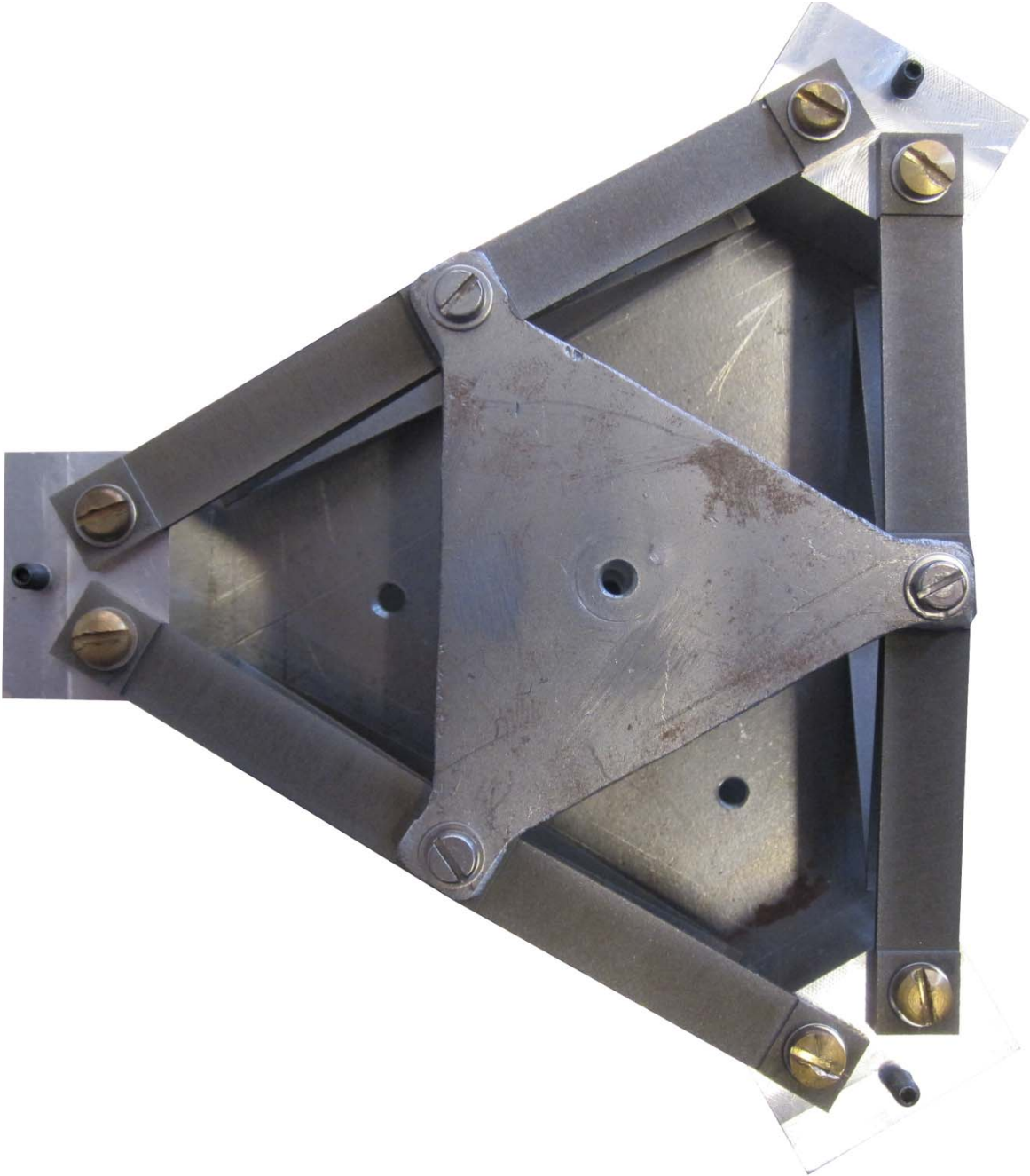
Appendix D

Measuring and Data Processing

D.1   Measurement setup

For measuring the stiffness in each direction a measurement setup was build. In Fig. D.1 and Fig. D.2 pictures of the measurement setup with the different modulus are shown.
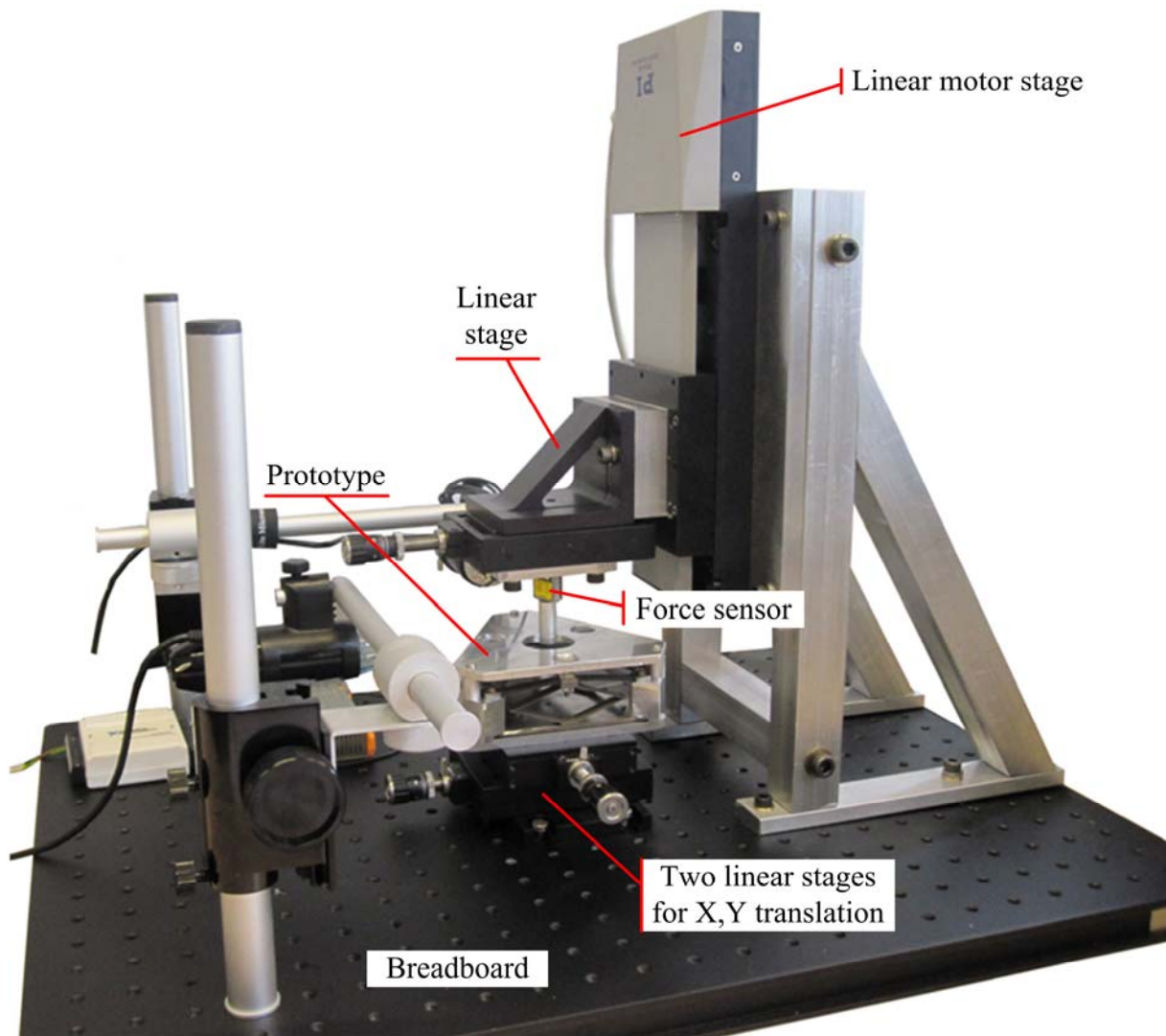
Fig. D.1. Perspective view of the measurement setup with the different modules.
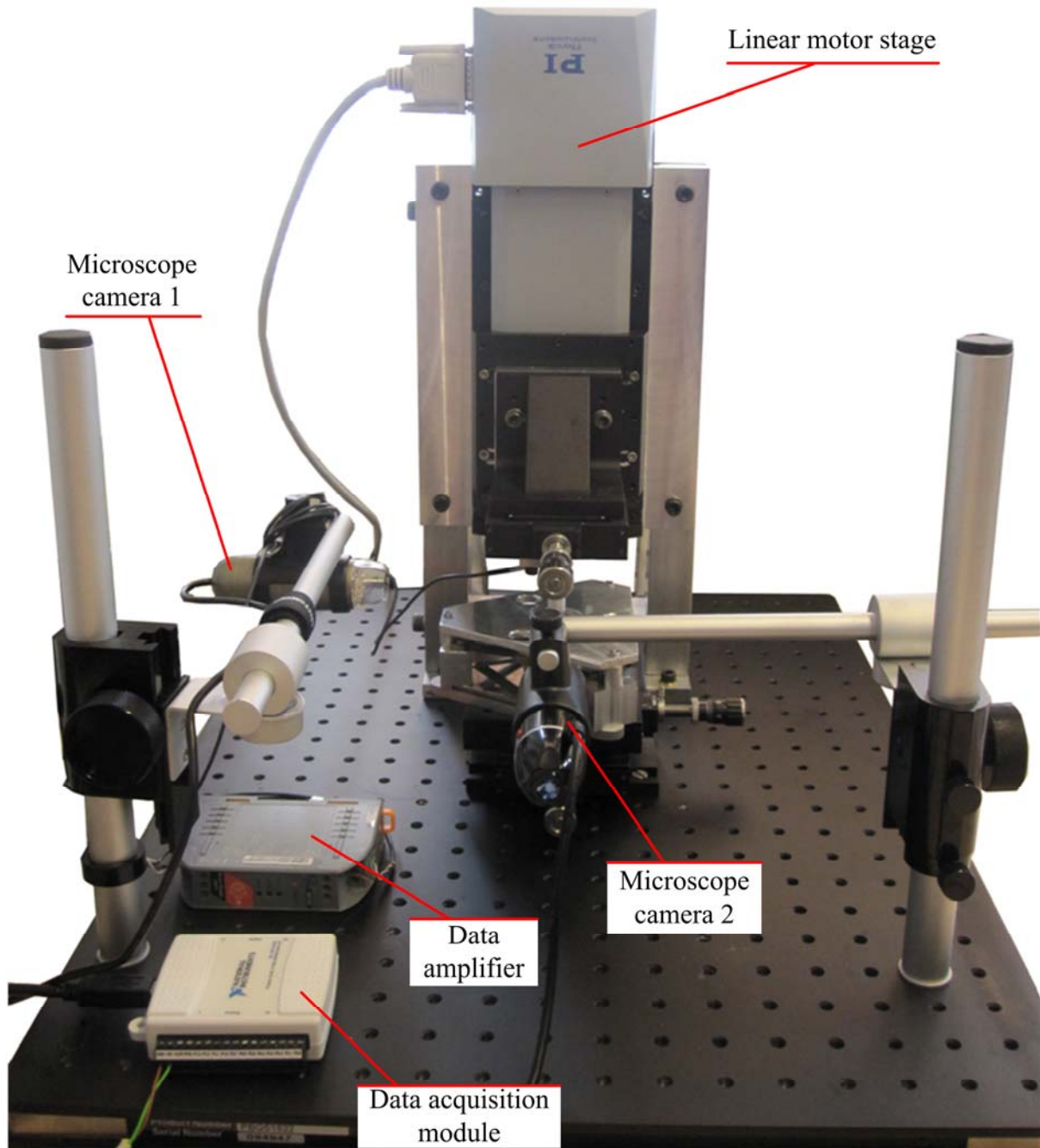
Fig. D.2. Side view of the measurement setup with the different modules.

During measurements the prototype was covered with an extra plate (Fig. D.3). This was to avoid that bending of the bottom plate and the blocks affect the bi-stable behavior of the bi-stable buckling beams. The bending is caused by the large horizontal reaction forces of the bi-stable buckling beams. Simulations showed that for this prototype the maximum horizontal reaction forces are 76N.
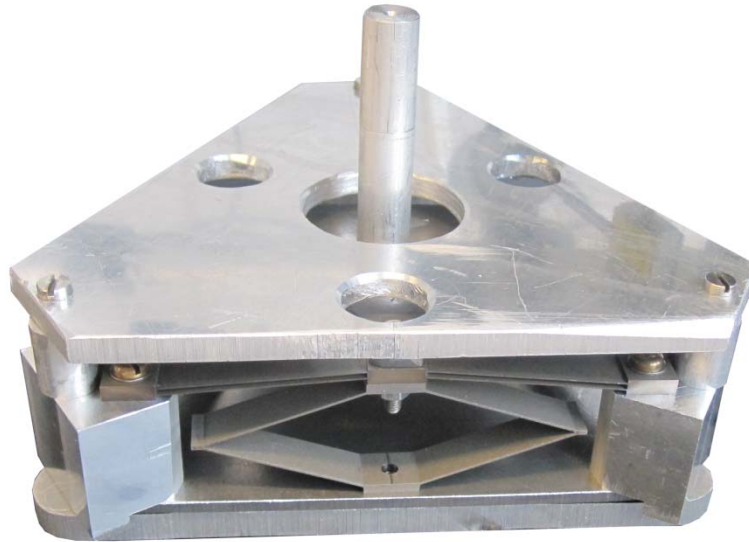
Fig. D.3. The prototype was covered with an extra plate, to avoid that bending in the bottom plate or blocks affect the bi-stable behavior of the bi-stable buckling beams.

The different modules in the measurement setup are the following:

1. Breadboard (Thorlabs PBG51522, dim. 600x450x25)

2. Three manual linear stages (Thorlabs PT3A/M, resolution: 25µm, travel range: 25mm)

3. Linear motor stage (Physik Instrumente M-505.4DG, resolution: 0.05µm, travel range: 100mm)

4. Force sensor (Futek LSB200, resolution 2mV/V, range: 0-44.5N)

5. Data amplifier (ICP DAS 3016)

6. Data acquisition module (National Instruments USB6008)

7. Microscope camera 1 (Dino-Lite AM-4013TL, frame rate: 30fps, magnification rate: 20-90x)

8. Microscope camera 2 (BW1008, frame rate: 30fps, magnification rate: 5-500x)

The data amplifier was set on an amplification factor of 1000. The input of ±10mV was amplified to an output of ±10V. The calibration factor for the force sensor was determined using weights, and for this experiment set to 5.6705 N/V. With the 'zero' screw on the data amplifier the force sensor can be set to zero, when there is no load on the force sensor.

For the measurements the speed of the linear motor stage was set to 4000 counts/s, which corresponds to 66 µm/s.

The software used to record and process the data are the following:

1. Labview 10 National Instruments
    a. File: MeasurementSetup.vi

2. Matlab R2011a

D.2 *Tz* direction

The force-displacement characteristic in *Tz* direction was measured and showed according to the following protocols.

Measurement protocol

1. Attach the prototype, without the rods, tight to the force sensor.
2. Make sure that the prototype is aligned horizontally.
3. Attach the mounting plate on top of the two linear stages.
4. Start Labview
5. Select file: MeasurementSetup.vi (Fig. D.4)
6. Press RUN.
7. If an error is given, the COM-port of the actuator is wrong.
8. Fill in the filename of the measurement: Tz_1.txt
9. Adjust the linear motor stage such that the prototype is slightly above the mounting plate with REL.MOVE in Labview.
10. Fill in the TRAVEL DISTANCE of 4500µm.
11. Activate TWO-WAY. The linear motor stage will go forwards and backwards.
12. Press CONTINUE.
13. When the linear motor stage is at its original position, press STOP.
14. Repeat the measurement 4 times.
15. Repeat the measurements for the bi-stable buckling beams (filename: BistableBeams_1.txt) and the v-shaped beams (filename: VshapedBeams_1.txt).

Data processing protocol

1. Open Matlab

2. Select file: Tz_balancing.m

3. Press RUN.

4. The program will show the force-displacement characteristic of the measurements for the bi-stable buckling beams, v-shaped beams and the complete prototype.
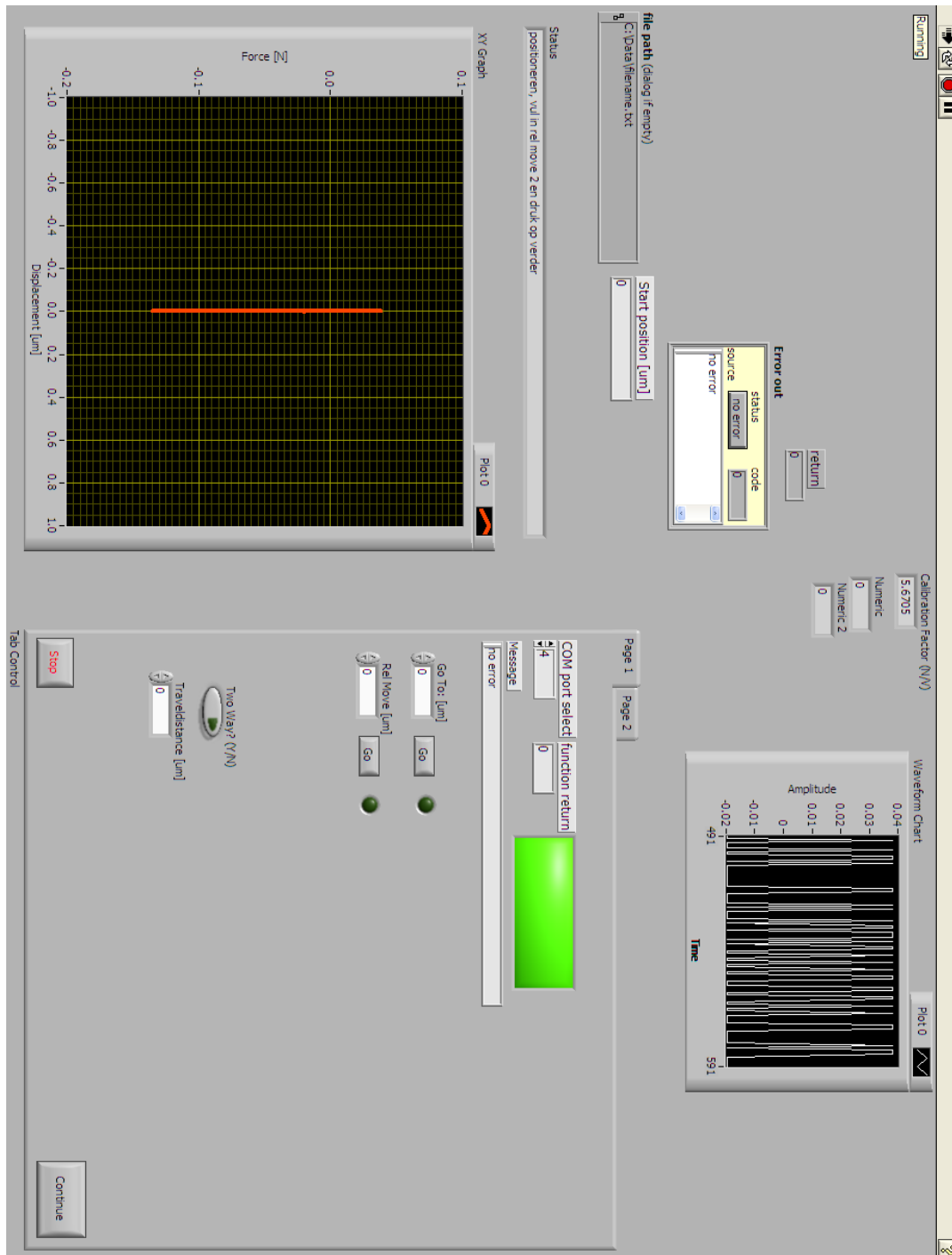
Fig. D.4. Interface of the Labview file: MesurementSetup.vi

D.3   *Rx, Ry* direction

The determine the rotational stiffness for out-of-plane motions, caused by the torsion of the bi-stable beams and v-shaped beams, the prototype was loaded with a weight, corresponding to the balanced force in T_z direction, and a moment was applied. This moment was calculated with the measured force, the moment induced by the weight and the moment induced by the three balanced mechanism. Fig. D.5 shows the calculation for the moment for *Rx* direction, induced by torsion of the bi-stable buckling beams and the v-shaped beams, where the characteristic lengths were measured from the middle of the stiff beam (Fig. D.7).

$$\theta = \tan^{-1}\left(\frac{X}{a}\right)$$

$$M_{Rx} = F_{meas} \cdot a + mg \cdot b \cdot \sin(\theta) - F_{mech} \cdot c - 2 \cdot F_{mech} \cdot d$$
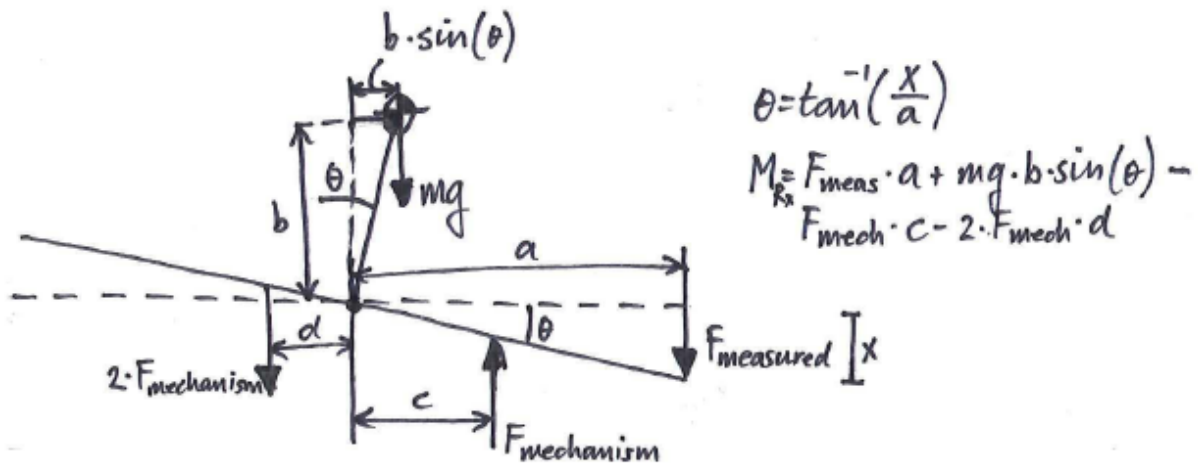
Fig. D.5. Calculation of the moment in Rx direction, induced by torsion: a=80mm, b=18.38mm, c=33mm and d=16.5mm. $F_{mechanism}$ is determined by dividing the stiffness in Tz direction with the displacement of the balanced mechanism.

Fig. D.6. shows the calculation for the moment for *Ry* direction, induced by the torsion of the bi-stable buckling beams and the v-shaped beams.

$$\theta = \tan^{-1}\left(\frac{X}{a}\right)$$

$$M_{Ry} = F_{meas} \cdot a + mg \cdot b \cdot \sin(\theta) - F_{mech} \cdot c \cdot 2$$
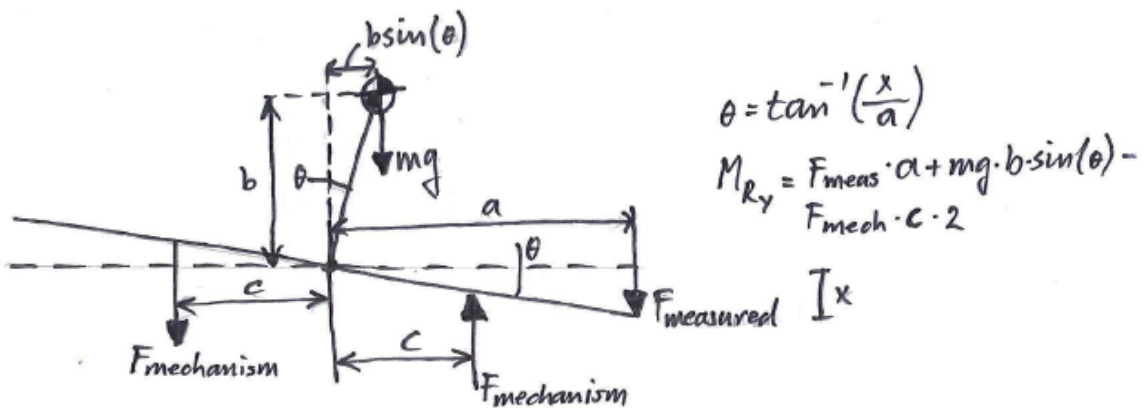
Fig. D.6. Calculation of the moment in Ry direction, induced by torsion: a=80mm, b=18.38mm and c=28.57mm. $F_{mechanism}$ is determined by dividing the stiffness in Tz direction with the displacement of the balanced mechanism.

Measurement protocol

1. Attach the mounting plate on top of the two linear stages.

2. Attach the prototype, without the rods, to the mounting plate.

3. Attach a stiff beam on top of the moving platform of the prototype perpendicular to a bi-stable buckling beam.

4. Put a weight of 3.508kg (balanced force determined in the first experiment) on top of the stiff beam an fix it with a nut.

5. Align the laser displacement sensor on one side of the stiff beam, 80mm from the middle en 25mm above the stiff beam (Fig. D.7).

6. Align the force sensor on the other side of the stiff beam, 80mm from the middle. Make sure the force sensor can load the beam through a ball contact. .

7. Start Labview

8. Select file: MeasurementSetup.vi (Fig. D.4)

9. Press RUN.

10. If an error is given, the COM-port of the actuator is wrong.

11. Fill in the filename of the measurement: Rx_1.txt

12. Adjust the linear motor stage such that the force sensor is slightly above the stiff beam, with REL.MOVE in Labview.

13. Fill in the TRAVEL DISTANCE of 2000µm.

14. Activate TWO-WAY. The linear motor stage will go forwards and backwards.

15. Press CONTINUE.

16. When the linear motor stage is at its original position, press STOP.

17. Repeat the measurement 4 times.

18. Repeat the measurements for rotation around the y-axis, by placing the stiff beam parallel to a bi-stable beam (filename: Ry_1.txt).

Data processing protocol

1. Open Matlab

2. Select file: Rxyz_balancing.m

3. Press RUN.

4. The program will show the moment-rotation characteristic of the measurements for the out-of-plane rotations.
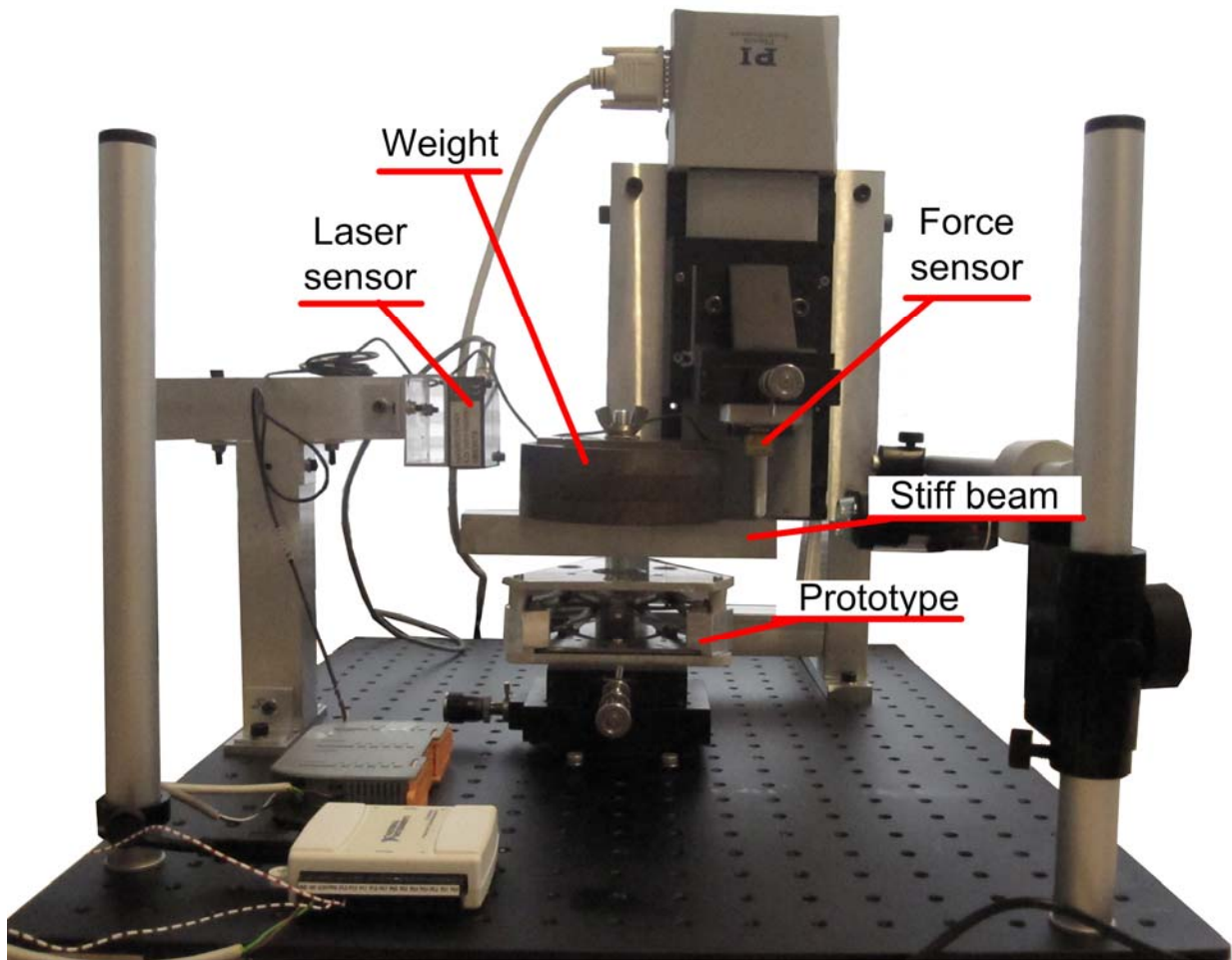
Fig. D.7. Side view of the measurement setup for out-of-plane rotation about the y-axis (Ry).

D.4   *Tx, Ty* direction

The behavior of the in-plane mechanism is the same for *Tx* and *Ty* direction. The force-displacement curve in *Tx* and *Ty* direction was measured and showed according to the following protocols.

Measurement protocol

1. Attach the mounting plate on top of the two linear stages

2. Mount the prototype with the rods on the mounting plate.

3. Load the prototype very carefully with 3,508kg (balanced force determined in the first experiment), placed in the middle of the prototype.

4. Mount the linear motor stage horizontally (Fig. D.8).

5. Start Labview

6. Select file: MeasurementSetup.vi

7. Press RUN.

8. If an error is given, the COM-port of the actuator is wrong.

9. Fill in the filename of the measurement: Txy_3508g_1.txt

10. Adjust the force sensor and the prototype with the linear stages such that the force sensor is in the middle of the prototype.

11. Fill in the TRAVEL DISTANCE of 2000μm.

12. Activate TWO-WAY. The linear motor stage will go forwards and backwards.

13. Press CONTINUE.

14. When the linear motor stage is at its original position, press STOP.

15. Repeat the measurement 4 times.

16. Repeat the measurements for a load of the prototype (filename: Txy_435g_1.txt).

Fig. D.8. Side view of the measurement setup for in-plane translation.

Data processing protocol

1. Open Matlab
2. Select file: Txy_balancing.m
3. Press RUN.
4. The program will show the force-displacement characteristic of the measurements.

D.5 R_Z direction

The moment-rotation characteristic for in-plane rotation was measured and showed according to the following protocols. The moment in R_Z direction was calculated by multiplying the measured force with the characteristic length of 65mm. A displacement of 1mm corresponds to a rotation of 15mrad (Fig. D.9).
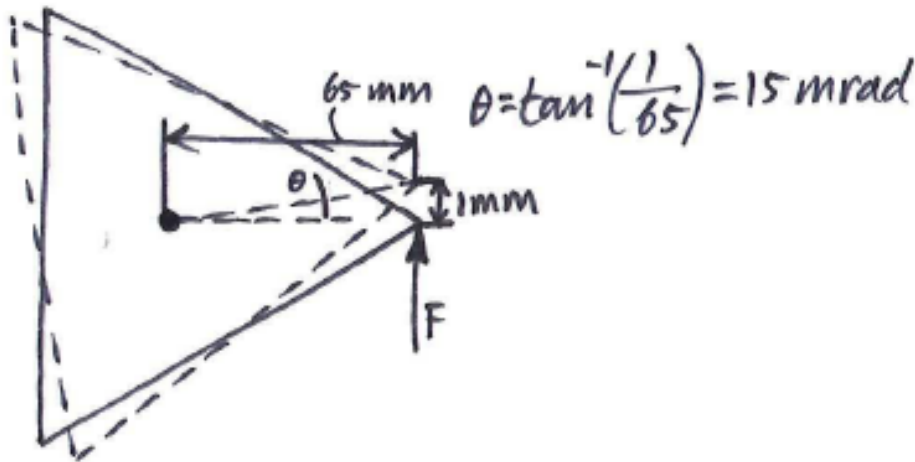
Fig. D.9. Sketch of the measurement setup to determine the moment-rotation characteristic for Rz direction. The moment was calculated by multiplying the measured force with the characteristic length of 65mm.

Measurement protocol

1. Attach the mounting plate on top of the two linear stages
2. Attach the ball bearing in the middle of the bottom plate.
3. Mount the prototype with the rods on the mounting plate., where the ball bearing is exactly in the middle of the mounting plate.
4. Load the prototype very carefully with 3,508kg (balanced force determined in the first experiment), placed in the middle of the prototype.
5. Mount the linear motor stage horizontally.
6. Start Labview

7. Select file: MeasurementSetup.vi

8. Press RUN.

9. If an error is given, the COM-port of the actuator is wrong.

10. Fill in the filename of the measurement: Rz_3508g_1.txt

11. Adjust the force sensor and the prototype with the linear stages such that the force sensor is 65mm from the middle of the prototype.

12. Fill in the TRAVEL DISTANCE of 1000μm.

13. Activate TWO-WAY. The linear motor stage will go forwards and backwards.

14. Press CONTINUE.

15. When the linear motor stage is at its original position, press STOP.

16. Repeat the measurement 4 times.

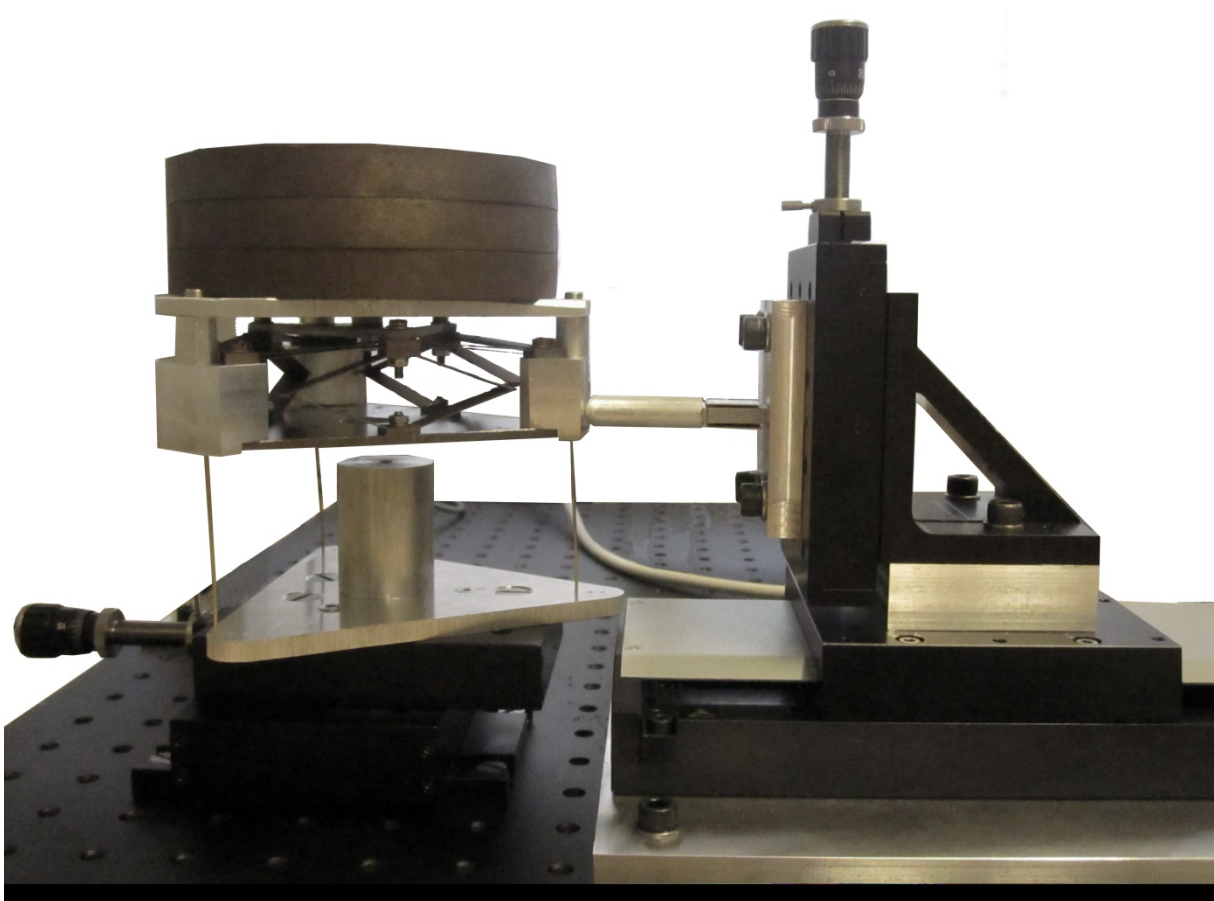17. Repeat the measurements for a load of the prototype (filename: Rz_435g_1.txt).

Data processing protocol

1. Open Matlab

2. Select file: Rz_balancing.m

3. Press RUN.

4. The program will show the moment-rotation characteristic of the measurements.

Appendix E

ANSYS Simulations

E.1   Out-of-plane motions

To model the bi-stable buckling beams and the v-shaped beams a finite element analysis model (FEA model) is required. In Dunning et al (2011b) a method is described to model the prototype. In this section the ANSYS code is showed and shortly explained. The code describes 1/6 of the prototype (Fig. E.1). This is because the ANSYS student version cannot define enough keypoints to model the complete prototype. Consequently, the results of the complete prototype is 6 times the results of this simulation. Furthermore, to have the result of the balanced domain positive, the part of the prototype is modeled upside down (Fig. E.1).
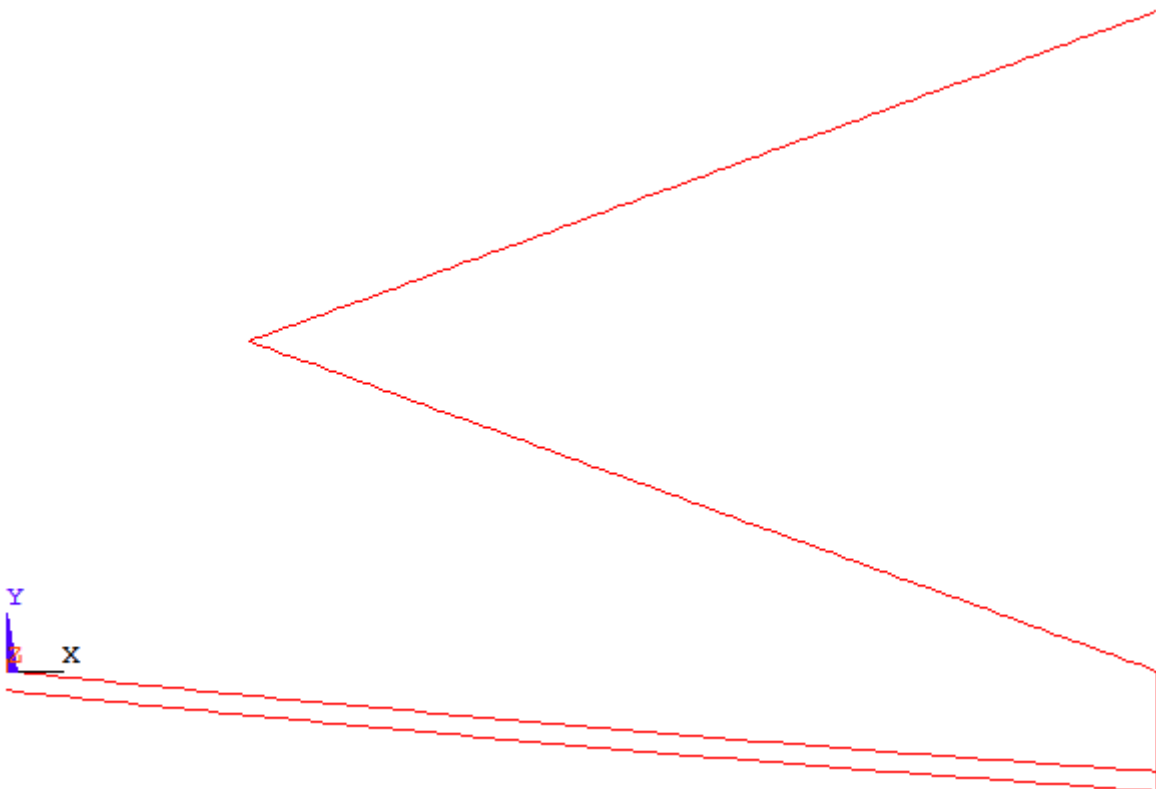

Fig. E.1. The shape of the FEA model of 1/6 of the prototype, modeled upside down.

E.1.1   ANSYS code

```
! ADJUSTABLE parameters-----------------------------------------------------------

      *SET,E,113e9                      ![Pa]  ,Young's modulus
      *SET,v,0.34                       ![]    ,Poisson Ratio
      *SET,l,35e-3                      ![m]   ,Length of bi-stable buckling beam
      *SET,w,9e-3                       ![m]   ,Width beams
      *SET,t1,0.25e-3                   ![m]   ,Thickness bi-stable buckling beams
      *SET,t2,0.45e-3                   ![m]   ,Thickness v-shaped beam
      *SET,alpha,5                      ![deg] ,Initial angle of the bi-stable beams
      *SET,b,27.5e-3                    ![m]   ,How wide is the v-shaped beam?
      *SET,h,20e-3                      ![m]   ,Height of the v-shaped beam


! FIXED parameters----------------------------------------------------------------
! 1/Curvature of bi-stable buckling beams:
      *SET,c,1                          ![m]
! Convert deg to rad:
      *SET,al_r,alpha*3.14157/180       ![rad]
! Calculate radios of the bi-stable buckling beams:
      *SET,R,sqrt((0.5*l*cos(al_r)+c*sin(al_r))**2+
            (-0.5*l*sin(al_r)+c*cos(al_r))**2)
! Total vertical displacement of the midpoint of the bi-stable buckling beams:
      *SET,travelrange,4.5e-3           ![m]
!---------------------------------------------------------------------------------


! Define element
      /PREP7
      ET,1,BEAM3


! Real constant of the bi-stable buckling beams (1) and the v-shaped beam (2)
      R,1,w*t1,w*t1**3/12,t1, , , ,
      R,2,w*t2,w*t2**3/12,t2, , , ,


! Material properties with Young's modulus and Poisson Ratio
      MPTEMP,1,0
      MPDATA,EX,1,,E
      MPDATA,PRXY,1,,v


! Define keypoints of the bi-stable buckling beams
      K,1,0,0,,
      K,2,0.5*l*cos(al_r)+c*sin(al_r),-0.5*l*sin(al_r)+c*cos(al_r),,
      K,3,l*cos(al_r),-l*sin(al_r),,
      K,6,0,-0.6e-3,,
      K,7,0.5*l*cos(al_r)+c*sin(al_r),-0.5*l*sin(al_r)+c*cos(al_r)-0.6e-3,,
      K,8,l*cos(al_r),-l*sin(al_r)-0.6e-3,,


! Define keypoints of the v-shaped beam
      K,9,l*cos(al_r),0,,
      K,10,l*cos(al_r)-b,h/2,,
      K,11,l*cos(al_r),h,,
```

```
! Draw lines between keypoints
      LARC,1,3,2,R,                     !Arc is needed for the small curvature
      LARC,6,8,7,R,                     !Arc is needed for the small curvature
      LSTR,3,8
      LSTR,3,9
      LSTR,9,10
      LSTR,10,11


! Glue the lines to one mechanism
      LGLUE, ALL,


! Mesh elements
      LESIZE,ALL, , ,100, ,1, , ,1,
      TYPE,        1
      REAL,        1
      LMESH,       1,4                  !Bi-stable beams has real constant 1
      REAL,        2
      LMESH,       5,6                  !V-shaped beam has real constant 2


! Define constraints for bi-stable beams (keypoint 3 and 8 can only translate in y-
direction)
      DK,1, ,0, , , ,ALL, , , , ,
      DK,3, ,0, , , ,ROTZ, , , , ,
      DK,3, ,0, , , ,UX, , , , ,
      DK,3, ,travelrange, ,0,UY, , , , , ,
      DK,6, ,0, , , ,ALL, , , , ,
      DK,8, ,0, , , ,ROTZ, , , , ,
      DK,8, ,0, , , ,UX, , , , ,


! Define constraints for v-shaped beams
      DK,9, ,0, , , ,ROTZ, , , , ,
      DK,10, ,0, , , ,ROTZ, , , , ,
      DK,11, ,0, , , ,ALL, , , , ,


! Defining analysis specifications
      NLGEOM,1
      AUTOTS,0
      NSUBST,200,0,0
      OUTRES,ALL,1


! Solve the analysis
      /SOL
            SOLVE
            FINISH


! Plot deformed shape
      /POST1
            PLDISP,1


! Plot force-displacement characteristic
      /POST26
            NSOL,2,2,U,Y,               !Displacements node 2 = keypoint 3
            RFORCE,3,2,F,Y,             !Forces node 2 = keypoint 3
            XVAR,2
            PLVAR,3
      /AXLAB,X,DEFLECTION [m]           !Renaming axis labels
      /AXLAB,Y,FORCES [N]
      /REPLOT
```

```
! Plot stresses in mechanism
      /POST1
            AVPRIN,0, ,
            ETABLE,SMAXI,NMISC, 1
            AVPRIN,0, ,
            ETABLE,SMAXJ,NMISC,3
            PLETAB,SMAXI,NOAV,1
            PLLS,SMAXI,SMAXJ,1,1
```

E.2   In-plane motions

The in-plane motions are performed by three flexible rods, loaded with the buckling load. One rod is modeled in ANSYS using a subsequent transient analysis. The buckling force of the rod is calculated according to Eq. E.1 (Gere, 2002).

$$F_b = \frac{\pi^2 EI}{L^2} \rightarrow \left(I = \frac{\pi d^4}{64} \right) \rightarrow F_b = \frac{\pi^3 E d^4}{64L^2} \tag{E.1}$$

The modeled rod is loaded in vertical direction with this buckling force. Subsequently, a small displacement in horizontal direction is applied to initiate a deformation. Finally, the force-displacement curve for the top of the rod is shown.

E.2.1   ANSYS code

```
! Define element
/PREP7
ET,1,BEAM3

! Material properties with Young's modulus and Poisson Ratio
MP,EX,1,97000                          ! Young's modulus (in Pa)
MP,PRXY,1,0.31                         ! Poisson's ratio

! Real constant of the rod
R,1,0.785398163,0.049087385,0.5        ! Area, I, height

! Define keypoints of the bi-stable buckling beams
K,1,0,0,0                              ! Lower node
K,2,0,50,0                             ! Upper node (50mm high)

! Draw lines between keypoints
L,1,2

! Mesh elements
ESIZE,1
LMESH,ALL


FINISH
/SOLU
```

```
! Defining analysis specifications
ANTYPE,4
NLGEOM,ON
OUTRES,ALL,ALL
NSUBST,20
NEQIT,1000
AUTOTS,ON
KBC,0
LNSRCH,ON
LUMPM,0
TRNOPT,FULL
/ESHAPE,1


! Time step 1 of the transient analysis
TIME,1


! Define constraints
DK,1,ALL,0                              ! Constrain bottom
DK,2, ,0, , , ,ROTZ, , , , ,
FK,2,FY,-11.47                          ! Buckling load
/SOL
SOLVE


! Time step 2 of the transient analysis
TIME,2
DK,1,ALL,0                              ! Constrain bottom
DK,2, ,0, , , ,ROTZ, , , , ,
FK,2,FY,-11.47                          ! Buckling load
DK,2, ,1, , , ,UX, , , , ,             ! Add a horizontal displacement


! Solve the analysis
/SOL
SOLVE


! Plot force-displacement characteristic
/POST26
RFORCE,2,1,F,X            !Displacements node 1
NSOL,3,2,U,X             !Forces node 1
XVAR,3
PLVAR,2
/AXLAB,X,DEFLECTION        !Renaming axis labels
/AXLAB,Y,LOAD
/REPLOT
```

Appendix F

Results and Discussion

F.1   Out-of-plane motions

F.1.1 T_Z direction

The results of the force-displacement characteristic for the first experiment, loading the mechanism in the centre in T_Z direction, is shown in Fig. F.1.
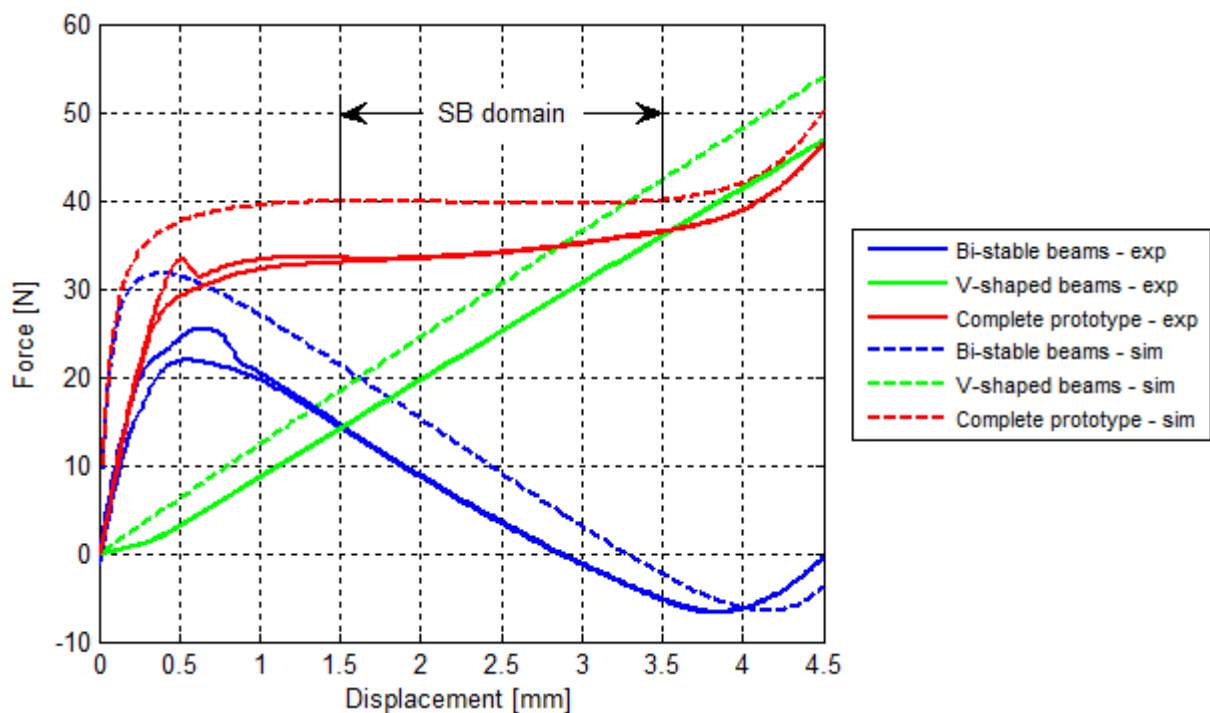

Fig. F.1. Force-displacement characteristic of the bi-stable buckling beams, v-shaped beams and the complete prototype, loaded in the centre of the moving platform in Tz direction for simulations in ANSYS (dashed) and experiments (solid). The residual stiffness in the balanced domain of the prototype is 1.75N/mm, from 1.5-3.5mm displacement.

The prototype is not perfectly balanced. The residual stiffness is 1.75N/mm over a domain of 2mm, from 1.5mm and 3.5mm displacement. The negative stiffness of the bi-stable buckling beams and the stiffness of the v-shaped beams are smaller than simulated. Due to small fabrication errors the total stiffness is influenced: the error in thickness for the bi-stable beams and the v-shaped beams is ±0.05mm and ±0.1mm, respectively; the error in width for the bi-stable beams and the v-shaped beams is ±0.05mm.

The negative stiffness of the bi-stable buckling beams is not perfectly linear and the positive stiffness of the v-shaped beams is not the exact opposite of the negative stiffness. This results in a non-linear behavior of the stiffness of the complete prototype in the balanced domain. Tuning the stiffness of the v-shaped beams can reduce the residual stiffness, but the smallest residual stiffness that can be achieved for this prototype remains 0.4N/mm (Fig. F.2).
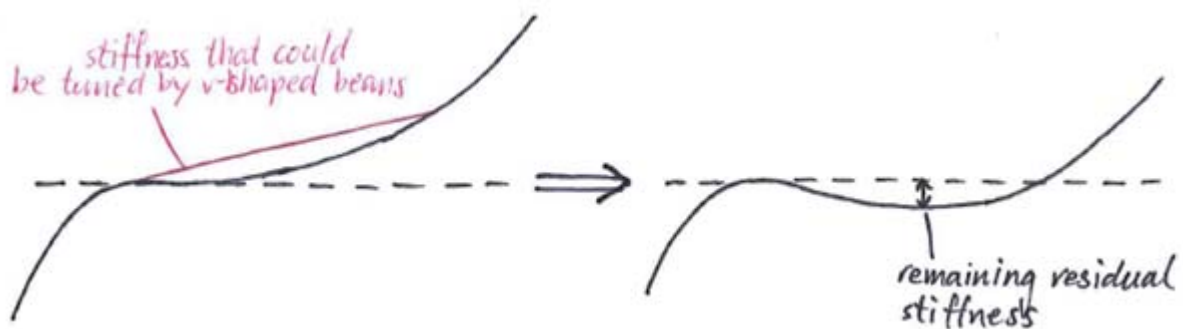

Fig. F.2. Schematic view of the balanced domain of the prototype. After tuning the v-shaped beams a small residual stiffness will always remain, due to the non-linear behavior of negative stiffness of the bi-stable buckling beams.

The small increase in force at the beginning of the negative stiffness domain of the bi-stable buckling beams is caused by the fact that the bi-stable buckling beams do not buckle symmetric. Small variations in the dimensions of the bi-stable buckling beams resulted in variation in the maximum force of the bi-stable beams (Fig. F.3). Consequently, the bi-stable beams are forced into different buckling modes in the beginning of the negative stiffness range. In the return motion, the bi-stable beams all have the same buckling mode, which results in a smoother behavior of the force-displacement characteristic.

The sum of the separate force-displacement characteristics of the bi-stable buckling beams and the v-shaped beams is not equivalent to the force-displacement characteristic of the complete mechanism. This is because the bi-stable buckling beams and the v-shaped beams probably have some parasitic torsion or bending, which result in a different force-displacement characteristic. Once the bi-stable beams and v-shaped beams are connected with the moving platform parasitic torsion and bending of the beams is reduced, resulting in a different force-displacement characteristic of the complete mechanism.
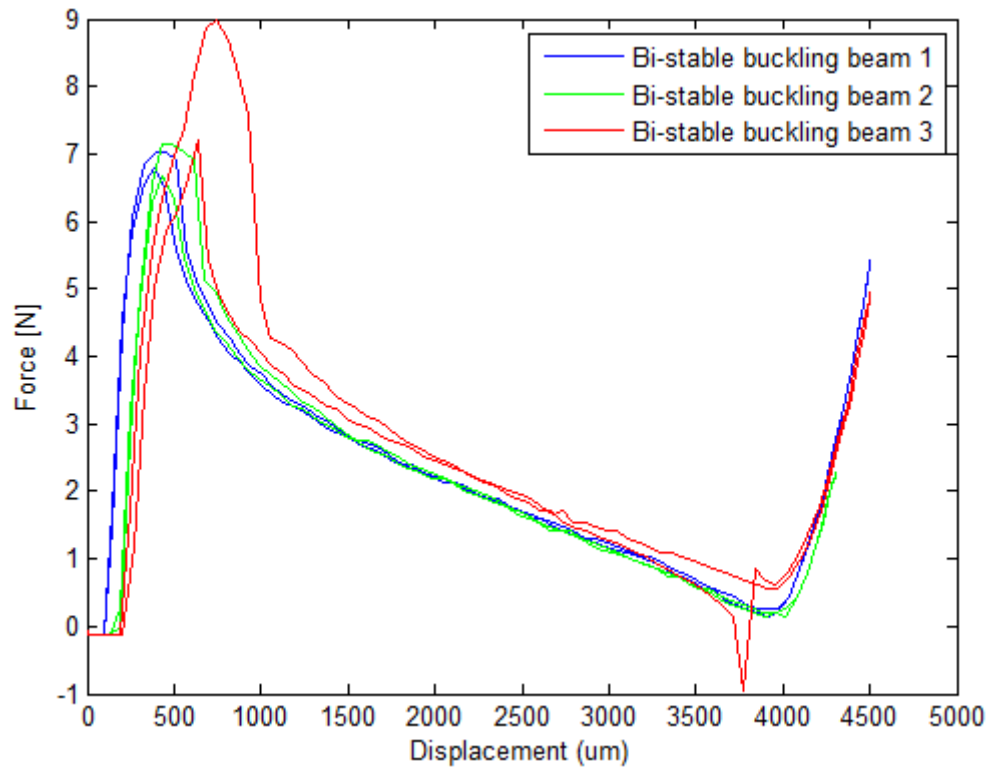
Fig. F.3. Force-displacement characteristics of the single bi-stable buckling beams used in the prototype. Bi-stable beam 3 has a peak in the force at the beginning of the negative stiffness domain, which results in different buckling behavior than the other bi-stable beams.

F.1.2   *Rx, Ry* direction

The measurements of the out-of-plane rotations gives a force and a vertical displacement of the stiff beam at 80mm right from the middle (Appendix D.3). Another vertical displacement is measured 80mm left from the middle with a laser displacement sensor. In Fig. F.4 the displacement on the left side, measured with the laser displacement sensor, are plotted against the displacement on the right side, measured with the linear motor stage.
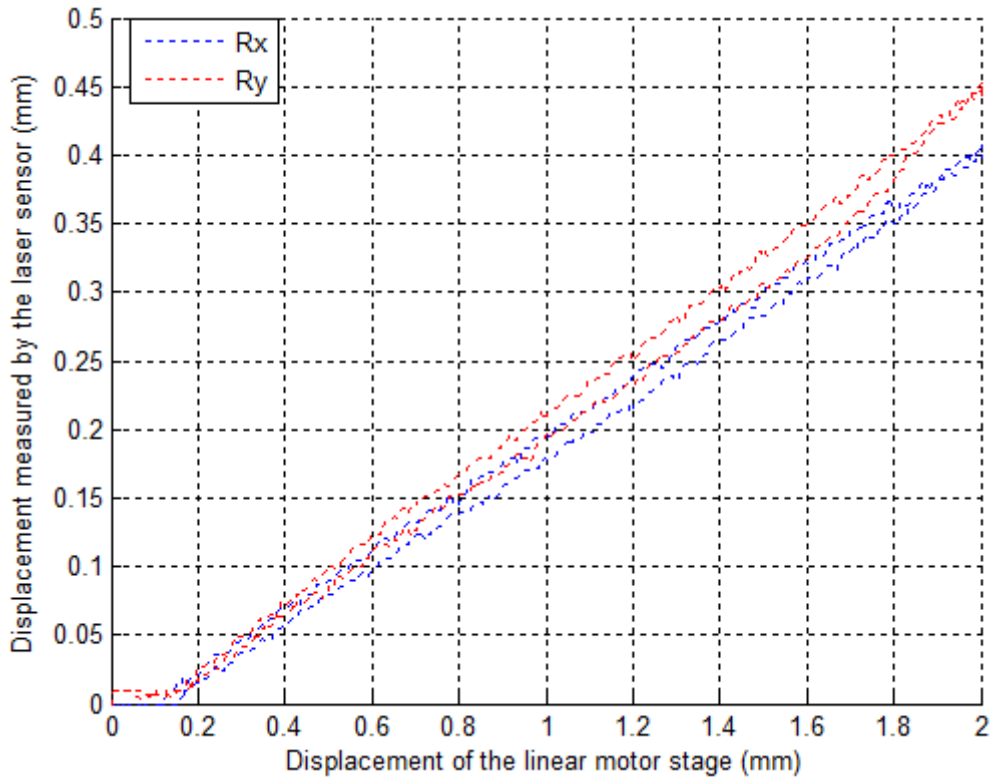
Fig. F.4. Plot of the vertical displacement measured by the linear motor stage vs. the vertical displacement measured by the laser displacement sensor.

The rotation of the stiff beam, and consequently the rotation of the platform is calculated according to these displacements. For small rotations the horizontal motion of the platform is neglected.
The moment-rotation characteristic induced by torsion of the bi-stable beams and the v-shaped beams is shown in Fig. F.5. It is seen that the stiffness in *Ry* direction (18.5Nm/rad) is higher than the stiffness in *Rx* direction (12Nm/rad). This is due to extra torsion in the bi-stable beams and v-shaped beams: due to the rotation about the y-axis, one pair of bi-stable beams and v-shaped beams (parallel to the stiff beam) are twisted about the y-axis (Fig. F.6).
If it is possible to reduce or even cancel out this rotational stiffness, the out-of-plane mechanism shows high potential to perform zero stiffness out-of-plane motion.
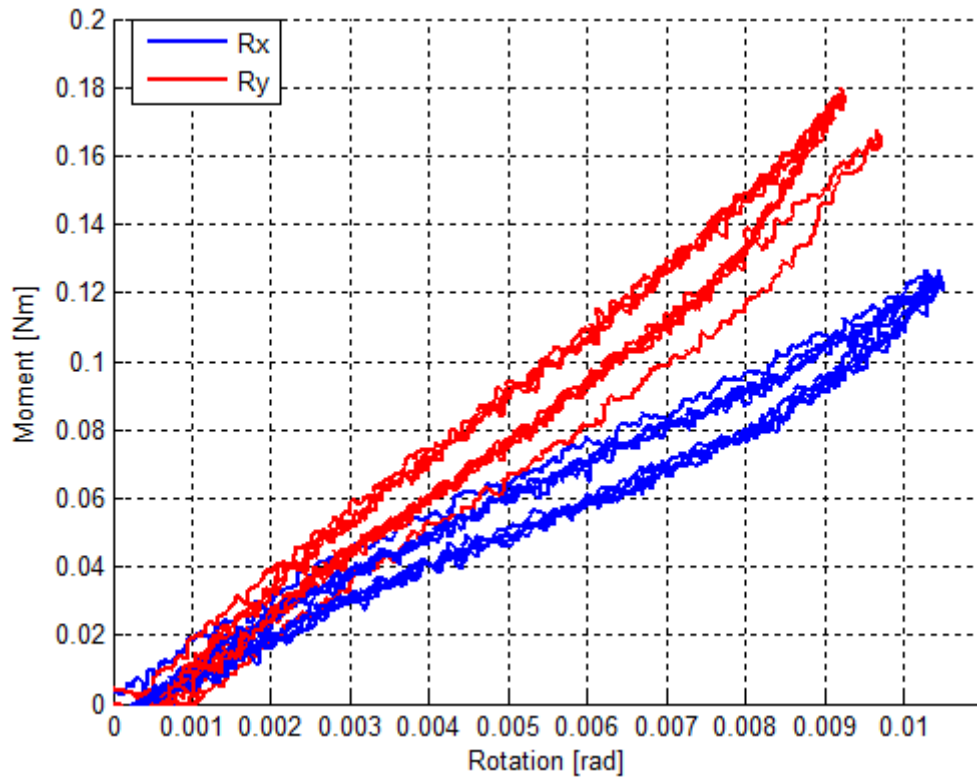
Fig. F.5. Moment-rotation characteristic of the measurements in Rx and Ry direction.
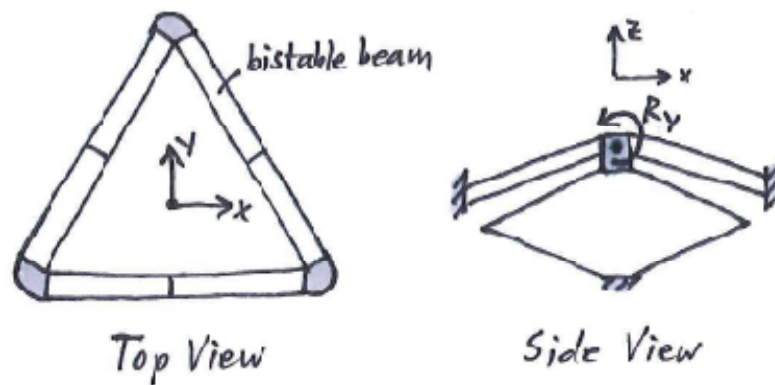
Fig. F.6. Sketch of the torsion in the bi-stable buckling beams and the v-shaped beams, induced by the rotation about the y-axis. This results in a higher stiffness in Ry direction, compared to the Rx direction.

F.2   In-plane motions

F.2.1   *Tx, Ty* direction

The force-displacement characteristic for the translation along the x-axis and the y-axis are the same. In Fig. F.6 the results are shown for two load cases: (1) with the load of the prototype (435g) on top of the flexible rods and (2) with a load of 3508g on top of the rods. The stiffness is reduced from 1.1N/mm to 0.4N/mm. The total buckling load of the three rods with length of 50mm and diameter of 1mm, made of brass (E=97 GPa), should be 56.4N, which corresponds to 5.75kg. So the stiffness could be reduces further by increasing the load on the rods.
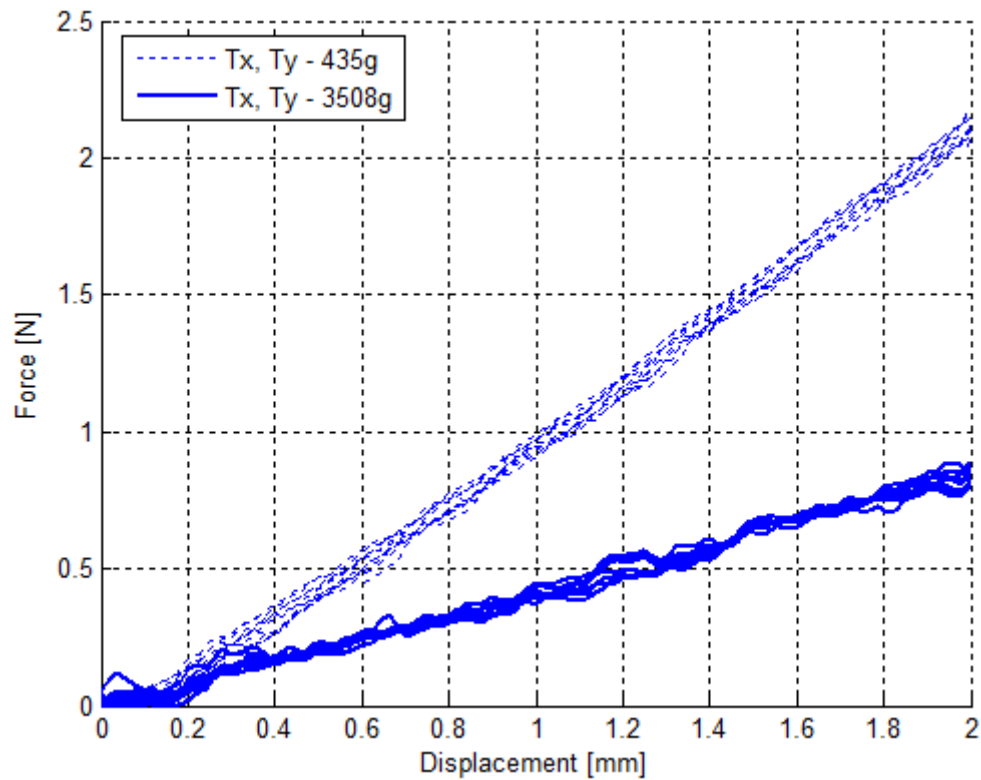
Fig. F.6. Force-displacement characteristic of the measurements in Tx and Ty direction for two different load cases.

F.2.2   *Rz* direction

To determine the moment-rotation curve for the rotation about the z-axis, first the moment and the rotations were determined from the measured force and displacement (Appendix D.5). In Fig. F.7 the results of the moment-rotation characteristic are shown for two load cases: (1) with the load of the prototype (435g) on top of the rods and (2) with a load of 3508g on top of the rods. The stiffness is reduced from 4.6Nm/rad to 2Nm/rad. The stiffness could be reduced further by increasing the load on the beams. But the rotational stiffness without the load is already lower than the required rotational stiffness from the design criteria.
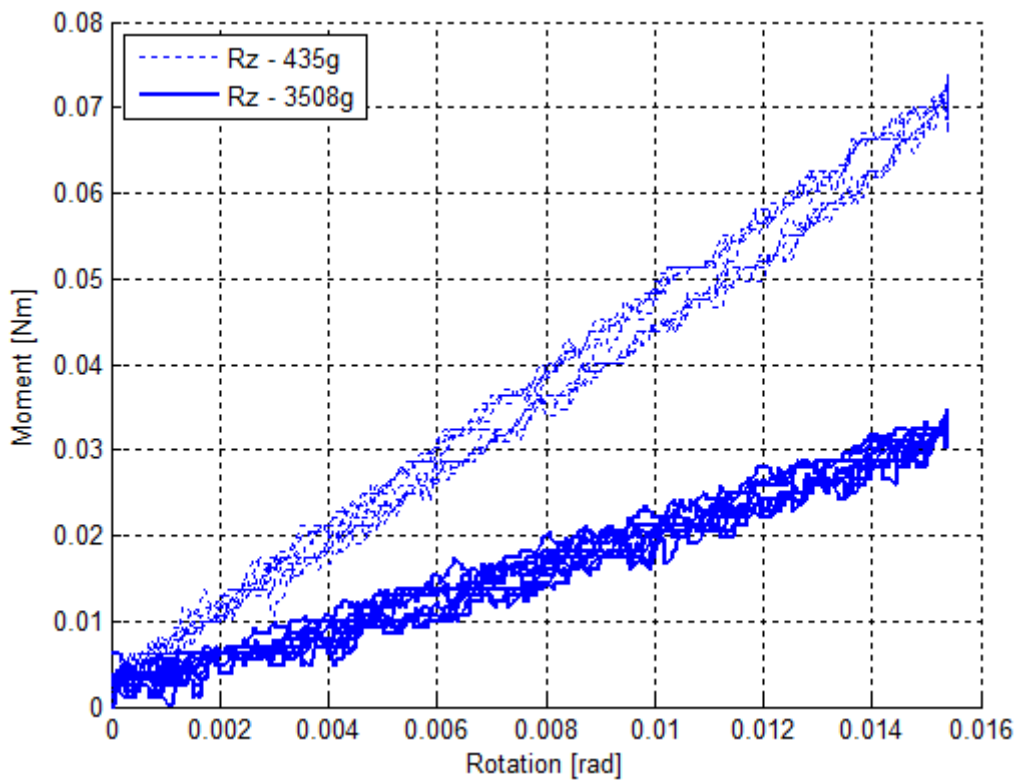
Fig. F.7. Moment-rotation characteristic of the measurements in Rz direction for two different load cases.

The required stiffness for in-plane motion described in the design criteria are reached. One important remark should always be taken into account. To reach a near zero stiffness, the rods are loaded to the buckling load. But the buckling load is very sensitive to variations in the diameter of the rods. When the rods are dimensioned, a safety factor on the buckling load should always be taken into account.

Appendix G

Conclusions and Recommendations

G.1   Conclusions

In this study a design for the first near zero stiffness 6 DoF compliant precision stage is presented. The precision stage was able perform 6 DoF with three statically balanced mechanisms, in triangular configuration, the perform translation along the vertical z-axis and rotations about the horizontal x-axis and y-axis, supported by three flexible rods for in-plane motions. An investigation was made to determine the optimal dimensions for the out-of-plane mechanism, in order to balance a gravity force with low negative stiffness of the b-stable beams and low positive stiffness of the v-shaped beams. It resulted that for the bi-stable buckling beams a high balanced force and low negative stiffness can be reached by designing the initial angle as large as possible. The width and thickness should be as small as possible, otherwise the relation between the balanced force and the negative stiffness is negatively affected. Simultaneously, decreasing the width and the thickness increases the robustness for fabrication errors. For the same reasons, the length of the beams should be as large as possible. The dimensions of the v-shaped beams are depending on the negative stiffness of the bi-stable beams, and the stiffness is sensitive to variations in thickness and length.

According to this investigation a prototype was made. The prototype is able to balance a gravity force of 34.4N in a balanced domain of 2mm in vertical direction, where a smallest residual stiffness of 0.4N/mm can be achieved. Parasitic torsion during the out-of-plane rotations induced a rotational stiffness of 12Nm/rad and 18.5Nm/rad in *Rx* and *Ry* direction, for a rotation to 10mrad.

The in-plane motions are performed by three flexible rods, loaded with the buckling load. The stiffness for in-plane translations to 2mm (*Tx, Ty*) is reduced from 1.1N/mm to 0.4N/mm, and the stiffness for in-plane rotations to 15mrad is reduced from 4.6Nm/rad to 2Nm/rad, when the load on the rods is increased from 435g to 3508g. The buckling load is highly sensitive to variations in the diameter, so a safety factor should always be taken into account.

G.2   Recommendations

A recommendation for improvements is the connection between the bi-stable buckling beams and the moving platform. In this prototype it is a fixed connection, resulting in torsion in the bi-stable beams and v-shaped beams, and consequently in a larger out-of-plane rotational stiffness than required. If this torsion is reduced or cancelled out, for example with a ball joint, the rotational stiffness is reduced.

Another important remark for the design is the large horizontal reaction force of the bi-stable buckling beams. The design should resist this reaction forces without parasitic motion of the end-tips of the bi-stable buckling beams. Otherwise, the bi-stable behavior is negatively affected, and consequently the zero stiffness behavior of the complete mechanism is negatively affected.

Finally, this first design for a zero stiffness 6DoF compliant precision stage, able to balance a gravity force, shows high potential to be used in precision engineering applications.

Appendix H

Design for Mapper Lithography

H.1 Machine architecture

To position the wafer with respect to the electron beam and with extremely high accuracy, a wafer positioning system (WPS) is developed. The process takes place inside a magnetically shielded vacuum chamber. This is to minimize the disturbance of temperature and magnetic fields on the electron beam. The WPS consist of a long stroke stage (LoS), which drives the system in Tx, Ty and Rz directions over relatively large distances (around 300mm), a short stroke stage (ShS), which correct the inaccuracies of the LoS, and a chuck, where the wafer is loaded on. The ShS consists of six Lorentz actuators to position the wafer in six degrees of freedom (DoF), three for providing degree of freedoms in the horizontal plane (Tx, Ty, Rz) and three for motions in the vertical plane (Tz, Rx, Ry) , and a spring system that compensates the weight of the chuck. This spring stiffness is 12N/mm in Tz direction and $1/10^{th}$ in X-Y motion. The accuracy of the positioning is 1mm translation and 10mrad rotation in each direction. A detailed drawing of the top and bottom part of the ShS is seen in Fig. H.1.

It is important that the wafer is positioned parallel to the electron beam. Due to the tolerances in every subsystem of the machine, it is possible that the wafer have to be positioned slanted with respect to the horizontal plane. In that situation the actuators constantly produce force and heat to keep the wafer in the required position, without correcting the errors.
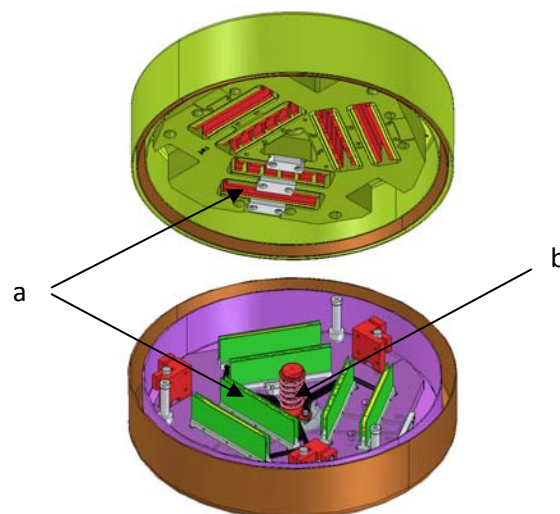

Figure H.1. Detailed drawing of the top and bottom part of the short stroke stage. Six Lorentz actuators (a) create the motion in 6DoF and a helical spring (b) balance the gravity force of the upper part and the chuck (not showed).

H.2　Design criteria

In the following section the design requirements and constraints for the zero stiffness 6 DoF compliant precision stage are discussed. Each of the requirements and constraints will be explained on their importance.

H.2.1　Performance requirements

Degrees of freedom - The ShS must be able to correct the inaccuracies of the LoS. Therefore the zero stiffness 6 DoF compliant precision stage must be able to position the wafer in six degrees of freedom (*Tx,Ty, Tz, Rx, Ry, Rz*).

Stroke - The statically balanced stroke must be 1mm translation in *Tx*, *Ty*, and *Tz* direction and 10mrad in *Rx, Ry, Rz*-direction. At this moment the stroke in *Tx* direction is 100um and 720um in *Ty* direction.

Stiffness - At this moment the spring has a stiffness of 12N/mm in *Tz* direction. With this stiffness the actuators produce too much heat. The stiffness of the new design must be smaller than 1N/mm in each direction. For rotations this corresponds to 8.15Nm/rad in *Rx* and *Ry* direction, and 1.81Nm/rad in *Rz* direction (Fig. H.2).
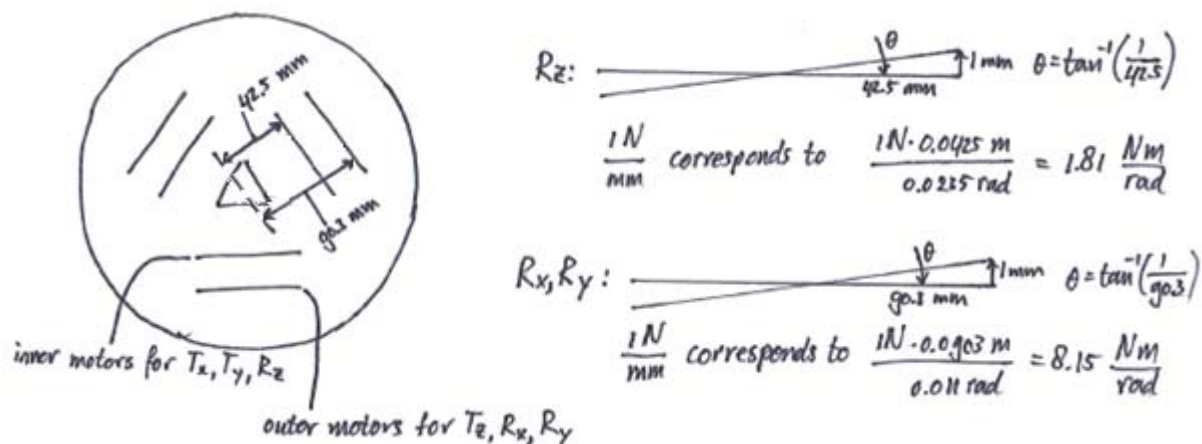
Fig. H.2. Calculation of the rotational stiffness for in-plane rotation (Rz) and out-of-plane rotations (Rx, Ry).

Static load - The precision stage must be able to balance the gravity force of the top part of the ShS and the chuck. The combined mass of the ShS top part and the chuck is 24kg.

Lifetime - The MAPPER machine has a lifetime of 3 years, doing 10 wafers per hour (24/7). The zero stiffness 6 DoF compliant precision stage must also have a lifetime of 3 years. In the power-off state the top part is resting on the end-stops and the stroke of the stage is the largest. During progress the strokes is usually smaller.

H.2.2   Manufacturing requirements

Assembly - The ShS consist of 2 parts. There are no fixed connections between the top part and the bottom part. The two parts are slid over each other when assembled. The mu-metal shielding is completely closed.

Attaching - The attachment points (in the stage and/or the ShS) have to be part of the design. It is preferable when the attachment points of the current design are used. Making some holes in the mu-metal shielding is possible in the bottom part, and strictly forbidden in the top part.

End-stops - When the machine is powered off the top part of the ShS is resting on some end-stops. These end-stops are positioned 0.5mm below the neutral position of the wafer. So during progress the actuators have to tilt the complete structure 0.5mm plus the required corrections. At the end-stops some gravity force is needed. The end-stops can be lowered when necessary.

Volume claim - The precision stage have to fit inside the current space for the spring. In Fig. H.3 the exact dimensions can be seen. When necessarily needed, it is possible to gain more space in the area between the motors, but then the whole ShS have to be redesigned.

Materials - Due to the outgassing of materials and the requirements about magnetism inside the vacuum chamber the materials that can be used are according to the 'MAPPER material list of approved materials'. Inside the mu-metal shielding more materials can be used than outside the shielding. The gravity balancer in the current design is made of phosphor-brass. Some material (e.g. spring steel) can give some problems, because the motors are calibrated for some amount of magnetic material inside the shielding.

Robustness to fabrication errors - The robustness to fabrication errors says something about the reliability of the design and how well it achieve all design requirements. The robustness to fabrication errors must be high, so not many manufactured mechanisms are rejected.
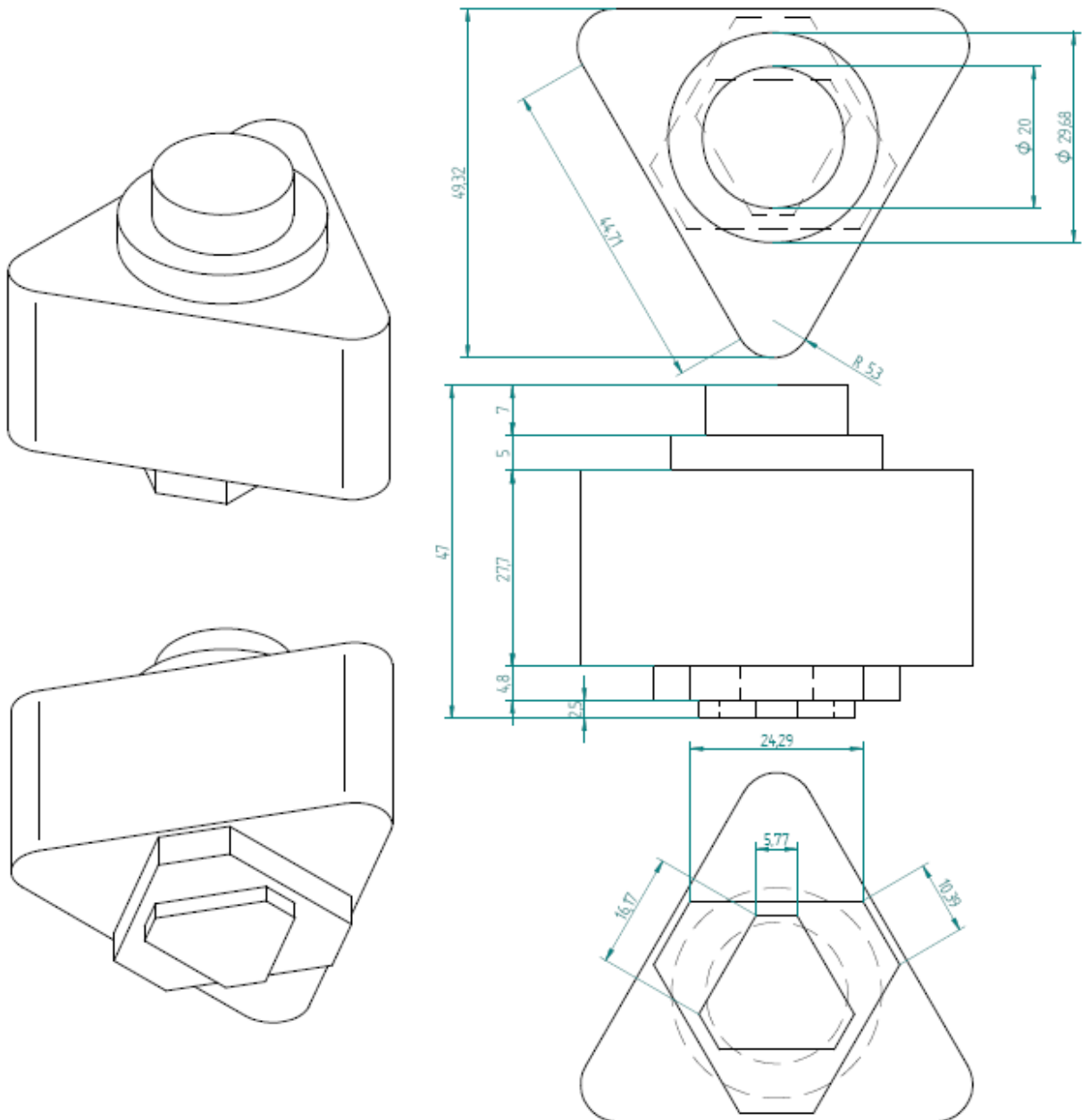
Figure H.3. Detailed drawing with dimensions of the volume claim.

An overview of the design requirements is found in table H.1.

Table H.1. Overview of the design criteria for a zero stiffness 6DOF compliant precision stage.

Parameter	Requirement
Performance requirements	
Degrees of freedom	Six: three translations and three rotations (Tx, Ty, Tz, Rx, Ry, Rz)
Stroke	1mm translation, 10mrad rotation in each direction
Stiffness	< 1N/mm in every translational direction, <8.15Nm/rad in Rx, Ry direction, <1.81Nm/rad in Rz direction.
Static load	24kg
Lifetime	3 years
Manufacturing requirements	
Assembly	No fixed connection between top part and bottom part.
Attaching	From current design, or redesign is needed.
End-stops	0.5mm below neutral position of wafer. Can be lowered.
Volume claim	See Fig. H.3.
Materials	See 'MAPPER material list of approved materials'
Robustness to fabrication errors	High

H.3 Design

H.3.1 Out-of-plane motions

The specific design for the machine of MAPPER Lithography requires a very high load in a small volume. This is a great challenge.

According to Dunning et al. (2011b) and the investigation on dimension parameter made in this research [Appendix B] the width and thickness should be as small as possible, and the length should be maximized. The most important design parameter is the initial angle of the bi-stable buckling beams. But for a higher initial angle, the beams should be thinner to stay below the allowed stresses. An optimization is found between initial angle, thickness, allowed stresses and the required number of bi-stable beams above each other. In Table H.2 an overview of the determined design parameters are shown. The dimensions of the mechanism are optimized to fit in the volume space, with 1mm space between the mechanism and the edge of the volume space, and a platform in the middle of the bi-stable buckling beams with a length of 3mm, to mount the moving platform on.

Table H.2. Overview of the design parameters of the mechanism for out-of-plane motions for the MAPPER Lithography machine.

Design parameter	Value
Bi-stable buckling beams	
Length	19.72mm
Width	5mm
Thickness	0.273mm
Initial angle	5°
Number of bi-stable beams above each other	5
Material	Titanium Grade 5 (Ti6Al4V)
V-shaped beams	
Length	20.22mm
Width	5mm
Thickness	0.58mm
Initial angle with ground	20°
Number of v-shaped beams above each other	3
Material	Titanium Grade 5 (Ti6Al4V)

The mechanism is modeled in ANSYS. Only 1/6 of the mechanism is modeled (Fig. H.4). Between every beam a space of 0.5mm is left. With this, the total height of the mechanism is 23.2mm, which fits in the volume space.
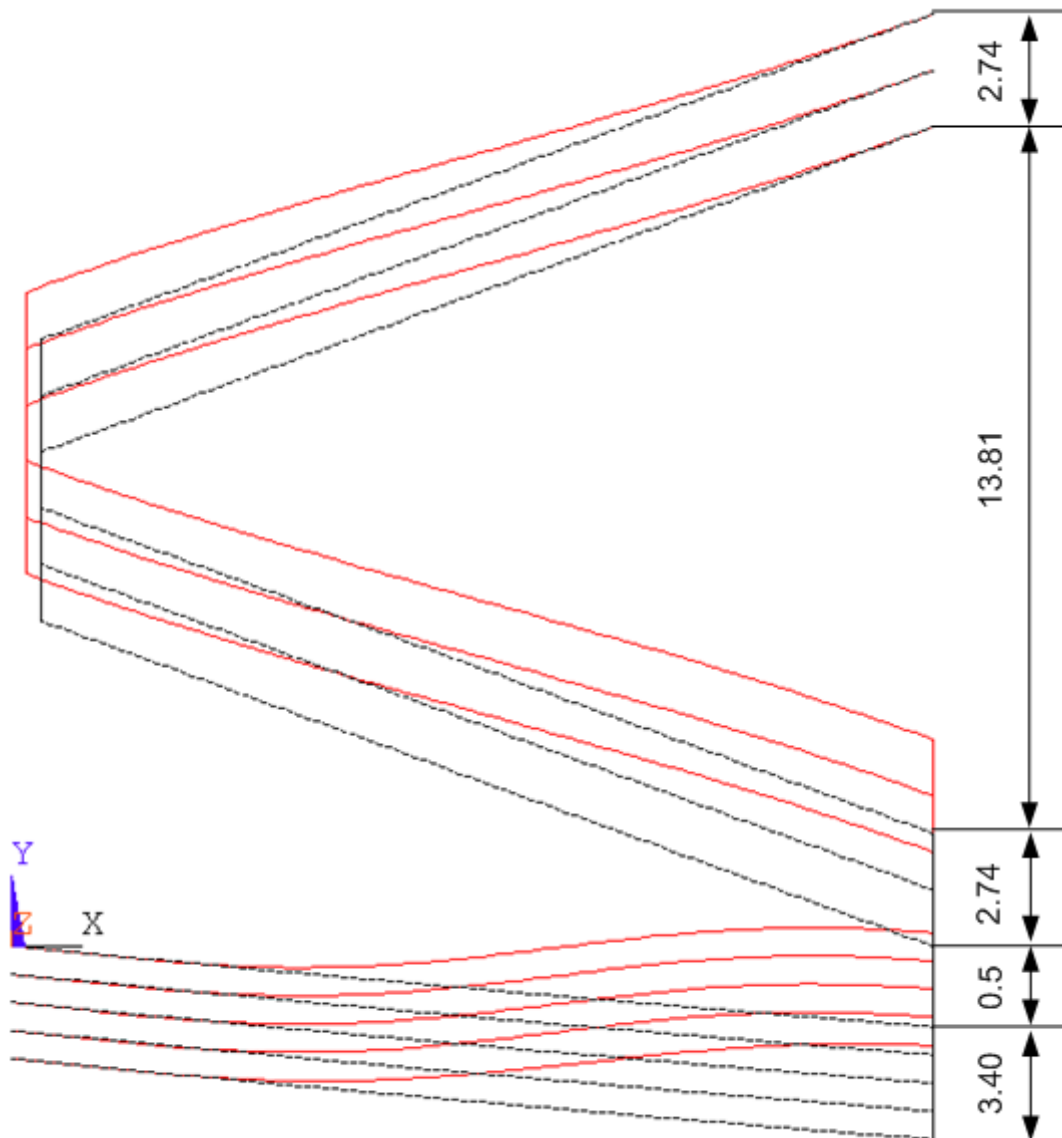
Fig. H.4. Shape of the mechanism in undeformed (black, dashed) and deformed shape (red).

This part of the mechanism should balance 235.44/6=39.2N in vertical direction. In Fig. H.5 the result of the mechanism for balancing the Tz direction is shown. The balanced force is 39.2N over a statically balanced stroke of 1mm, from 0.75-1.75mm displacement. The minimum residual stiffness is 0.4N/mm [Appendix F.1.1]. To fulfill the requirement of a stiffness lower tan 1N/mm the maximum manufacturing tolerance is determined by calculating the two worst scenarios. In the first scenario the stiffness of the bi-stable buckling beams is lower, and the stiffness of the v-shaped beams is larger than modeled, resulting in a mechanism with a low positive stiffness in the balanced stroke. In the second scenario the stiffness of the bi-stable buckling beams is larger and the stiffness of the v-shaped beams is

lower than modeled, resulting in a mechanism with a low negative stiffness in the balanced stroke. The maximum manufacturing tolerance on the dimensions must be smaller than 3µm to fulfill the requirements. The proposed solution for tuning the stiffness is not very suitable for this design. It would require very small and strong parts.
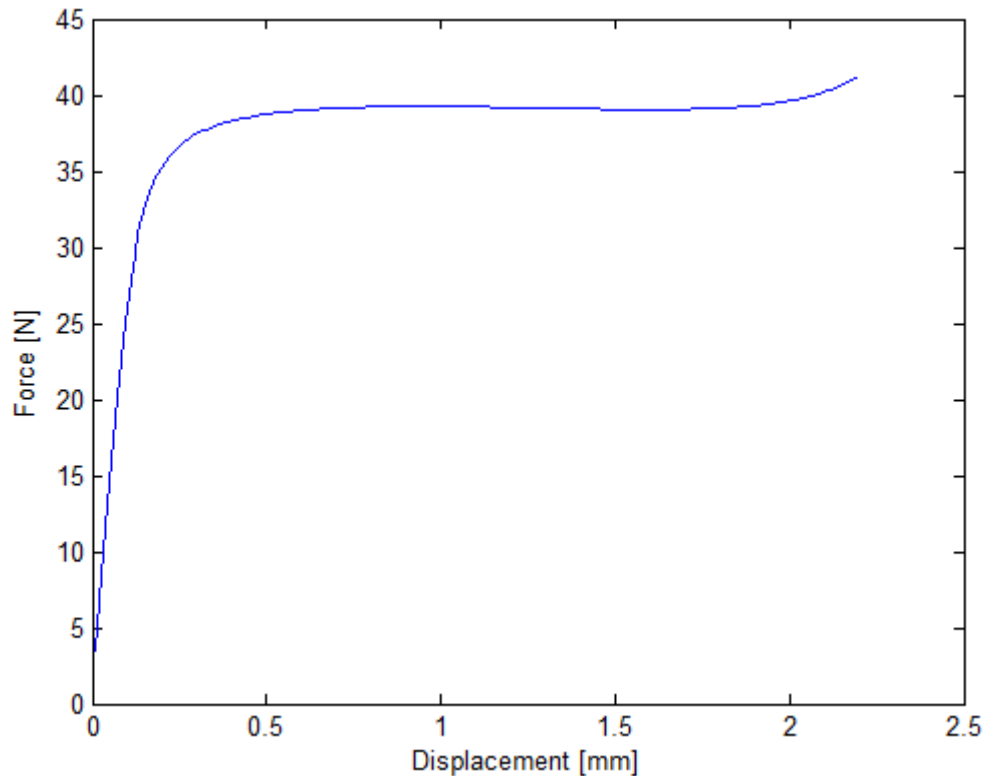
Fig. H.5. The force-displacement characteristic of the balanced mechanism in vertical direction; the balanced force is 39.2N over a stroke of 1mm.

In Fig. H.6 the stresses in the mechanism are shown. The max. stress in the mechanism is 551MPa, at the end tips of the v-shaped beams. The ultimate tensile strength of the titanium Grade 5 is approximately 950MPa (Salomon's Metalen). The endurance limit is around 0.5 of the ultimate tensile strength, so the max. stresses are around the stress where the mechanism can endure an infinite number of load cycles[1]. Further investigation on the specific material and the exact endurance limit is needed.

[1] Ashby, M.F.: Materials Selection in Mechanical Design, Fourth Edition, Elsevier Ltd., Oxford UK, 604pp., 2011.
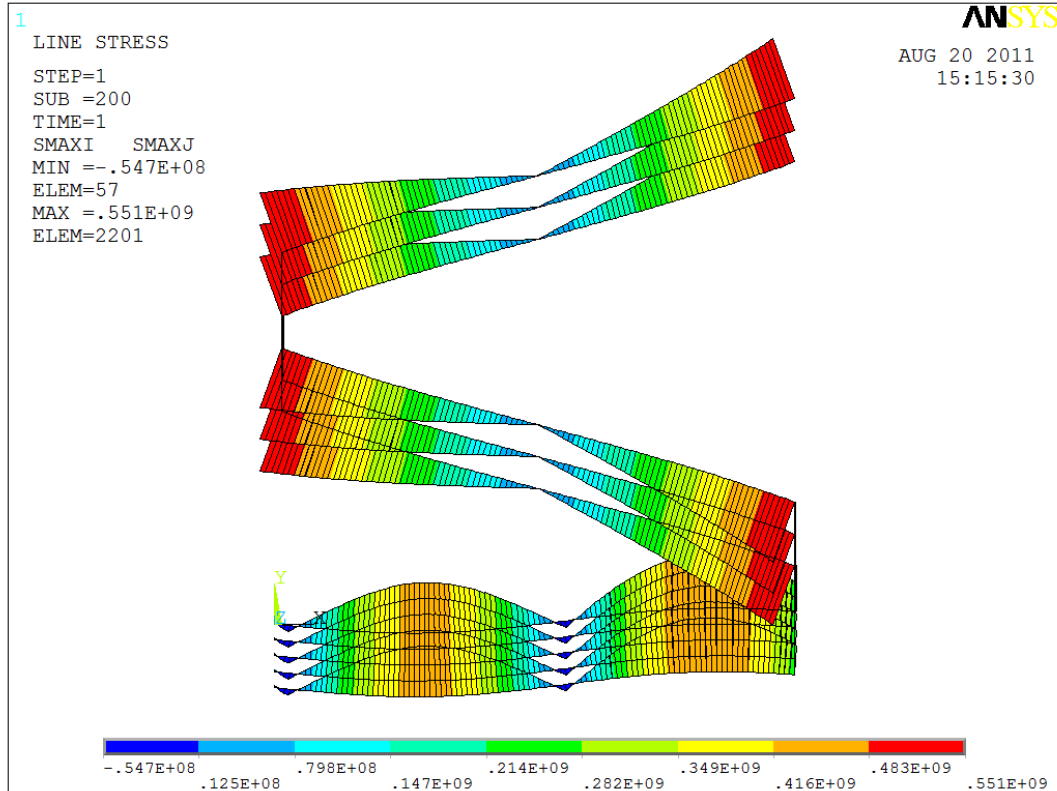
Fig. H.6. Results of the stresses in the mechanism. The max. stress is 551MPa in the end tips of the v-shaped beams.

In the design the horizontal reaction forces of the bi-stable buckling beams should be taken into account. Simulations showed that the max. horizontal reaction force is 450N. The design of the out-of-plane mechanism should be able to withstand these forces without parasitic horizontal motion of the end-tips of the bi-stable buckling beams, otherwise the bi-stable behavior and consequently the statically balanced behavior of the complete mechanism is affected.

In this research it has been shown that the rotational stiffness due to torsion of the bi-stable buckling beams and the v-shaped beams is larger than the required stiffness. The torsional stiffness of a single cantilever beam can be calculated with Eq H.1 (Gere, 2002):

$$\frac{T}{\theta} = \frac{G \cdot I_p}{L}, \qquad with \left(I_p = \frac{1}{12} wt(w^2 + t^2) \right) \tag{H.1}$$

From the equation it is expected that the stiffness due to torsion in the beams will reduce compared to the prototype made in this research, because decreasing the width and the thickness has the most influence on reducing the stiffness. Compared with the prototype, the width in this design is decreasing the most. The stiffness due to torsion can be reduced by using a different connection between the bi-stable beams and the moving platform. In the current design, this is a fixed connection, but when, for example, a frictionless ball joint is used, the stiffness due to the torsion in the beams will reduce.

H.3.1.1   ANSYS code

```
! ADJUSTABLE parameters-------------------------------------------------------
        *SET,E,113e9                    ![Pa]  ,Young's modulus
        *SET,v,0.34                     ![]    ,Poisson Ratio
        *SET,l,19.72e-3                 ![m]   ,Length of bi-stable buckling beam
        *SET,w,5e-3                     ![m]   ,Width beams
        *SET,t1,0.275e-3                ![m]   ,Thickness bi-stable buckling beams
        *SET,t2,0.578e-3                ![m]   ,Thickness v-shaped beam
        *SET,alpha,5                    ![deg] ,Initial angle of the bi-stable beams
        *SET,b,19e-3                    ![m]   ,How wide is the v-shaped beam?
        *SET,h,13.83e-3                 ![m]   ,Height of the v-shaped beam


! FIXED parameters-----------------------------------------------------------
! 1/Curvature of bi-stable buckling beams:
        *SET,c,1                        ![m]
! Convert deg to rad:
        *SET,al_r,alpha*3.14157/180     ![rad]
! Calculate radios of the bi-stable buckling beams:
        *SET,R,sqrt((0.5*l*cos(al_r)+c*sin(al_r))**2+
            (-0.5*l*sin(al_r)+c*cos(al_r))**2)
! Total vertical displacement of the midpoint of the bi-stable buckling beams:
        *SET,travelrange,2.2e-3         ![m]
!-----------------------------------------------------------------------------


! Define element
        /PREP7
        ET,1,BEAM3


! Real constant
        R,1,w*t1,w*t1**3/12,t1, , , ,
        R,2,w*t2,w*t2**3/12,t2, , , ,


! Material properties with Young's modulus and Poisson Ratio
        MPTEMP,1,0
        MPDATA,EX,1,,E
        MPDATA,PRXY,1,,v


! Define keypoints of the bi-stable buckling beams
        K,1,0,0,,
        K,2,0.5*l*cos(al_r)+c*sin(al_r),-0.5*l*sin(al_r)+c*cos(al_r),,
        K,3,l*cos(al_r),-l*sin(al_r),,

        K,4,0,-0.6e-3,,
        K,5,0.5*l*cos(al_r)+c*sin(al_r),-0.5*l*sin(al_r)+c*cos(al_r)-0.6e-3,,
        K,6,l*cos(al_r),-l*sin(al_r)-0.6e-3,,

        K,7,0,-1.2e-3,,
        K,8,0.5*l*cos(al_r)+c*sin(al_r),-0.5*l*sin(al_r)+c*cos(al_r)-1.2e-3,,
        K,9,l*cos(al_r),-l*sin(al_r)-1.2e-3,,

        K,10,0,-1.8e-3,,
        K,11,0.5*l*cos(al_r)+c*sin(al_r),-0.5*l*sin(al_r)+c*cos(al_r)-1.8e-3,,
        K,12,l*cos(al_r),-l*sin(al_r)-1.8e-3,,

        K,13,0,-2.4e-3,,
        K,14,0.5*l*cos(al_r)+c*sin(al_r),-0.5*l*sin(al_r)+c*cos(al_r)-2.4e-3,,
        K,15,l*cos(al_r),-l*sin(al_r)-2.4e-3,,
```

```
! Define keypoints of the v-shaped beam
        K,16,l*cos(al_r),0,,
        K,17,l*cos(al_r)-b,h/2,,
        K,18,l*cos(al_r),1.2e-3,,
        K,19,l*cos(al_r)-b,h/2+1.2e-3,,
        K,20,l*cos(al_r),2.4e-3,,
        K,21,l*cos(al_r)-b,h/2+2.4e-3,,
        K,22,l*cos(al_r)-b,h/2+3.6e-3,,
        K,23,l*cos(al_r),h+3.6e-3,,
        K,24,l*cos(al_r)-b,h/2+4.8e-3,,
        K,25,l*cos(al_r),h+4.8e-3,,
        K,26,l*cos(al_r)-b,h/2+6.0e-3,,
        K,27,l*cos(al_r),h+6.0e-3,,

! Draw lines between keypoints
        LARC,1,3,2,R,                       !Arc is needed for the small curvature
        LARC,4,6,5,R,                       !Arc is needed for the small curvature
        LARC,7,9,8,R,                       !Arc is needed for the small curvature
        LARC,10,12,11,R,                    !Arc is needed for the small curvature
        LARC,13,15,14,R,                    !Arc is needed for the small curvature
        LSTR,3,6
        LSTR,6,9
        LSTR,9,12
        LSTR,12,15
        LSTR,3,16
        LSTR,16,18
        LSTR,18,20
        LSTR,16,17
        LSTR,18,19
        LSTR,20,21
        LSTR,17,19
        LSTR,19,21
        LSTR,21,22
        LSTR,22,24
        LSTR,24,26
        LSTR,22,23
        LSTR,24,25
        LSTR,26,27

! Glue the lines to one mechanism
        LGLUE, ALL,

! Mesh elements
        LESIZE,ALL, , ,100, ,1, , ,1,
        TYPE,        1
        REAL,        1
        LMESH,       1,9                    !Bi-stable beams has real constant 1
        REAL,        2
        LMESH,       10,23                  !V-shaped beam has real constant 2

! Define constraints for bi-stable beams
        DK,1, ,0, , , ,ALL, , , , ,
        DK,3, ,0, , , ,ROTZ, , , , ,
        DK,3, ,0, , , ,UX, , , , ,
        DK,3, ,travelrange, ,0,UY, , , , , ,

        DK,4, ,0, , , ,ALL, , , , ,
        DK,6, ,0, , , ,ROTZ, , , , ,
        DK,6, ,0, , , ,UX, , , , ,
```

```
        DK,7, ,0, , , ,ALL, , , , ,
        DK,9, ,0, , , ,ROTZ, , , , ,
        DK,9, ,0, , , ,UX, , , , ,

        DK,10, ,0, , , ,ALL, , , , ,
        DK,12, ,0, , , ,ROTZ, , , , ,
        DK,12, ,0, , , ,UX, , , , ,

        DK,13, ,0, , , ,ALL, , , , ,
        DK,15, ,0, , , ,ROTZ, , , , ,
        DK,15, ,0, , , ,UX, , , , ,

! Define constraints for v-shaped beams
        DK,16, ,0, , , ,ROTZ, , , , ,
        DK,16, ,0, , , ,UX, , , , ,
        DK,18, ,0, , , ,ROTZ, , , , ,
        DK,18, ,0, , , ,UX, , , , ,
        DK,20, ,0, , , ,ROTZ, , , , ,
        DK,20, ,0, , , ,UX, , , , ,

        DK,17, ,0, , , ,ROTZ, , , , ,
        DK,19, ,0, , , ,ROTZ, , , , ,
        DK,21, ,0, , , ,ROTZ, , , , ,
        DK,22, ,0, , , ,ROTZ, , , , ,
        DK,24, ,0, , , ,ROTZ, , , , ,
        DK,26, ,0, , , ,ROTZ, , , , ,
        DK,21, ,0, , , ,ROTZ, , , , ,

        DK,23, ,0, , , ,ALL, , , , ,
        DK,25, ,0, , , ,ALL, , , , ,
        DK,27, ,0, , , ,ALL, , , , ,

! Defining analysis specifications
        NLGEOM,1
        AUTOTS,0
        NSUBST,200,0,0
        OUTRES,ALL,1

! Solve the analysis
        /SOL
                SOLVE
                FINISH

! Plot deformed shape
        /POST1
                PLDISP,1

! Plot force-displacement characteristic
        /POST26
                NSOL,2,2,U,Y,            !Displacements node 2 = keypoint 3
                RFORCE,3,2,F,Y,          !Forces node 2 = keypoint 3
                XVAR,2
                PLVAR,3
        /AXLAB,X,DEFLECTION [m]          !Renaming axis labels
        /AXLAB,Y,FORCES [N]
        /REPLOT
```

```
! Plot stresses in mechanism
      /POST1
              !PLNSOL, U,SUM, 0,1.0
              AVPRIN,0, ,
              ETABLE,SMAXI,NMISC, 1
              AVPRIN,0, ,
              ETABLE,SMAXJ,NMISC,3
              PLETAB,SMAXI,NOAV,1
              PLLS,SMAXI,SMAXJ,1,1
```

H.3.2   In-plane motions

The three flexible rods for the in-plane motions must be able to support 24kg. The buckling load of one rod should be 235.44/3 = 78.5N. The maximum length of the rods is set to 20mm. Due to fabrication errors both the diameter and the length can vary. Extracting the error from the diameter and adding to the length ('worst-case 2') decrease the buckling force. In this case the rod should balance 78.5N. In table H.3 the buckling force of the three cases is shown.

Table H.3. The calculated buckling force of one flexible rod for three different cases. In the middle the normal case is shown. The other cases are the limits for an error of 5μm.

Length Diameter	'worst-case 1': 19.995mm	20mm	'worst-case 2': 20.005mm
0.875mm			80.19N
0.88mm		82.08N	
0.885mm	84N		

A simulation is done using the length and diameter of 'worst-case 1' with the buckling load of 78.5N. The complete in-plane balancing mechanism will have a stiffness less than 1N/mm when the maximum manufacturing tolerance is smaller than 5µm (Fig. H7).
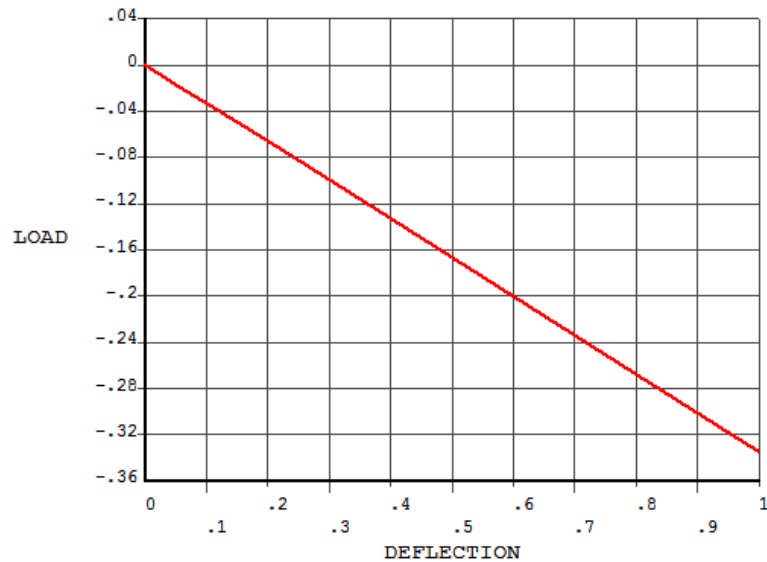
Fig. H.7. Force-displacement characteristic of one flexible rod, where 'worst-case 1' is loaded with the buckling load of 78.5N. The stiffness of the complete mechanism (three rods) is 1N/mm.

H.3.2.1   ANSYS code

```
! Define element
     /PREP7                  ! Enter the preprocessor
     ET,1,BEAM3              ! Define element as beam3

! Material properties with Young's modulus and Poisson Ratio
     MP,EX,1,113000              ! Young's modulus (in Pa)
     MP,PRXY,1,0.34             ! Poisson's ratio

! Real constant
     R,1,0.615143477,0.030112234,0.4425     ! area, I, height

! Define keypoints
     K,1,0,0,0
     K,2,0,19.995,0

! Draw lines between keypoints
     L,1,2

! Mesh elements
     ESIZE,1
     LMESH,ALL

     FINISH
     /SOLU

! Defining analysis specifications
     ANTYPE,4
     NLGEOM,ON
     OUTRES,ALL,ALL
     NSUBST,20
     NEQIT,1000
     AUTOTS,ON
```

```
        KBC,0
        LNSRCH,ON
        LUMPM,0
        TRNOPT,FULL
        /ESHAPE,1
```

```
! Define constraints for time step 1
        TIME,1
                DK,1,ALL,0                      !Constrain bottom
                DK,2, ,0, , , ,ROTZ, , , , ,
                FK,2,FY,-78.5                   !Apply buckling load
        /SOL
        SOLVE
```

```
! Define constraints for time step 2
        TIME,2
                DK,1,ALL,0                      !Constrain bottom
                DK,2, ,0, , , ,ROTZ, , , , ,
                FK,2,FY,-78.5                   !Apply buckling load
                DK,2, ,1, , , ,UX, , , , ,      !Apply 1mm displacement on top
        /SOL
        SOLVE
```

```
! Plot force-displacement characteristic
        /POST26
                RFORCE,2,1,F,X          !Reaction force node 1 (bottom)
                NSOL,3,2,U,X            !Displacement node 2 (top)
                XVAR,3
                PLVAR,2
        /AXLAB,X,DEFLECTION [MM]        !Renaming axis labels
        /AXLAB,Y,LOAD [N]
        /REPLOT
```
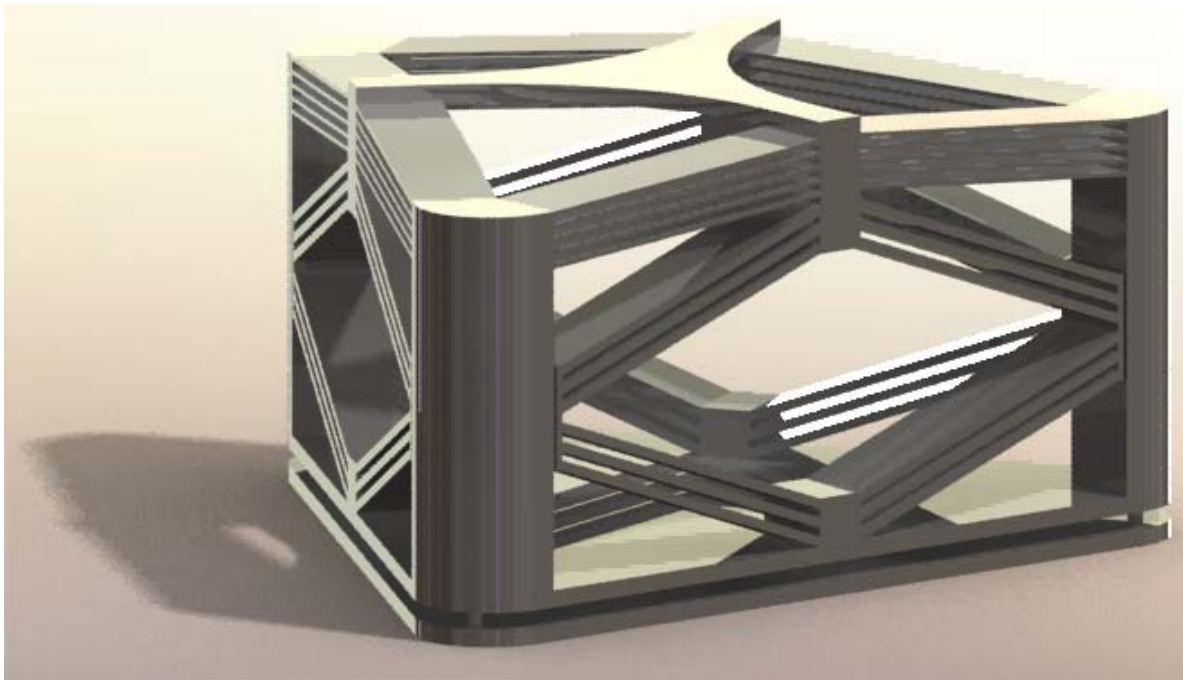
H.4 CAD model

Fig. H.8. Render of the CAD model of the design for Mapper Lithography.

H.5 Conclusions

The proposed design for a zero stiffness 6 DoF precision stage show high potential to be used in the machine of Mapper Lithography. The mechanism is able to balance a mass of 24kg with a residual stiffness smaller than 1N/mm in a domain of 1mm in vertical direction. The stiffness for in-plane translations and rotation are also smaller than the required stiffness. The stiffness for out-of-plane rotations caused by torsion in the bi-stable buckling beams and the v-shaped beams is to large, but can be reduced with a different design.

The stresses in the mechanism are around the endurance limit of the material, so the mechanism can endure an infinite number of load cycles. More research on the exact material properties is needed.

Before implement the current design into the current machine of Mapper Lithography, some design criteria should be taken into account where the current design did not focus on. The end-stops should be build in, to constrain the position of the mechanism when the machine is powered off. The attachment points should also be integrated in the design, to fix the mechanism in the Mapper machine.

Finally, due to the small manufacturing tolerances for the mechanism, another tuning mechanism could be considered, to increase the robustness to fabrication errors.